University of Leeds

DOCTORAL THESIS

Development of a Low Cost Bio-magnetometer for the Detection of Myocardial Infarction

Author:
Shima Ghasemi Roudsari

Supervisor:
Prof. Benjamin T H Varcoe

A thesis submitted in fulfillment of the requirements for the degree of Doctor of Philosophy

in the

Experimental Quantum Information
School of Physics and Astronomy

May 2017

Development of a Low Cost Bio-magnetometer for the Detection of Myocardial Infarction

Shima Ghasemi Roudasri

May 2017

Abstract

The aim of the present study was to design, develop and examine a portable and low cost magnetometer for cardiac imaging. Magnetocardiography (MCG) involves capturing magnetic field maps (MFM's) of current distributions resulting from cardiac action potentials. Particular emphasis was given to the diagnostic performance of distinguishing cardiac patients, mainly with ischemic heart disease, from healthy individuals with the aim of potentially expanding the clinical utility.

The current magnetocardiography is known as a superconducting quantum interference device (SQUID). It was first used in 1970 in a magnetically shielded room and the device produced an MCG waveform that could be visualised just as clearly as the conventional electrocardiogram. This popularity is largely attributable to the appearance of unshielded SQUID devices in the late 1990s. However, continued reliance on large immovable equipment that is expensive to maintain, has limited the clinical application of MCG to a small but expanding group of research clinicians worldwide. Despite this, a large body of evidence suggests that an unshielded MCG device is a potentially powerful tool for detecting a multitude of cardiac abnormalities in the human heart. Over the course of this research, I have constructed an induction coil magnetometer that is not only portable, low cost and non-invasive, but also reaches into the sensitivity range needed for magnetocardiography and produces magnetic field maps that are medically diagnosable. Therefore, this technology provides a real alternative to other costly diagnostic tools, such as Superconducting Quantum Interference device-SQUIDs.

While MCG sensors are an established diagnostic tool to diagnose cardiac conditions, for other groups around the world [1], this device is a newly developed apparatus using a less complicated design. This study determines the extent to which the device can provide a clear image across test subjects with a range of age and genders and to identify which parameters from the MCG data are markers for ischemic heart disease when compared with healthy controls.

A pilot study was conducted using 40 patients with ischemia and 20 with post myocardial infarction (MI) as well as 60 healthy age matched controls to evaluate the capability of MCG to detect myocardial ischemia. To identify the optimal recording of MCG, we looked at 55 patients with ischaemic heart disease and 10 post MI patients. In addition, 49 healthy age matched controls underwent examinations. In the MCG pilot study, we defined standard features or "lobes" of

MCG signals, which are common to all healthy normal subjects. For the purpose of evaluating the diagnostic performance of the MCG these are referred to as cursors, and consist of 6 parameters that can be estimated, QR and RS, T-wave (T_1-T_4), as well as the RT interval and zero crossings (ZCs). We also consider QR length and RS length, T length, and angles and genders. They were examined in the detection of myocardial ischemia in both the patient group and the healthy controls. The results showed that MCG is able to distinguish patients from healthy regardless of the presence or absence of a history of remote MI.

Stepwise regression was performed using the Forward Logistic Regression-LR method. Using this approach, any variable with $p > 0.20$ was removed at each step. Thereafter, the two-way interactions were included in a stepwise analysis with other significant predictors. Candidate predictors entered at step 1 include the following; T2_corr by T2_length, QR cursor, QR_angle, T1_angle, T_zcMDIS, QR_length by RS_length, and GENDER(1) by T_stdcorrvar. The aforementioned parameters are spatial and temporal diagnostic variables of the MCG that we used in o

ur study to distinguish healthy from patient. T1 is the magnetic Field Map (MFM) at the beginning of depolarization and T2 is the MFM at the peak of the depolarsation. Length, angle and correlation of each of these were measured. We also defined some other parameters such QR that is repolarisation at the peak of R-wave. More definitions are detailed in chapter 6. As a result of the final model, we find the following interactions are significant predictors: QR_length by RS_length, GENDER(1) by T_stdcorrvar and T2_corr by T2_length.

In conclusion, 15 channel- MCG can detect myocardial ischemia at rest and supine position in an unshielded environment. In MCG several factors can be used to distinguish unhealthy from healthy: QR, RS length and T-wave correlations. The interactions between some of the parameters can also produce significant predictions. We also found that T-wave changes during the period of time corresponding to T_1 to T_4 are very useful in detecting abnormalities. Furthermore, the T-wave parameters such as angles and lengths may contain information on separate physiological stages of the ischemia development. This will be subject to future research.

Acknowledgements

Seek knowledge from the cradle to the grave

I praise God for all His mercy and grace, the beauties of the world and the chance that he has given us to discover its laws.

I would like to give my special thanks to my supervisor, Professor Ben Varcoe, for giving me the opportunity to take part in this very exciting project. He taught me how to do research and what Physics is. I would also like to acknowledge EPSRC (Medical Devices) and The National Innovation Centre for funding this research. I would like to especially thank York Neuroimaging centre for access to their shielded room and Prof G. Green, who gave us opportunities to test the sensors in a shielded environment. To Leanne Burgin thanks for taking responsibility of being the project manager for the trial. Also many thanks to Prof M. Kearney, M.Williamson, Lorraine Falk, Roo Byrom and the rest of the clinical team in the LGI for their assistance during the project.

Great thanks to John Mooney, QI current PhD candidate, whose heart was and is my MCG healthy standard template and without his programing the data analysis wouldn't be ready that soon. Also thanks to Dr. Paul Wathall from QuantumImaging and Charlotte Kelly for the statistics work they have done as part of the MCG analysis .

I am so thankful to Abbas Al-Shimary for helping me with the systematic review as my time was so tight to play with some QUADAS tools. Also he has to be thanked so much as he spent many hours making this thesis legible.

The mechanical and electrical workshops of the Physics department at Leeds University, for their help with the sensor layout design, deserve a special mention. Their enthusiasm and their skills in designing equipment are admirable. I also thank the wider QIX family for making this group a fun place to work.

Also many thanks to Catherine and Ben Varcoe for the barbecue. It helped to reduce stress. Thanks also to dear Emma for giving medals to the winners of the garden jenga challenge, which Beth and I won versus all the boys, including Ben.

My special thanks have to go to my lovely and loyal family, who have been very understanding at my lack of visits and were always willing to listen to my non-sense when things were not going to plan. To my Mum and Dad; without their guidance and financial support I would have never had this opportunity. To my dear brothers, Abbas and Alireza, who although are in another part of the world, were never too far away to call and check in on their sister and show lots of support and an interest in my achievements. To my aunties and my cousin Reyhaneh, for being most of her time with my mum and supporting me during my PhD (keeping my mind calm by being always available).

To everyone else, cheers for everything.

In the hope of union, my very life, I'll give up
As a bird of Paradise, this worldly trap I will hop.
In the hope of one day, being your worthy servant
Mastery of both worlds I'll gladly drop.
May the cloud of guidance unload its rain
Before I am back to dust, into the air I rise up.
Beside my tomb bring minstrels and wine
My spirit will then dance to music and scent of the cup.
Show me your beauty, O graceful beloved of mine
To my life and the world, with ovation I put a stop.
Though I am old, tonight, hold me in your arms
In the morn, a youthful one, I'll rise up.
On my deathbed give me a glimpse of your face
So like Hafiz, I too, will reach the top.

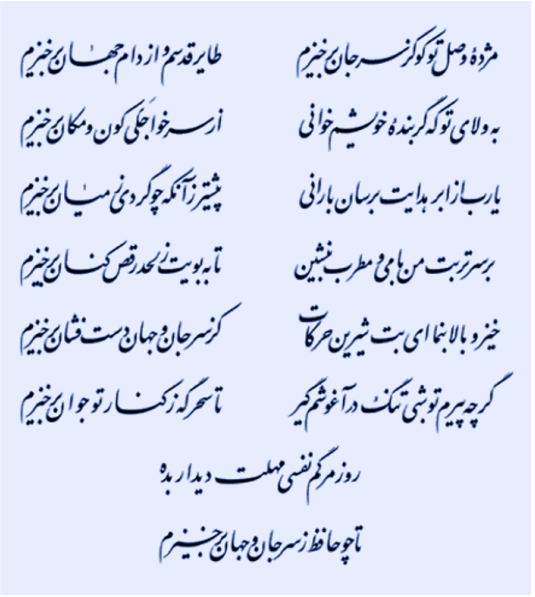

Contents

List of Figures

List of Tables

Abbreviations

MCG	Magnetocardiogram
ED	Emergency Department
IHD	Ischemic Heart Disease
ECG	Electrocardiogram
MI	Myocardial Infarction
AMI	Acute Myocardial Infarction
CAD	Coronary Artery Disease
ACS	Acute Coronary Disease
SQUIDs	Superconducting Quantum Interference Devices
AMI	Acute Myocardial Infarction
fT	Femto Tesla
ELF	Extremely Low Frequency
MFM	Magnetic Field Map
NPV	Negative Predictive value
PPV	Positive Predictive Value
NSTEMI	Non-ST Elevation Myocardial Infarction
MCV	Maximum current Vector
TCV	Total Current Vector
CHD	Coronary Heart Disease
CDPs	Current Distribution Parameters
VT	Ventricular Tachycardia
VF	Ventricular fibrillation
SVT	Supra-Ventricular Tachycardia
PSVT	Paroxysmal Supra-Ventricular Tachycardia

WPW	Wolff-Parkinson-White
AF	Atrial Fibrillation
TPE	T wave Peak to T wave End
AP	Action Potential
RMS	Root Mean square
PCA	Principal Component Analysis
PVC	Premature Ventricular Contraction
VPx	Ventricular Pre-excitation
CRBBB	Complete Right Bundle Branch Block
CAM	Current Arrow Map
W-HEBEMS	Whole-Heart-Electrical Bull's Eye Map
AV	AtrioVentricular node
VA	Ventricular Arrhythmia
LVH	Left Ventricular Hypertrophy
HCM	Hypertrophic Cardiomyopathy
ECHO	Echo-Cardiogram
ATP	Adenosine TriphosPhate
TMP	Trans-Membrane Potential (TMP)
PET	Positron Emission Tomography
CD	Current Density
BSPM	Body Surface Potential Mapping

I would like to dedicate this thesis to my love, Abbas and to my loving parents, Fatemeh Dastoum and Khosro Ghasemi

Preface

This dissertation is an original intellectual product of the author, Shima Ghasemi Roudsari. The fieldwork reported in Chapters 4- 6 received approval by the NRES Committee Yorkshire & The Humber - Leeds Central, with Ethics Certificate number 12/YH/0562. This thesis describes the research conducted during my Ph.D. study, at the University of Leeds, UK, under the supervision of Professor Ben Varcoe. The majority of the work was carried out since 2011 at the Department of Physics and Astronomy, in the Experimental Quantum Information Laboratory. The clinical trial data were obtained in Leeds General Infirmary, and were analysed in the Experimental Quantum Information Laboratory. All the written work and electronic files were kept secure on a password protected computer, and all the obtained data were kept in an encrypted hard drive which was only accessed by the authorised researchers. Research of this nature needs a high level of confidentiality and, as a result, no publications were permitted until the device patent process was completed.

Magnetocardiography is a non-invasive, non-contact and emission free technique that measures the magnetic field generated by the heart. Currently, the two most commonly used methods by clinicians for clinical diagnostics in the cardiac field at a preliminary stage of a heart disease, such as myocardial infarction, are electrocardiograms (ECG) and blood troponin tests. Both of these methods have serious drawbacks. The ECG measures fluctuations in the potential difference across the whole body, and thence give no spatially resolved data on the heart. Furthermore, the produced waveform is sometimes difficult to read, due to the high level of noise in the signal. On the other hand, while blood troponin tests are highly sensitive for the detection of acute myocardial infarction (AMI), these can only be obtained between 10-12 hours following the onset of symptoms, during which time patients require prolonged observation within a clinical decision unit.

Hence, early and accurate identification of AMI patients is fundamental to a successful chest pain triage in an emergency department. Diagnostic techniques based on magnetocardiography (MCG), promise speedy and accurate detection of AMI, thus reducing diagnostic procedures without compromising patient safety.

The aim of this thesis is to present a novel MCG technology that can detect MI and CAD patients while addressing the drawbacks of existing MCG devices. This

thesis also provides a description of magnetocardiographic solutions that have been proposed to date.

Research questions and solutions

Chapter 1 presents a literature review of the applicability of magnetocardiography to the diagnosis of cardiac conditions. In particular, it focuses on the major cardiac conditions, ischaemic heart disease, and plans a study based on that. The subsequent work was completed with the assistance of two undergraduate students.

Chapter 2 consists of two parts. The first part provides an overview of the principles of cardiac electrophysiology. The second part presents a systematic review of the use of magnetocardiography for ruling out coronary artery disease. In the process, I reviewed 3884 articles on magnetocardiography based on defined search criteria.

Data extraction was conducted by myself and reviewed by an independent reviewer A. Al-Shimary. The extracted data was summarized using the Hierarchical Summary Receiver Operator Curve (HROC) technique with the help of C. Kelly from the Institute of Transport Studies, who also performed the statistical analysis. Dr R. Charles and Prof J. Camm provided medical oversight and Prof B. Varcoe supervised, motivated, and managed the research program.

Chapter 3 represents the main work of this thesis. It describes the design and optimization of the novel apparatus. The research addressed the following challenges and proposed possible solutions to improve the performance of the system. These challenges and proposed solutions are given below:

Challenges

Magnetocardiography (MCG) offers high accuracy diagnosis for numerous heart conditions but its practical implementation suffers from several limitations, meaning that the technology remains largely unused in clinical environments.

During the course of the project I identified the existing problems and introduced alternative solutions to overcome these. The design of a state-of-the-art MCG technology, therefore, has to be studied in full to check:

- What is the best sensor layout, and how many sensors are required to map the magnetic field obtained from the heart in sufficient resolution for it to be medically beneficial?

- How to locate the sensors to give the best data and readings?
- How to design a portable MCG device that can achieve sufficient resolution in images without the requirement for a shielded room?

Solutions

Several experiments were set up using inductive coils to optimise the layout and the number of sensors required for designing an optimal medical magnetometer. Over the course of these experiments (detailed in chapter 3), different numbers of sensors were tested with different layouts, they are as follows:

- Two sensors placed in series in a tube,
- Four sensors located in a square layout,
- Nine sensors placed hexagonally,
- 15 sensors also placed hexagonally.

It was concluded that 15 sensors in a hexagonal layout is the minimum requirement for mapping the magnetic field generated by the heart. The hexagonal design of the magnetic sensor head was defined based on heart anatomy (detailed in chapter 5). In the process, Leeds University electrical and mechanical workshop assisted with the electronics and the mechanical needs for the device. J. Mooney's contribution was the formal evaluation of the sensor calibration and noise floor, E. Reade Banham produced the software to drive the device, C. Symonds was an undergraduate project student who assisted in coil evaluation, and N. Pawlowski generated the COMSOL models. All the works have been completed under Prof B. Varcoe's supervisons.

Challenges

The research sought and was granted approval from the University Ethics Committee to test the device on a healthy group from the University of Leeds (ethics number MEEC 12-034).

This process served to test the design in respect to the previously discussed problems and it was found to work perfectly on this healthy group. There was a requirement to evaluate the medical magnetometer device performance on patients with heart conditions.

Solutions

Based on the literature reviewed in chapter 1, it was decided to conduct a clinical trial on patients with ischaemic heart disease. In order to examine the 15 channel MCG on patients with heart conditions, further ethical approval was required to use the device at Leeds General Infirmary (LGI). I applied for a second ethical approval, this time to use the device in hospital (in the LGI). This process was completed through the Integrated Research Application System (IRS) with the project title 'Solid state Magnetocardiography Technical Performance Study'. For the IRAS form, the assistance of Sarah Brown from CTRU, Leeds University was taken into account, to ensure the project meets the health-care legal policy. The clinical trial was designed and conducted at Leeds general Infirmary (LGI). The study protocol is detailed in chapter 4. The device was operated by two research nurses trained by myself. Over the entire clinical trial I supervised all the scans as well as data collection successfully.

Chapter 5 concentrates on how the performance of the device can be optimised by reducing noise. It also describes several experiments to optimise issues such as the distance between the sensor and the body, along with the scan environment and positioning of the device.

This state-of-the-art study has established bio-markers to enable the use of the MCG variables as diagnostic parameters by taking and analysing over 500 MCG scans from healthy volunteers and analysing a vast number of MCG data. This understanding of the MCG signal was translated into a potential diagnostic algorithm, which was subsequently implemented by J. Mooney using Python Language.

Following the completion of the study, detailed analysis of the algorithm output for each subject was performed, comparing magnetic field maps and other variables. An independent statistician, Dr P. Wathall, was employed to perform the statistical analysis. Results suggested outstanding diagnostic performance, paving the way for future clinical trials.

Summary of the contributions of this work

The principal contributions to the current research are as follows:

- Identification of a number of cardiac conditions for which better diagnostic techniques are required

- A substantial systematic review of the use of Magnetocardiography to rule out CAD patients
- Obtained two ethical approvals; one was for healthy subjects, in the university and the other one was for a clinical trial on patients with cardiac conditions
- Sensor layout optimisaton was proposed in respect to the number of sensors that were required to map the magnetic field of the heart with sufficient resolution to make it medically beneficial
- Identification of sensor head position on the thorax to obtain the most accurate data possible from the heart
- Conduction of a clinical trial in Leeds General Infirmary (LGI). The study resulted 89% sensitivity, 41% specificity on patients with ischemic heart disease and an age matched healthy group.
- Determination of the key diagnostic features of MCG images.

Publications

Chapter 2 *" Magnetocardiography for Detection and Rule-Out of Coronary Syndrome and Significant Coronary Artery Disease: Systematic Review and Meta-Analysis"*. S. Ghasemi-Roudsari, A. Al-shimary, C. Kelly, B. Varcoe, R. Charles and J. Camm. Academic Emergency Medicine, (2017) [January 2017 submitted].

Chapter 3 *"A Portable Diagnostic Device for Cardiac Magnetic Field Mapping"*. J. W. Mooney, S. Ghasemi-Roudsari, E. Reade Banham, C. Symonds, N. Pawlowski, and B. T. H. Varcoe . Biomedical Physics& Engineering Express (2017). 3(1): 015008. [It is an open access and available online].

Chapter 6 *"Ghost Imaging in Magnetocardiography"*, S. Ghasemi-Roudsari, J. W. Mooney, R. Byrom, L. Kearney, M. Kearney and B. Varcoe. Scientific Reports, (2017) [in submission].

Chapter 4 and 6 *"A new portable magnetometer to differentiate between ischemic and non-ischemic heart disease in patients presenting with chest pain"*.S. Ghasemi-Roudsari, Abbas Al-Shimary, B. Varcoe, R. Byrom, L. Kearney, M. Kearney, Journal of the American College of Cardiology (2017) [March 2017 submitted].

I also gave several internal seminars and a symposium talk at the university of Leeds:
Talk by Shima Ghasemi R, *Magnetocardiography - A Novel Diagnostic Technology to Detect Ischemic Heart Disease-IHD.* (2014).

This thesis aims to provide a complete description of the development of an innovative magnetocardiography to date.

Chapter 1

Introduction

The purpose of this thesis and corresponding experiment is to design a magnetometer useful for cardiac imaging. Over the course of the introduction I will explain the motivation for this research and review some cardiac conditions and MCG responses to them. I will also provide an overview of current and upcoming methods in bio-magnetic measurements. At the end of the chapter I will provide an outline of this thesis.

1.1 Motivation

Electrical activity in the heart results in current flow with an associated magnetic field. The magnetic fields created by the heart are the largest in the body, nevertheless they are still very small with a peak field of the order of tens of picotesla and are 10^{-8} times smaller than the earth's field. Nevertheless it has been demonstrated that these small fields have a have a sound diagnostic capability for cardiac dysfunction [2]. Magnetocardiography (MCG) is the creation of diagnostic images of the magnetic field of the heart and its analysis is a developing field of cardiac research. Magnetocardiograhy has been studied since 1963 [3] as a medical diagnostic technique and these images have been shown to have additional diagnostic information compared to ECG. This is due to the fact that magnetic fields, unlike electric fields, are not distorted and diffused by intervening tissue and are therefore capable of giving a clear image of the electrical activity of the heart. Also the magnetic field is a direct measurement of the field map rather than a measurement of the potential difference between two points.

This technique will be able to speed up the treatments of patients with cardiac conditions. Magnetocardiography is an emission-free, non-invasive and non-contact diagnostic, which works through clothing and delivers a relatively accurate initial diagnosis. These aspects therefore make it a desirable diagnostic tool.

In benchmarked studies, the MCG has been shown to have an excellent diagnostic capability that is both superior to ECG and is presented in a form that is easier and faster to diagnose. These aspects therefore make it a highly desirable diagnostic tool. Hence, MCG has the potential to play a central role in the rapid triage of patients with chest pain very early in the diagnostic pathway. It could, for example find a role in the ambulance service, directing patients to the correct centre for appropriate treatment. However, despite its successes as a diagnostic, and given the length of time that MCG has been studied, including the availability of commercial devices, it has yet to make an impact on medical practice. The reason for this is that all current commercial MCG devices use superconducting magnetic sensors and are therefore large and expensive, requiring liquid helium and specialist operators. They are also extremely magnetically sensitive requiring a low noise environment; in practice this means either a shielded room, or location restrictions are imposed on the installation. Therefore, the added benefit of MCG typically does not overcome the expense.

Chest pain is one of the most common emergency department (ED) presenting complaints and is related to the leading cause of death worldwide. While some patients present with potentially life threatening diagnoses (i.e. acute coronary syndrome (ACS), pulmonary embolism, aortic dissection) the majority have conditions that are relatively benign (i.e. musculoskeletal pain, gastro oesophageal reflux disease (GORD), pericarditis). The challenge for the physician is to distinguish an acute coronary syndrome (ACS) from the variety of other cardiac and non-cardiac causes of chest pain. The current cardiac pathway is summarised in Fig.1.1. In approximately 35% of cases there is an obvious non-cardiac explanation and these patients can quickly be discharged or reassigned to a more appropriate non-cardiac care pathway. In approximately 14% of cases a diagnosis can be made quickly based on ECG evidence of ST elevation myocardial infarction (STEMI). However, for the remaining 52% of patients the diagnosis is considerably less certain [4].

At present, clinicians use the ECG and blood troponin as their clinical judgment. However, the image obtained from ECG is a single 10 to 12 second period of

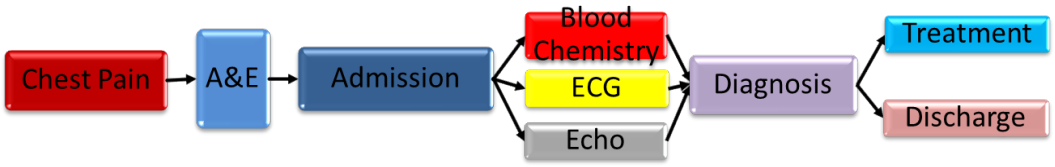

FIGURE 1.1: The current pathway is accurate and effective but requires multiple tests and patient observation, which takes time.

the cardiac cycle that has insufficient accuracy of detection for all areas of the myocardium [5, 6] and sometimes the waveform production is difficult to read [7], which could be due to noise in the signal. On the other hand the sensitivity of troponin testing for AMI is obtained between 10–12 hours following the onset of symptoms. Therefore, many patients required serial blood tests and prolonged observation within a clinical decision unit. Hence, identifying all AMI patients in the early stage is the fundamental key to a successful chest pain triage in an emergency department.

FIGURE 1.2: Cardiac magnetometer diagnostic tree. It takes < 3 hours.

Using an MCG scanner allows us to significantly reduce the diagnostic procedure time, to less than 3 hours, Fig.1.2. New diagnostic methods for acute coronary syndromes are required to reduce the risk for patients and save the cost of missed treatments. These are factors that have significant impacts on reducing deaths from coronary artery disease (CAD) and AMIs. Magnetocardiography can be a suitable candidate to improve the evaluation of MI patients, in terms of sensitivity and specificity. Also the portability of the MCG can play an effective role in accelerating the diagnosis.

1.2 Review of Cardiac Magnetometers

1.2.1 Background

For more than a decade, MCG has been used in magnetically shielded rooms and considered mostly of interest for research activity. However, an increasing number of papers have been published indicating magnetocardiography can also be useful to improve diagnostic accuracy. Most recently, the development of standardized instrumentation for unshielded MCG, and its ease of use and reliability, even in emergency rooms, has triggered a new interest from clinicians leading to several new installations of unshielded systems worldwide. In this review, clinical applications of magnetocardiography are summarized, along with the existing medical magnetometers responses to both myocardial diseases and other cardiac conditions, and recent results of other medical magnetometers. There are a number of technologies that can be used to reach this sensitivity including SQUID Magnetometers [8, 9], atomic physics based sensors [10], induction coils [3, 11, 12] and recently, giant magneto-resistance [13].

The first systematic magnetocardiography recordings were performed after the invention of the Superconducting QUantum Interference Device (SQUID) and reported in the early 1970s [12]. Cohen was the first to use a shielded measuring chamber for MCG recordings. The development of the SQUID magnetometer allowed the recording of real-time MCGs [12]. In addition, the development of second-order SQUID gradiometers and low-cost aluminum shielding has allowed MCG recordings to be used in a hospital environment [14–16]. Nevertheless, scientists throughout Europe were unable to reach a consensus, and developed substantial experience with two fundamentally different approaches, MCG recordings in a shielded room [12, 17, 18] and MCG recordings in an unshielded room [19–22].

1.3 MCG Applicabilities in Clinical Environment

The capability of MCG has been studied mainly in the following clinical conditions. The following sections provide an overview of cardiac conditions and MCG responses to them.

1.3.1 Coronary Artery Disease - CAD

Studies have been done to examine the ability of MCG to detect changes in current dipole parameters as well as in spatial and temporal aspects of the QT interval in patients with CAD at rest. The QT interval is the distance between T-wave and Q-wave in a cardiac cycle. QT dispersion values were significantly higher for CAD, differences appear in the total amount of dispersion, degree of QT variability between registration sites, and overall pattern [23]. Hailer et al.[24] enhanced the ability of CAD detection both at rest and under stress for the evaluation of spatial distribution of QT dispersion in MCG compared to ECG. Comparing spatial distribution of QT dispersion between CAD and controls gave a sensitivity of 74% and specificity of 80% [25].

However, another group of MCG studies [26], [27], focused on the ST segment, which is the distance between S-wave and T-wave, at rest, using Current Density Maps, and found that MCG gave a correct classification ratio of 74%. Furthermore, Chaikovsky et al. in 2000 [28] revealed that CAD patients showed 1-3 additional areas of current vectors in $> 1/3$ maps. In 81% there was a correct correlation between location of additional current areas and the stenos-ed vessel. In 2003 Brisinda et al.[29] found MCG mapping abnormality of depolarization, at rest, in 95.2% of CAD patients, with sensitivity of 92.6%, specificity of 92.3% and predictive vale 92.3%. Later on in 2005, Hailer et al.[30] reconstructed current density vector maps every $10ms$ within the ST-T interval using an unshielded system. They were able to identify CAD patients at rest with sensitivity 73.3% and specificity 70.1%. For comparison between patients with and without relevant stenosis, a sensitivity of 62.8% and specificity of 61.3% were found. In addition, Park et al.[31] applied four variables during the ST-T interval (orientation of the positive and negative pole and its movement as well as the ratio between the field strength of the positive and that of the negative pole), an experienced reader had correct identification of 97.8% for CAD patients and 84.8% for those without, for an inexperienced reader these were 92.6% for CAD group and 66.7% for those without. Both were superior to automatic computer analysis. Also Kown et al.[32] applied the 4 parameters that represent directional changes of electrical activity in the R-ST-T interval. Therefore, in their study CAD has been detected with sensitivity of 84.1% and specificity 81.4%.

Lim et al. [33], studied unstable angina pectoris and NSTEMI patients with CAD, using 10 parameters based on the T-wave segment and computing a total score out of 10, which quantifies the number of parameters outside the normal range. Based on the following four current distribution parameters (CDPs): maximum current vector (MCV), total current vector (TCV), current integral map, and current rotation, coronary heart disease (CHD) can be detected with a sensitivity of 85.7% and specificity of 74.3%. However, it is found that current angles at the T-wave peak were most effective for distinguishing electrical current abnormalities in CHD patients [34].

Interestingly, for patients with no indication of ischemia with suspected CAD, sensitivity of 78.1% and NPV 70.4% were higher than that for ECG, whereas specificity of 82.6% and PPV of 87.7% were comparable to patients with no indication of ischemia on ECG, sensitivity was 73.5%, specificity 82.3%, PPV 84.3% and NPV 70.7% [35]. Kandori et al. [36] used a new subtraction MCG method and it showed CAD patients have significant residual ST-T components in a current-arrow map (CAMs), and could be detected with sensitivity 74.6% and specificity 84.1%.

1.3.2 Myocardial Ischemia (Ischaemic Heart Disease - IHD)

Early on, Cohen, et al. [37] revealed changes relating to ischemia not detected by ECG. The TQ baseline elevation and ST depression were found after exercise testing in CAD patients. Ischemic ST depression appeared in the MCG from CAD patients, indicating a greater ST amplitude shift/R amplitude ratio in MCG than that found in ECG [38, 39].

According to Hanninen et al. [39], despite the smaller spatial mapping area of the MCG compared to BSPM, MCG was capable of detecting reciprocal ischemia-induced changes in the ST-segment and T-wave parameters. It was able to detect exercise-induced myocardial ischemia caused by stenosis in any of the main coronary arteries, regardless of presence or absence of a remote infarction. ST-segment parameters and T-wave amplitude, performed equally well in ischemia detection. In non-MI patients, ST elevation and increase in ST slope performed best. In post-MI patients, decrease in ST slope and in T-wave amplitude were best. The optimal

locations for ischemia-induced ST depression, decrease in ST slope, decrease in T-wave amplitude and decrease in ST-T integral area were over the middle inferior thorax and abdomen. Moreover, information on physiological stages of ischemia development and resolution can be found in the ST-segment and T-wave upon exercise testing.

Also, transient acute myocardial ischemia is well-recognized in MCG. In addition, the localization of Myocardial Ischemia by MCG has been successfully attempted using a current density reconstruction method [40]. Tavarozzi et al.[41] added that transient acute myocardial ischemia causes easily recognizable changes in the MCG on the ST segment and the T-wave. To determine these changes, the orientation of the maximum spatial gradient of the MF was used. MCG abnormalities during the re-polarization phase were detected in all patients with severe coronary lesions in vector arrow maps and iso-integral maps .

Interestingly, MCG parameters from ST interval and T-wave in IHD patients at rest were found to be sensitive markers for myocardial ischemia [31, 42–45].

Another study [46] used Machine Learning as their diagnostic tool. Machine learning for diagnosing ischemia teaches a computer to learn patterns of MF maps and to differentiate between healthy and IHD patients, Direct Kernel based Self-Organizing Maps (DK-SOMs) were used for unsupervised learning and Direct Kernel Partial Least Squares (DK-PLS) and (Direct) Kernel Ridge Regression for supervised learning.

Hanninen et al.[47] also found it is possible to differentiate between different stenosed vessel regions, with T-wave and ST segments giving equal capability. Optimal locations for detection of exercise-induced ischemia depend strongly on ischemic regions.

In a study with 13 parameters [48], the most successful in separating ischemic patients from controls was RSI (Re-polarization stabilization interval) measured post-exercise, with post-exercise ST- T integrals in both channels and the T-wave amplitude over the upper left thorax also performing well. The best parameters at rest were; T-wave amplitude, ST slope and ST-T integral in the channel over the upper left thorax.

For the detection of re-polarization abnormalities, 7 parameters around the peak of the T-wave were used (pre-peak T-wave mean frontal angle, trajectory, angle

deviation; post-peak T-wave mean frontal angle, trajectory, angle deviation; and difference in mean frontal angle between pre- and post-peak T-wave). It was found that the MCG effective magnetic dipole vector score had the strongest relationship with an ischemic outcomes when compared with ECG and stepwise logistic regression analysis [42].

1.4 Current Medical Magnetometers

Despite the ease of use of MCG, explained in the previous sections, the spread of MCG in the clinical environment has been relatively slow, thus in this section I give an overview of promising current MCG devices. Magnetocardiography (MCG) is a noninvasive technique to detect the magnetic fields of the heart generated by the same bio-electric currents as the ECG.

The first MCG from a human was recorded in 1963 [3]. Unlike electric fields, magnetic fields do not suffer badly from varying attenuation as they pass through the different tissue types. Therefore, MCG is more sensitive to tangential currents [49], while the chest leads of ECG are more sensitive to radial currents with respect to chest. Moreover, the magnetic field is a direct measurement of the field rather than a measurement of the potential difference, meaning MCGs could provide important diagnostic information, such as better spacial resolution. Since MCG may show pathological deviations from the normal depolarization and re-polarization in a different manner to that of ECG, application of MCG to ischemia research is of interest.

1.4.1 Superconducting Quantum Interference Device

Nowadays, superconducting quantum interference devices (SQUID) are the most common magnetometer detectors for weak magnetic fields [1]. They are sensitive to fields as small as a few fT and have been used in cardiac magnetometers for several decades [33, 36, 50, 51]. The development of SQUID magnetometers has resulted in the recording of real-time MCGs [12]. Currently, MCG is used mainly as a research tool, and most MCG studies so far have focused on arrhythmia risk assessment [15]. Highly sensitive magnetometers are required that have to be capable of discriminating between very small fields with remarkable accuracy.

There are, however, some limitations of SQUIDs, such as the requirement of a cryostat and high levels of shielding or low frequency DC background subtraction. Hence, their overall cost tends to be very high ($> £1m$). Although SQUIDS can produce high resolution medical images, the cost and immovability, hesitated the interest of medical societies. Therefore, it is not yet being used or known as a medical diagnostic device, Fig.1.3.

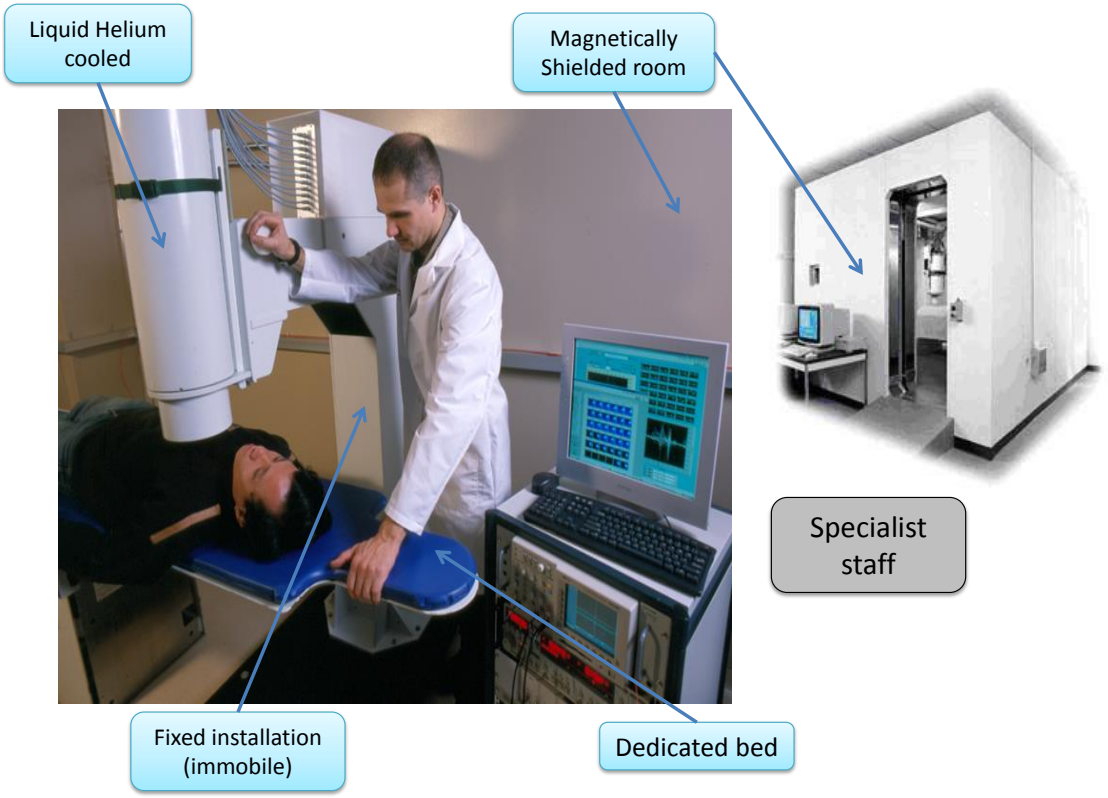

FIGURE 1.3: The figure shows SQUID device that is used in a shielded environment. It requires specialist staff and a dedicated bed.

1.4.2 Atomic Physics and Induction Coil Magnetometers

There are two other approaches that have been used for MCG very successfully, atomic physics packages [1] and induction coil magnetometers [37]. A feature that both atomic physics magnetometers and SQUID sensors share is that they are both sensitive to DC magnetic field levels, making them equally sensitive to very low frequency changes in the local environment (e.g. the movement of cars and equipment in the general location can have a measurable impact on performance). Typically, therefore, both SQUID sensors and atomic physics sensors require extensive shielding from the background field.

On the other hand, induction coil magnetometers are inexpensive, relatively easy to manufacture and can be put to a wide range of applications and have no DC sensitivity. They have been shown to have an excellent signal detection noise floor and are capable of reaching a noise performance of 50 $fT/\sqrt{Hz}$ for signals of 1 kHz [52]. It seems reasonable to replace SQUID sensors with induction coil sensors in MCG devices, in order to create an inexpensive and portable device that can do away with the need for DC field shielding. However, despite the apparent benefits of an induction coil magnetometer, to match the sensitivity of other sensors, they need to be both bigger and heavier, they have a frequency dependent response and their sensitivity is typically somewhat lower than a SQUID (typically >0.1 pT). Hence, they were effectively abandoned as MCG sensors soon after the development of the field in the 60's.

1.4.3 Induction Coil Magnetometer

The field started when Baule and McFee [3] noticed that a differential inductive magnetometer (two coils with the opposite orientation wired in series to reduce common mode noise) was capable of detecting the magnetic field created by electrical excitation of the heart, Fig.1.4. The coils used for this measurement were 30 cm long, 9 cm in diameter ferrite 'dumbbell' cores with 2×10^6 windings. Although it was successful, this coil setup was impractically large as a device and was not suitable for medical imaging, primarily because the sensitive area of the coil was too large and the resulting position resolution would have been very low. Cohen et al.[53] subsequently used a shielded room to reduce background field fluctuations reducing the need for a differential probe and reducing the complexity of the apparatus to a single 8 cm in diameter, 5 cm long coil with 200,000 turns of wire. However, although a single coil was in principle sensitive enough to see a signal, in practice two coils were stacked in series on a ferrite rod making a coil of 400,000 turns and 10 cm long making this still an impractical device for mapping the field of the heart both in terms of size and weight.

Induction coil magnetometers have continued to be developed for biomagnetic field sensing applications [52, 54], using coils of 20 cm in diameter and 10 cm in height with an optimized (shaped) cross section and a 300 mm long, 18 mm wide coil with a laminated ferrite core respectively. Although both achieved a low background noise level, each of these is impractical as an MCG sensor either due to the width,

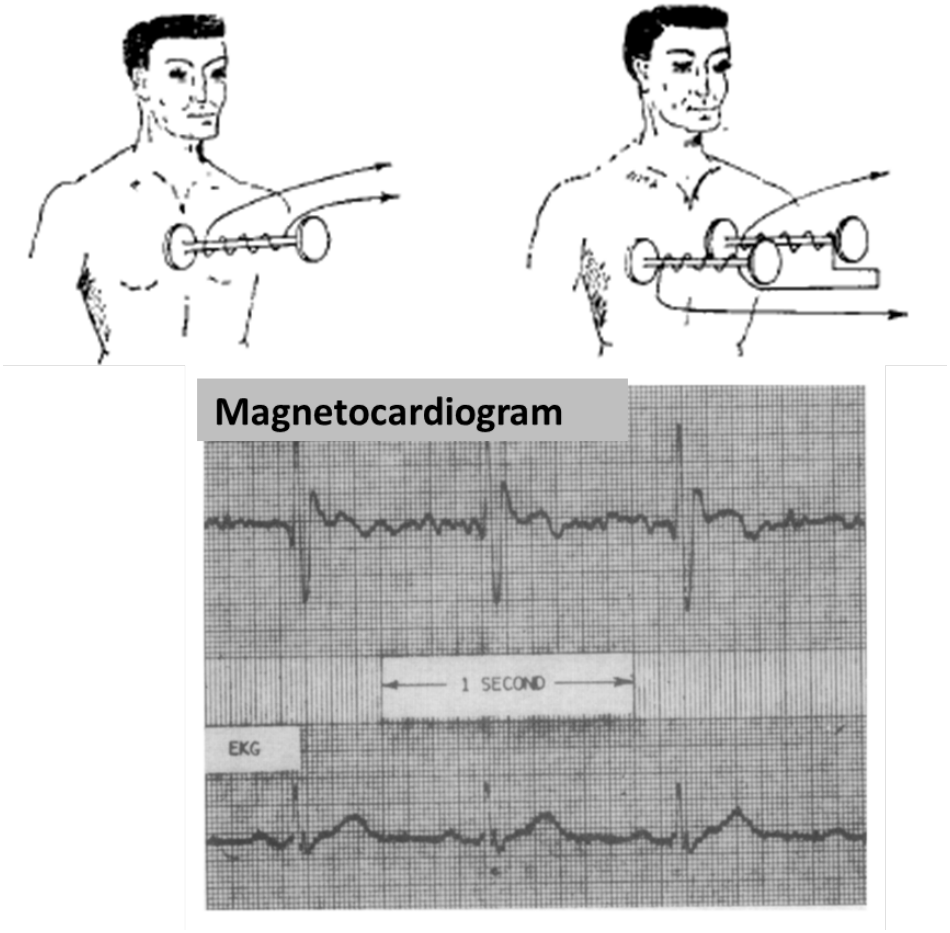

FIGURE 1.4: Magnetocardiograph pick up coils. Diagram taken from [3].

which limits the resolution, or the length, which limits the strength of the field due to field dispersion.

The properties of SQUID sensors include their excellent noise floor and gradiometry (used to remove global noise affecting both coils while maintaining signal applied to a single coil) is easily achieved with simple coil configurations. On the other hand induction coil gradiometers are bulky, producing matching coils is difficult and they have a typical noise floor of $>0.1\ pT/\sqrt{Hz}$ at 10 Hz.

1.5 Thesis Outline

The current research explains the importance of a novel magnetocardiography, using inductive coils as a medical magnetometer to detect cardiac conditions. In

addition to these, the aim of the current research is to develop a low cost alternative to current devices with the aim of potentially expanding the clinical utility.

The beginning of this chapter detailed the concept and motivation for this research. Also, a literature review of several cardiac conditions that have been diagnosed by MCG and the existing medical magnetometers are outlined. In the next chapter cardiac electro physiology and our recent systematic review about MCG for the ruling out of NSTEMI in patients with chest pain that play a part in this research, are presented. This will build up our base knowledge of fundamental heart electro physiology activities and the capabilities of magnetocardiography.

From the general interactions we move to Chapter 3, where the details of the key features of the newly built magnetometer present in this experimental system, are outlined. The most important of these are the design and method (discussed in section 3.3). It will detect very small magnetic fields. In this section the noise correlation and setting arrays are discussed. Chapter 4 explains the study protocol detailing the clinical research procedures, which have been done in Leeds General Infirmary. Prior to the main study (clinical test), which will be explained in chapter 6, chapter 5 defines several tests and outlines the accuracy of the MCG in different circumstances. Chapter 6 is related directly to the apparatus, and results obtained during the course of this research from Leeds General Infirmary (LGI). The apparatus used is mentioned in Chapter 3. However, Chapter 6 outlines not only the capability of the MCG but also an explanation of how to distinguish healthy subjects from abnormals, with 98.15% and 30.61%, sensitivity and specificity, respectively.

The conclusions and future work are described in the last chapter which ends this thesis. This chapter closes with a conclusion on distinguishing between healthies and patients with ischemic heart disease along with the future prospects of the experiment. A series of appendices are included at the end to give further details of aspects of importance that were omitted from the main text to maintain the flow.

We have developed a new device at the University of Leeds that is both smaller and cheaper, operates at room temperature, and is capable of operating in an ordinary clinical environment whilst still giving the same information as larger and more expensive commercial devices.

Chapter 2

Diagnosis of Cardiac Conditions - Myocardial Infarction

The goal of this chapter is to provide the current research design. We start by briefly reviewing cardiac physiology, in particular, action potential (AP) performance [1, 55], is described in section 2.2. We then focus on cardiac ischemia and evaluate MI patients. Finally, in the last section of the chapter, we present our recent systematic review that detailed how MCG is able to rule-out NSTEMI patients with chest pain.

2.1 Cardiac Electro-physiological Activities

The electric currents flowing in the muscle tissue of the heart (myocardium) can generate a weak magnetic field. The currents are carried by ions in the myocardium, evoking the electro-physiological processes that activate the mechanical contraction of the heart. In principle, these electrical currents are measurable by an electrocardiogram at the surface of the body.

The cardiac tissue consists of muscle cells that are about 100 μm long with a diameter of about 15 μm [56]. As can be seen in Fig.2.1 the cells sit together with discs inserted between them. Each cell consists of a membrane separating the inner volume of the cell from the surrounding intracellular liquid [1, 55]. The outer membrane provides a barrier of cells and the surrounding intracellular liquid. Although the membrane is highly permeable to water and some other molecules,

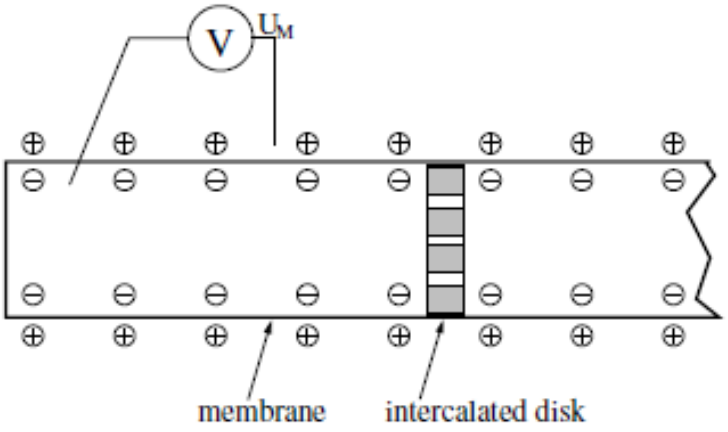

FIGURE 2.1: Schematic diagram of the myocardial cell. The outer bound of the cell is formed by the membrane. The ions can penetrate the disk that separate the individual cells. Diagram taken from [1].

it is impermeable to charged particles and ions. The following ions are known to be the key physiologically significant ions: Na^+, K^+, CL^- and Ca^{2+} [1]. The exchange of these ions between the inner cell and the surrounding volume controls the electro-physiology of the muscles and nerves. Ion channels control their flow of movement through the membrane by acting as gating proteins. These gating proteins control the permeability of the membrane and actively pump Na^+ out of the cell and K^+ into it, using physiological energy [1, 55]. The fluctuations of the ion concentration across the membrane result in a trans-membrane potential (Um), which is produced by a voltage difference across the membrane. As the capacitance of the membrane is very small (approximately $1\mu F/cm^2$), any minor difference is therefore measurable. At rest Um it is almost -70 mV. When the cell is electrically stimulated so that Um increases over the threshold potential, the ion channels open, in the case of Na^+ allowing the ions to flow into the cell, which raises Um towards zero. This process is referred to as depolarization and travels as a wave through the muscle cell. To explain more clearly what these steps are going to be, I define cardiac action potentials in the following section.

2.2 Cardiac Action Potentials

In the right atrium of the heart there is a group of cells called the sinoatrial (SA) node where the cardiac action potential originates. The action potential

sequence is essential for neural communication. A nerve cell goes through steps of depolarization from its rest state followed by re-polarization back to that rest state. There are a variety of types of ionic channels in cardiac muscle that play active roles in the action potential mechanism. Furthermore, different locations in the heart produce different action potentials [57]. We will consider the action potential of ventricular myocytes. The ventricles are usually the last part of the heart to undergo an action potential during each cardiac cycle which is described as 'classical' cardiac action potential in almost all textbooks. The most important ionic channels that can be taken into account in the production of action potentials are the voltage-gated Na^+ and K^+ channels. There is a rapid change within the purkinji fibre system that results in the initiation of depolarization of the ventricular myocytes which takes 30 to 40 ms and is recorded as the QRS complex in the electrocardiogram [57]. Action potentials serve to stimulate the excitatory and conductive muscle fibres of the heart to induce contractions. They begin with sharp changes in membrane potential, usually from resting level between -70 mV and -90 mV, then becoming positive 30 mV to 40 mV.

2.2.1 Action Potential Performance (AP)

The action potentials have several sequences that can be subdivided into different phases and these phases will be explained. Fig.2.2 illustrates the simplified time profile of an AP generated by ventricular cardiac myocytes.

- Provided the Na^+ channels open sufficiently, the interior potential changes from -70 mV rest potential to -55 mV. This rest depolarization is electrically as well as magnetically detectable as the P-wave. Leaving K^+ rectifier channels keep the trans-membrane potential (TMP) stable at -90 mV.
- The fast Na^+ channels flow into the interior cell of the membrane. TMP approaches -70 mV, the threshold potential in cardiomyocytes is the point at which enough fast Na^+ channels have opened to generate a self-sustaining inward Na^+ current. The increase Na^+ current rapidly depolarizes the TMP to slightly above 0 mV. Fast Na+ channels are time-dependent.
- If both Na^+ and K^+ channels open, the process becomes neutral and prevents the creation of action potential. Hence, the Na^+ channels close and the K^+ channels open briefly and an outward flow of K^+ returns the TMP

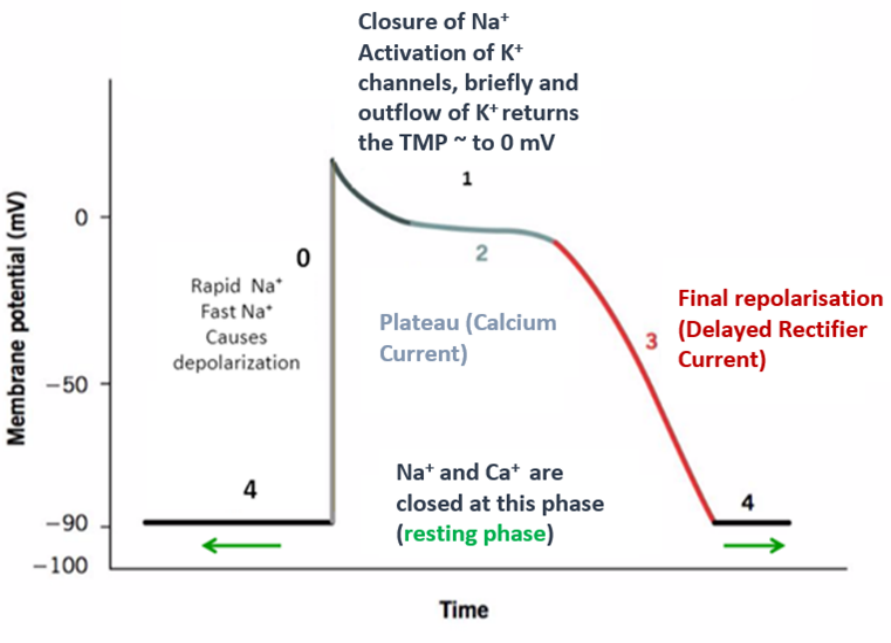

FIGURE 2.2: The figure shows the sequences in a classic cardiac action potential subdivided into to five steps.

to approximately 0 mV. In this step there is sufficient time to complete the depolarization as the current open channels move much slower. Therefore, with the K^+ channels the membrane starts to re-polarize.

- Next is a period of time in which the membrane potential remains relatively constant, as there is long AP duration in cardiac cells. This is caused by a balance between the inward Ca^2+ current through L-type calcium channels that becomes significant in the excitation-contraction coupling process described below, and the outward K^+ channels that are known as the delayed rectifier k^+ channels. These two counter currents are electrically balanced, and the TMP is maintained at a plateau just below 0 mV throughout phase 2.

- Prior to the last sequence, it is vital in the transmission of information that hyper-polarization (so called as its rest potential is about -90 mV) occurs. It prevents any other stimulus within the neuron and raises the threshold for any new stimulus. In other words, hyper-polarization is responsible for the signal proceeding in only one direction. Thereafter, the $Na^{\pm}$ and $K^{\pm}$ pump eventually returns the membrane back to its resting state of -70 mV. The final re-polarization phase (Delayed Rectifier Current) is caused by the

outward current overcoming the inward current, $\uparrow Ca^{2+}$ and $\downarrow K^{+}$, respectively.

The complete set of action potential effects can only produce a very weak biomagnetic field. The heart's magnetic field ranges from approximately a hundred picotesla to femtotesla, making them hard to measure, when compared to the magnetic noise produced by environmental sources.

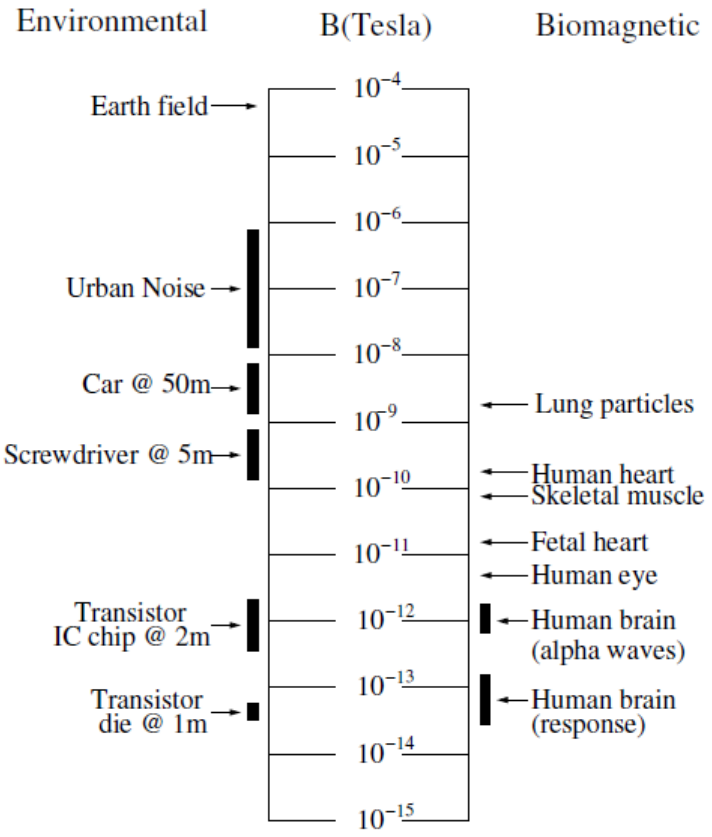

FIGURE 2.3: The diagram shows the scale of different magnetic fields, biological and environmental. Diagram adapted from [58] .

Fig.2.3 shows the relative strengths of the main biomagnetic fields as well as source environmental fields. Therefore, when the measurement of the heart 's magnetic field is taken, the noise sources have to be considered during the measurements.

2.3 Action Potential Delays Versus ECG

To study the delay caused by calcium channels, we used a non contact ECG, which uses the same detection electronics as the MCG signal, so that any phase delay is identical on both signals. The graph comparing integrated non contact ECG with MCG signals, shows that the MCG is in advance of the ECG signal, Fig.2.4.

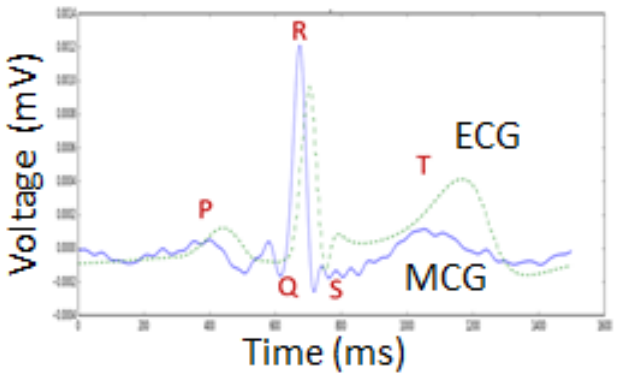

FIGURE 2.4: The morphological features within the MCG show marked similarity to those of the ECG, such as a P wave, QRS complex, and a T wave.

Through use of a new inductive magnetocardiogram design we have been able to accurately measure the phase between MCG and ECG signals, which is about 21 ms. We have also found that in all cases the MCG signal occurs in advance of the ECG. This suggests the QRS region of the MCG signal is produced from the Na^+ influx during myocyte action potential. This may coincide with the cardiac action potential, Fig.2.5.

2.3.1 Action Potentials Response to Cardiac Ischemia

Myocardial ischemia occurs when blood flow in the heart muscle is decreased by a partial or complete blockage of the coronary arteries. The decrease in blood flow reduces the heart's oxygen supply which can damage the heart muscle, reducing its efficiency which may result in a heart attack. There is a dramatic reduction in the levels of adenosine triphosphate (ATP) if ischemia is prolonged [59]. Myocardial ischemia induces changes in the electrophysiological properties of the myocardium, resulting in a decrease in resting membrane potential and conduction velocity, with a dispersion of the activation wavefront. During ischemia the intracellular Na^+

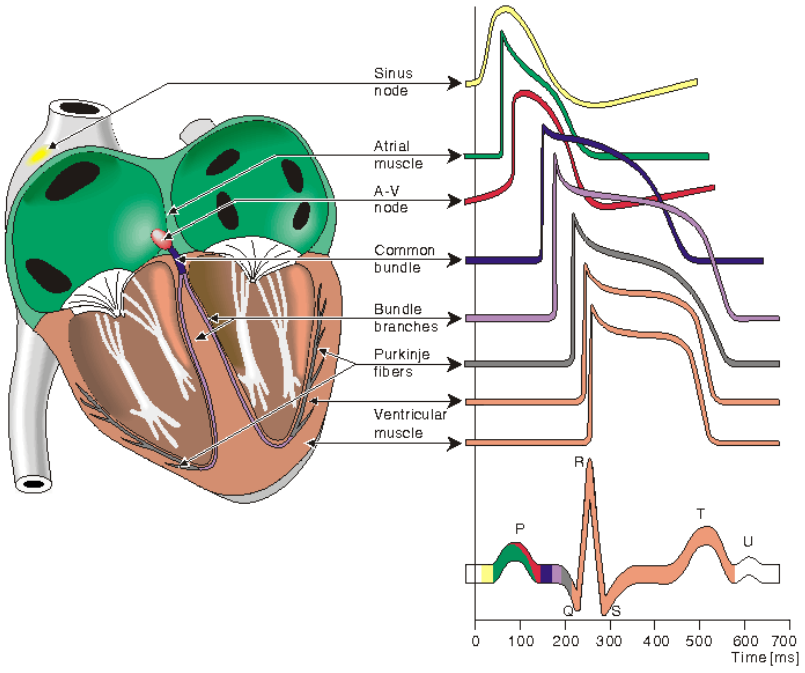

FIGURE 2.5: Electrophysiology of the heart and the different waveforms for each of the specialized cells. The latency stage shown approximates that normally found in the healthy heart. Diagram was taken from http://www.bem.fi/book/06/06.htm.

increases. This procedure causes a reduction in active outward pumping and an increased inward leak through the Na^+/H^+ exchanger [59]. In this situation the ion concentrations of cardiac myocytes (cardiac muscle cells) change. Extracellular potassium associations increase due to the following factors:

- An outflow of potassium due to the ATP-dependent K^+ channel activation [60],
- A reduction in K^+ influx resulting from a deduction in $Na^+ - K^+$ pump activity [61],
- A reduction in extracellular space because of the rise in osmotically active particles inside the cell [62].

While cardiac ischemia happens, the intracellular calcium tends to rise gradually. There are several factors that can be taken into account, as follows [59]:

- Less effective removal to the extracellular space
- A reduction in the sarcoplasmic reticulum (SR) uptake
- An increased inward leak
- Displacement by protons from binding sites

Increased Ca^{2+} overload can cause the spontaneous release of Ca^{2+}. The result can be Early After Depolarizations (EAD) and/or Delayed After Depolarizations (DAD) [59]. Acute ischemia results in a depolarization from the normal resting membrane potential, producing a transient increase in excitability. Depending on the extent of further depolarization, fast Na^{+} current is either partially or completely inhibited. These changes in ion concentrations seem to be a major factor behind changes in AP morphology. After almost all acute ischemia the action potential morphological features recover during re-perfusion. Nevertheless, there is still a chance that action potential morphological features remain at their abnormality during re-perfusion, due to oxygen radical stress [63]. The amount of departed oxygen in the system is consumed by oxidative phosphorylation. Phosphocreatine (PCr) are demolished to keep a steady production of ATP, which is the factor for the body's principal source of energy. However, they can be fully consumed with prolonged ischemia. As a result of the consumption of ATP and the inability of the tissues to regulate metabolic waste accumulation, the inorganic phosphate (Pi) levels increase. To keep the ATP at reasonable levels, glycolysis which is produced from the Anaerobic metabolism, is initiated. But it is only able to maintain ATP levels for a short time due to limited ATP production efficiency and the buildup of lactic acid and hydrogen ions.

2.4 QT Dispersion in Patients With Myocardial Infarction

QT dispersion, defined as maximum QT interval minus minimum QT interval, was originally proposed as an index of the spatial dispersion of ventricular recovery times. In reality, QT dispersion is an approximate measure of a general abnormality of re-polarization [64, 65].

Attempts to characterize and quantify the inhomogeneity of ventricular re-polarization from the magnetocardiogram using mathematical methods, such as principal function analysis of the T wave, can be traced back to 1996 [66]. In clinical practice, however, the ECG assessment of ventricular re-polarization has been limited to the measurement of the QT interval and its heart rate-corrected value (QTc) and to the description of the ST-T morphology, often using vague terms such as "non-specific ST-T wave changes."

So far many different parameters have been defined as MCG interpreter data, based primarily on signal morphology, source parameters, time intervals or magnetic field map analysis. Main work on signal morphology concentrates on ST-depression, ST-T signal amplitude [39] as well as QRS and ST-T integrals. With respect to time intervals most studies focus on QT interval. By considering QT dispersion in MCG, as it reflects regional heterogeneity of re-polarization, the ability of the identification of CAD patients can improve [24].

In one approach magnetic field orientation, defined as the angle between the line joining the centres of gravity of the positive and negative field components and the right-left line of the torso, was calculated during the QT interval at rest. These values separated ischemic patients with normal or abnormal ECG from the control group in this study. Abnormal MFM patterns were firmly related to severe stenosis in patients with coronary artery disease. It is found that the re-polarization period is strongly related to coronary artery disease [44, 67, 68].

According to Lim et al. [69] most patient dipoles in the MFMs were compressed, stretched, broken, or rotated poles. In contrast, the MFM patterns of the controls were consistently normal and completely identical, Fig.2.6. Abnormal shapes (the position and shapes of poles) supported the idea that cardiac conductivity changes during ischemia [70] and the MFM rotation at the T wave are due to ischemia [71].

During our study, we identified several MCG parameters that enabled us to approach these results. In order to determine which were the most effective, we started to write a systematic review in NSTEMI patients with chest pain that will be described in the next section.

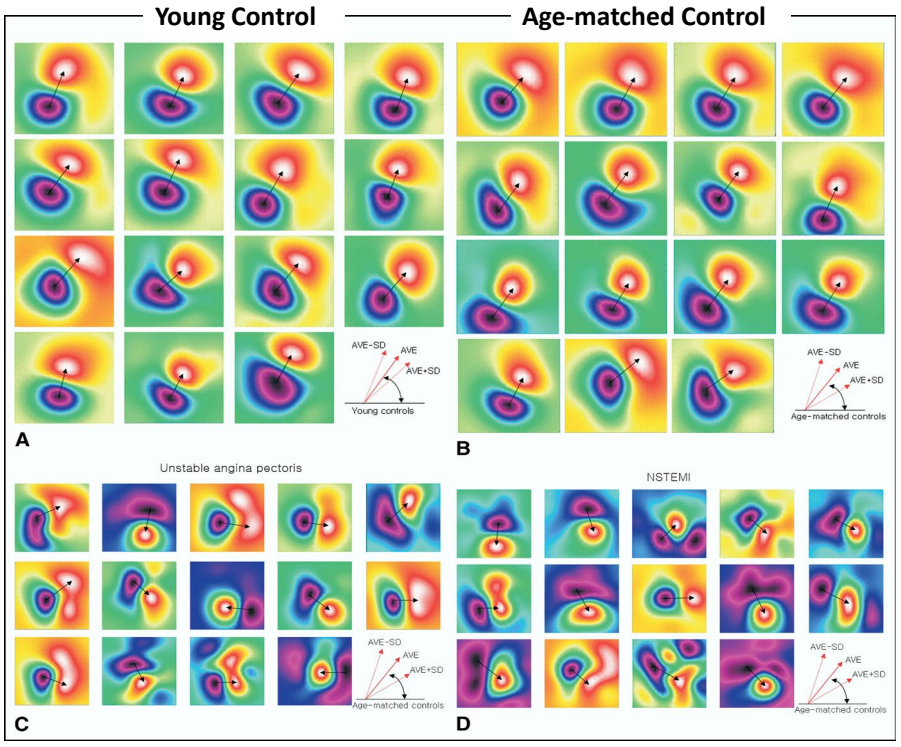

FIGURE 2.6: MFMs at T-wave peak on the basis of the total scores of 10 parameters. Maps were plotted on the basis of the scores from YCs (A), AMCs (B), patients with UAP (C), and patients with NSTEMIs (D). Arrows on each map are shown for clarity [69].

2.5 Systematic Review MCG for the Rule-out of Non ST Elevation MI in Patients With Chest Pain

The problem of distinguishing an acute coronary syndrome (ACS) from the variety of other cardiac and non-cardiac causes of chest pain is a challenging one. In the UK every year, just over half the total number of patients with chest pain, who visit the accident and emergency (A&E) department, do not exhibit clear evidence of ST elevation myocardial infarction (MI), based on ECG [4],[72]. These patients are classified as Non-ST elevation MI (NSTEMI). Common diagnostic tools such as 12-lead electrocardiogram (ECG) and cardiac troponin, although highly specific, are either inconclusive or very insensitive in the first few hours following the onset of symptoms. As a result, the majority of patients will have a normal or inconclusive result necessitating further evaluation and testing to achieve an accurate diagnosis.

The assessment and safe disposition of these patients are a significant challenge as a missed NSTEMI can result in major adverse outcomes, including the risk of death [73]. Data obtained using multichannel MCGs provide an alternative diagnostic tool to the conventional ECG. Several recent studies reported promising sensitivity and specificity values for MCG in identifying patients with ACS. This raises the question of whether MCG could be useful for the early triage of patients with acute chest pain. In this paper, we perform a systematic review and meta-analysis to evaluate the diagnostic efficacy of MCG for the rule-out of NSTEMI in patients with chest pain.

2.5.1 Search Methodology

Our search included studies published in English language, from 1963 onwards, restricted to adult humans. We searched the following electronic databases, MEDLINE, Cochrane DSR, ACP journal DARE, CCTR, CRDTAS, CMR, HTA and NHSEED, web of science, CINAHL and the Cochrane Central Register of Controlled Trials. We also searched the following physics related electronic databases; ArXiv.org, Engineering Village, SciFinder, Scopus, ADS and the Technology research database. Search terms were structured following the PICO convention, for a variety of relevant keywords under following definitions:

Population: IHD, CAD, ACS, MI, STEMI, NSTEMI, Angina, Stable Angina etc. **Intervention**: MCG, SQUID, MFM etc. **Comparator**: CA, ECG, Troponin etc. **Outcomes**: Performance Evaluation, Sensitivity, Specificity etc. The search was Population AND Intervention AND Outcome.

2.6 Selection Criteria

Our selection strategy consisted of three-stages. First, titles and abstracts identified in our search were screened by one reviewer. A minimum of 10% was reviewed independently by a second reviewer. Second, all articles meeting inclusion criteria underwent full-text review. Again, a minimum 10% was reviewed independently by a second reviewer. Studies were included if they evaluated either patients with MI or patients presenting initially with chest pain and subsequently diagnosed

with MI. Furthermore, we included studies that reported the diagnostic performance of MCG (e.g. sensitivity, specificity, NPV, PPV, PLR, NLP). Finally, the reference list of the included papers was checked for completeness.

2.7 Quality Assessment

Two independent reviewers (myself and Abbas-Alshimary) assessed the quality of the included papers, using the Quality Assessment of Diagnostic Accuracy Studies (QUADAS 2) tool [74]. This tool is recommended for use in systematic review to evaluate the risk of bias and applicability of primary diagnostic accuracy studies. QUADAS 2 consists of four domains: patient selection, index test, reference standard, flow and timing and it is applied in four phases: summarise the review question, tailor the tool to the review and produce review-specific guidance, construct a flow diagram for the primary study and assess risk of bias and concerns regarding applicability. For each study, the risk of bias was evaluated according to the quality assessment tool shown in Table B.1 in Appendix B. Furthermore, applicability concerns were considered for each study. Studies are considered to be of high standard if they have a low risk of bias and low applicability concerns.

2.8 Data Extraction

Data were extracted from the selected review papers using a standardized data extraction tool (separate from the quality assessment tool). The extracted data included specific details about the interventions, populations, study methods and outcomes of significance to the review question and specific objectives. The year and country of origin was recorded. The primary variables of interest were sensitivity and specificity as well as negative and positive predictive values.

2.9 Quantitative Data Analysis

Meta-analyses of sensitivity and specificity for the data was performed by Abbas Al-shimary and Charlotte Kelly. Where possible, we examined sources of significant homogeneity, using various study level covariates. We also evaluated the

pooled sensitivity and specificity values across the 40 studies. We used Stata, which is a complete, integrated and Bayesian analysis and statistical software package. It's capabilities include data management, statistical analysis, graphics, simulations, regression, and custom programming. Moreover, we used MetaDAS is a SAS (Statistical Analysis Software) macro developed to automate the fitting of bivariate and HSROC models for meta analysis of diagnostic accuracy studies. This procedure fits nonlinear and generalized linear mixed models using likelihood based methods and the MetaDAS macro v1.3 [75], to fit the HSROC model to the data. The HSROC curve graphs the sensitivity (or true positive rate) against $(1 - specificity)$ (or false positive rate). Each point on the curve represents a different study. The area under the curve (AUC) is also an indicator of the overall performance or accuracy of the test. Overall test accuracy is indicated by the closeness of the graph to the top left corner or equivalently an AUC close to unity. It is a function for joint meta-analysis of sensitivity and specificity of a diagnostic test. HSROC is a function that can be used to predict the parameters of a hierarchical summary receiver operating characteristic (HSROC) model allowing for the reference standard to be possibly imperfect, assuming it is conditionally independent from the test under evaluation. Stata is a complete, integrated and Bayesian analysis and statistical software package. Its capabilities include data management, statistical analysis, graphics, simulations, regression, and custom programming. MetaDAS is a SAS (Statistical Analysis Software) macro developed to automate the fitting of bivariate and HSROC models for meta analysis of diagnostic accuracy studies. This procedure fits nonlinear and generalized linear mixed models using likelihood based methods.

2.10 Study Selection

Our literature search yielded 3684 articles. Screening of titles and abstracts yielded 196 articles. Full text screening yielded 40 articles that met our inclusion criteria. These results are summarized in the PRISMA flow diagram in Fig.2.7.

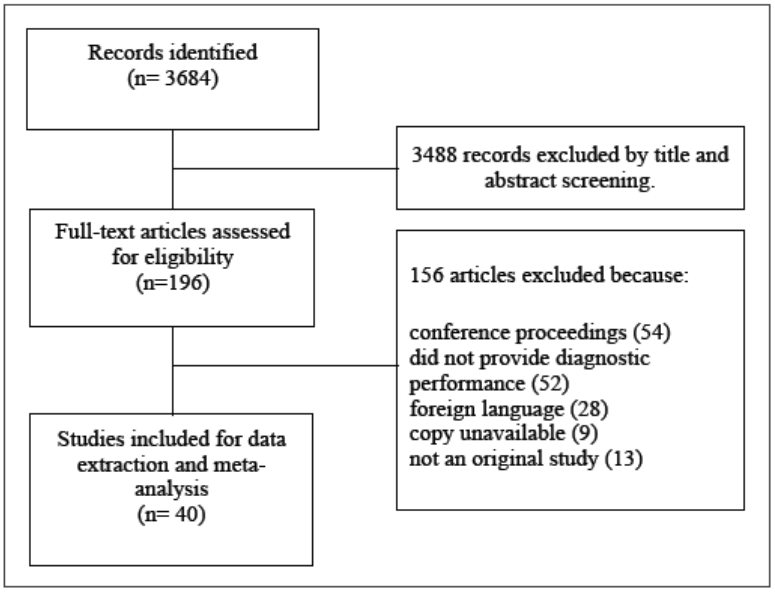

FIGURE 2.7: Flow diagram for selection of included studies.

2.11 Study Characteristics

We extracted the study characteristics for all the 40 studies, these are shown in Table B.2 in the Appendix. In more than half of these studies, 22, the included patients had stable IHD or CAD. Most of these patients had coronary angiograms (the golden reference standard) with documented epicardial coronary artery stenosis greater than 50-75%. In 12 studies, patients presented with acute chest pain and subsequently diagnosed with MI (STEMI, NSTEMI and unstable angina). The studies were conducted using unshielded rooms in 10 studies and magnetically shielded rooms in 26 studies. Ten studies used an MCG device with less than nine channels and 21 studies used more than nine channels. Of particular interest are those studies that considered NSTEMI patients. Out of the total 40 included studies, nine considered NSTEMI patients [31, 35, 44, 69, 76–80], study characteristics of these studies are listed in Table 2.1. Four out of these nine studies, namely [35, 69, 77], and [79], fit our study model, i.e. they consider patients presenting with chest pain without ST-segment elevation, which were subsequently diagnosed.

Author (Year)	Study Design	Test	Control	Room (#channels)
Goering, 2009	Case-control	Patients who suffered MI more than 28 days earlier with angographically proven stenosis > 70% stenosis (108)	Heathly subjects (70)	Shielded (31)
Kwon, 2010	Case-control	Patients admitted to hospital with suspected ACS diagnosed CAD with angiographically proven > 50% stenosis of a vessel (237)	Patients with angiographically proven nonobstructive CAD (127)	Shielded (64)
Leithauser, 2013	Registry study	Parients with CAD and BBB chosen from patients with ACS and NSTEMI angiographically proven > 50% stenosis (46)	Patients with ACS and BBB angiographically proven nonobstructive CAD (16)	Unshielded (Not specified)
Lim, 2009	Case-control	Patients with unstable angina pectoris and NSTEMI patients (193)	Young subjects with normal ECG and no history of heart diseas, Age-matched controls admitted to hospital for chest pain, normal clinical results (203)	Shielded (64)
Park, 2005	Registry study	Patients presenting with chest pain diagnosed as CAD with ECG, troponin elevation, echocardiography or coronary angiography (143)	Subjects with normal ECG, troponins or coronary evaluation presenting with chest pain (42)	Unshielded (Not specified)
Park, 2004	Case-control	Patients with symptoms of unstable angina, who were diagnosed with CHD angographically (53)	Patients with normal troponin levels in whom CHD could be ruled out (33)	Unshielded (13)
Lim, 2007	Case-control	NSTEMI patients (83)	Subjects presenting with chest pain but there was no clinical evidence to indicate MI (57)	Shielded (64)
Muller, 1999	Case-control	Patients with CHD and history of sustained VT and angiographically proven stenosis > 75% in at least one vessel (43)	Post MI patients without arrhythmic event (42)	Shielded (49)
Lin, 2011	Registry study	Patients with suspected ACS with STEMI (144)	Patienst with NSTEMI (143)	Shielded (Not specified)

TABLE 2.1: Study characteristics of 40 studies with NSTEMI patients.

2.12 Study Quality Assessment

The outcome of applying the study quality assessment tool to the papers reviewed is shown in Table 2.2. The reasons for withdrawal were not explained in six studies [30, 31, 78, 81–83]. Three studies, [69, 84, 85] showed risk of bias in more than one domain. Remarkably, half of the studies did not specify the amount of delay between the reference and index tests.

Domain	Patient Selection		Index Test		Reference Standard		Flow And Timing	
Patient	Risk of Bias?	Applicability Concerns?	Risk of Bias?	Applicability Concerns?	Risk of Bias?	Applicability Concerns?	Accepetable Delay?	Withdrawals Explained?
Brisinda, 2003	-	+	+	+	+	+	?	+
Chen,2014	+	+	?	+	+	+	?	+
Endt, 2000	+	+	+	+	+	+	+	+
Fenici, 2004	?	+	+	+	?	+	+	+
Fenici, 2005	+	+	+	+	+	+	?	+
Gapelyuk, 2007	+	+	+	+	+	+	+	+
Gapelyuk, 2010	+	+	+	+	?	+	+	+
Godde, 2001	+	+	-	?	?	?	?	+
Goering, 2009	-	+	?	+	+	+	?	-
Hailer, 2005	+	+	+	+	+	+	+	-
Hren, 1999	+	+	+	+	+	+	?	+
Kandori, 2010	+	+	?	?	?	-	?	+
Kanzaki, 2003	-	-	+	+	?	+	+	+
Karvonen, 2002	+	+	+	+	+	+	?	+
Korhonen, 2000	?	+	+	+	+	+	?	+
Korhonen, 2001	?	+	-	+	-	?	?	+
Kwon, 2010	+	+	+	+	+	+	?	+
Kwon,2006	+	+	+	+	+	+	?	+
Leeuwen	+	+	?	+	+	+	?	+
Leithauser, 2013	?	+	+	+	+	+	?	+
Lim, 2007	+	+	+	+	+	+	+	+
Lim, 2009	+	+	-	+	-	+	+	+
Lin, 2011	+	+	+	+	+	+	+	+
Makijarvi, 1993	+	?	+	+	+	+	+	+
Muller, 1999	+	+	+	+	+	+	?	+
Ogata, 2009	+	+	+	+	?	+	+	+
On, 2007	+	+	+	+	+	+	+	+
Park, 2004	+	+	+	+	+	+	-	+
Park, 2005	+	+	+	+	+	+	+	-
Park, 2008	+	+	+	+	+	+	+	+
Park, 2015	+	+	+	+	+	+	+	-
Steinberg, 2005	+	+	+	+	+	+	+	-
Tantimongcolwat, 2008	+	+	-	-	-	-	?	+
Tolstrup, 2006	+	+	+	+	+	+	+	?
Van Leeuwen, 2003	+	+	?	?	+	+	?	+
Van Leeuwen, 2011	+	+	+	+	?	?	+	-
Wu, 2008	+	+	+	+	+	+	?	+
Wu, 2013	+	+	+	+	+	+	?	+
Wu, 2013,	+	?	+	+	-	-	?	+
Wu, 2014	+	+	+	+	+	+	?	+

TABLE 2.2: Study characteristics of a subgroup of 9 studies with NSTEMI patients.

2.13 Test Characteristics

Synthesizing information on test performance metrics, such as sensitivity, specificity, predictive values and likelihood ratios, is often an important part of a systematic review of a medical test. Due to the fact that many metrics of test performance are of interest, the meta-analysis of medical tests is more complex than the meta-analysis of interventions or associations. Sometimes, a helpful way to summarise medical test studies is to provide a 'summary point', a summary sensitivity, against summary specificity meta-analysis. This yielded a pooled sensitivity of 84.1% (95% CI 81.24% to 86.6%) and a specificity of 78.6% (95% CI 75.4% to 81.4%). Fig.2.8 graphically shows the HSROC summary curve and the summary point.

The sample size of the studies was large enough to allow additional analysis to be completed by adding covariates into the HSROC model. Covariates examined were: NSTEMI subgroup studies vs. the remaining studies, setting where test was performed (shielded vs. unshielded), and the number of MCG channels used (< 9 vs. ≥ 9).

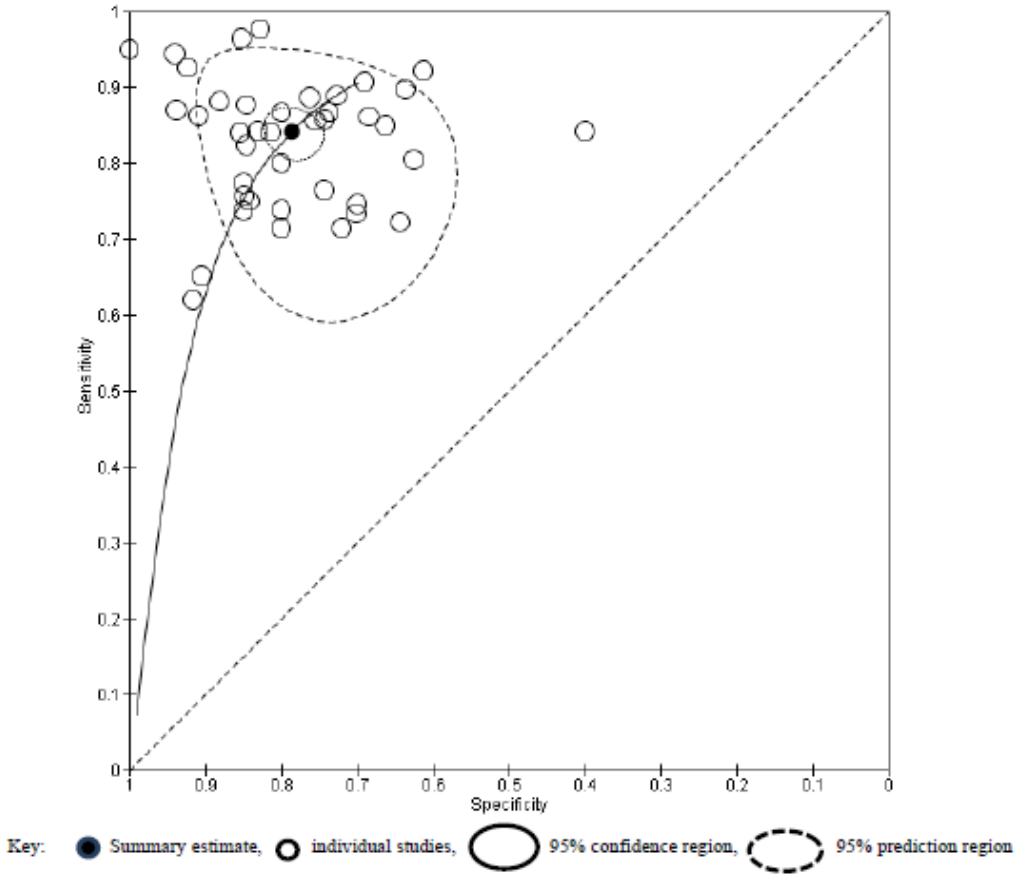

FIGURE 2.8: The graph displays HSROC summary curve, estimates and 95% confidence region.

2.13.1 NSTEMI Subgroup Patients

The key covariate tested was whether the MCG can be used to rule-out NSTEMI in patients with chest pain. To evaluate this, the subgroup of 9 NSTEMI studies was compared with the remaining 31 studies. The analysis, summarized in Table 2.3 and Fig.2.9, showed a small difference in the specificity estimates between the two subgroups, indicating the high efficacy of MCG in ruling out NSTEMI in patients with chest pain. On the other hand, the analysis showed a significant

difference in the sensitivity estimates, indicating high efficacy of MCG in ruling-in NSTEMI in patients with chest pain.

	9 studies considering NSTEMI patients (CI 95%)	31 remaining studies (CI 95%)
Sensitivity	0.8876 (0.8405 – 0.9221)	0.8156 (0.7803 – 0.8464)
Specificity	0.7841 (0.7278 – 0.8315)	0.7971 (0.7529 – 0.8351)

TABLE 2.3: A focus on the 9 studies subgroup (pooled results and confidence intervals).

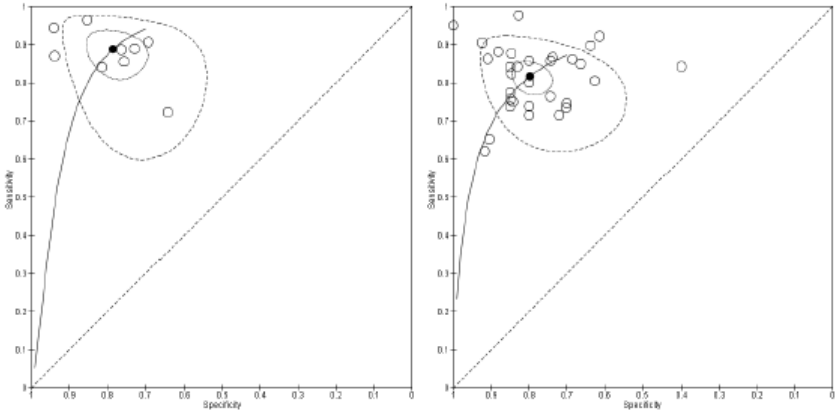

FIGURE 2.9: HSROC Curve of the 9 studies that were identified as most similar to the Leeds model study (left). HSROC curve of the other 31 studies (right).

There are several potential sources of bias in the 9 NSTEMI studies subgroup, that could have influenced the above estimates. At study level, three studies showed at least one source for risk of bias [44, 69, 78], according to the study quality assessment shown in Table 2.2. Using the study characteristics shown in Table 2.1 one can see that six out of the nine studies were conducted in a shielded room. Seven out of the nine studies had MCGs with more than nine channels, with the other two not specified. Finally, six out of the nine studies in the NSTEMI patients subgroup are relatively modern, published in 2007 or after. Given the rapidly developing nature of the medical technologies field, improved technology could have influence on the high sensitivity estimate of the NSTEMI subgroup.

2.13.2 Shielded vs. Unshielded

The study investigated whether the test environment, shielded or unshielded, could have influence on the sensitivity and specificity estimates. The data is displayed

in Table 2.4. We divided the studies into two groups, 26 studies in shielded environment and 10 studies in an unshielded environment. 4 Studies [34, 83, 85, 86] did not specify whether the analysis had been completed in a shielded or unshielded environment and were removed from this analysis.

		Pooled estimates	Confidence levels (95%)
Shielded	Sensitivity	0.8482	(0.8142 - 0.8769)
	Specificity	0.7868	(0.7497 - 0.8197)
Unshielded	Sensitivity	0.8201	(0.7620 - 0.8665)
	Specificity	0.7860	(0.7174 - 0.8416)

TABLE 2.4: Shielded and unshielded test environments.

The results in Table 2.4 show that the pooled estimate for the sensitivity of the shielded room environment is higher than the unshielded environment, but the confidence levels overlap. The shielded environment improves the sensitivity levels compared to the model without this covariate included.

2.13.3 Number of Channels

We also examined whether there was a difference in the sensitivity and specificity for MCG devices that run on ≤ 9 and > 9 channels. 10 studies did not specify the number of channels used. The analysis showed that the sensitivity and specificity levels were higher for those studies that had used more than 9 channels compared to studies that used ≤ 9 channels. Table 2.5 describes sensitivity and specificity of MCG studies which used more than 9 channels compared to those with ≤ 9 channels.

2.14 Discussion and Conclusions

MCG is a relatively new technology, that could potentially transform the way health-care providers diagnose patients with suspected MI. This review is an attempt to systematically identify and analyze all evidence available on the diagnostic performance of MCG within this setting. Our pooled test characteristics produced a sensitivity of 84.1%, and a specificity of 78.6%. The main objective of this systematic review was to evaluate the efficacy of MCG as a test for the

	Number		Pooled estimates	Confidence levels (95%)
≤9	13	Sensitivity	0.8395	0.7930 – 0.8771
		Specificity	0.7700	0.7007 – 0.8273
> 9	25	Sensitivity	0.8442	0.8002 – 0.8799
		Specificity	0.7845	0.7468 – 0.8180
Unknown	4	Sensitivity	0.8544	0.7598 – 0.9159
		Specificity	0.8342	0.6878 – 0.9200

TABLE 2.5: Sensitivity and specificity of MCG using more than 9 channels compared to studies that used less than 9 channels.

rule-out of NSTEMI in patients with chest pain. This was done by comparing the performance of MCG for the subgroup studies with NSTEMI patients, against the remaining studies. The analysis showed a significant advantage for the sensitivity results 88.8% compared to 81.6%, respectively. Similarly estimates for specificity results in 78.4% compared to 79.1%. Also, for a given prevalence of NSTEIM in a population, the pooled sensitivity and specificity of MCG can be used to calculate positive and negative predictive values for the test. For instance, the age-adjusted prevalence of NSTEIM in the United Kingdom is 17% and yields a positive predictive value of 50% and a negative predictive value of 97% for MCG, suggesting that MCG could be useful in this population to rule out NSTEIM in patients with chest pain. The limitations of our analysis stem from the currently small amount of available evidence on this technology. Several covariates such as shielded vs. unshielded environment and number of MCG channels, were shown to have influence on the test accuracy estimates. Furthermore, as the majority of considered NSTEMI studies were relatively modern, published in 2007 or after, this could potentially introduce a risk bias due to technology improvements.

Chapter 3

Optimisation and Performance of Induction Coil Magnetometer

To explore the limitations of an induction coil magnetometer in low field ($< nT$), low frequency ($<10\ Hz$) sensing, we start by looking at the development of Magnetocardiography (MCG) over the last several decades. Induction coil sensors [87–89] are one of the oldest and best known types of magnetic sensors that can be used in medical devices for diagnostic purposes. They have a relatively low signal to noise ratio, requiring long averaging times to reach the same signal to noise ratio as other devices. Their physical size also puts limits the resolution that can be obtained. However, the magnetic field is so small in comparison to typical background fields, in order to be suitable for bio-magnetic imaging, the magnetometer must be capable of discriminating between very small fields with remarkable accuracy. This places the emphasis of magnetometer design on noise rejection rather than striving for higher sensitivity. Suppression of background noise is typically performed using gradiometers which help extract the signal from this large noisy background field and it therefore normally requires very high precision manufacturing to achieve sufficient background suppression. These are good reasons not to continue with induction coils and the principle reason that the literature teaches us away from induction coil magnetometers. This being said, there are several factors in favour of induction coil magnetometers. They are as follows;

- They are relatively cheap, which is important because in real life medical purchasing decisions, a substantially reduced cost can overcome objections to the length of time required for averaging signals.

- They are sufficiently sensitive. The typical peak magnetic emission from the heart is 50-150 pT at around 30 Hz. Hence, the few Femto-Tesla noise floor achievable with a SQUID magnetometer is not necessary.
- They can be incorporated into a portable apparatus, which can be used with limited training and without liquid cryogens.

However, to make them medically useful, three significant factors that do need to be overcome:

1. There needs to be sufficient spatial resolution to achieve the minimum required resolution.
2. The signal output of the coil must be large enough to be detectable.
3. The Johnson noise of the coil needs to be $\leq 1\,pT/\sqrt{Hz}$ to avoid the signal being swamped by noise.

In this chapter, I'll present several different setups of magnetocardiography based on the induction coil, explaining the limitations of each set and introducing solutions as well as the results from different experimental methods. The key results obtained in using the 15-channel MCG, are displayed in chapter 6.

3.1 Induction Coil Magnetometer

3.1.1 Two-channel MCG - Test 1

A feature of our research is that the experimental setup evolves as the project moves along, as a result of this several experimental methods used to obtain high resolution Magnetic field map-MFM will be discussed, not only as a diagnosable technique but also a marketable MCG mapping device. In order to capture the heart's magnetic field, which is in the range of 50-150 pT at around 30 Hz, very sensitive sensors with specific features are required. Fig.3.1 illustrates the structure of the coils used in this research, more details of which will be explained later in this chapter.

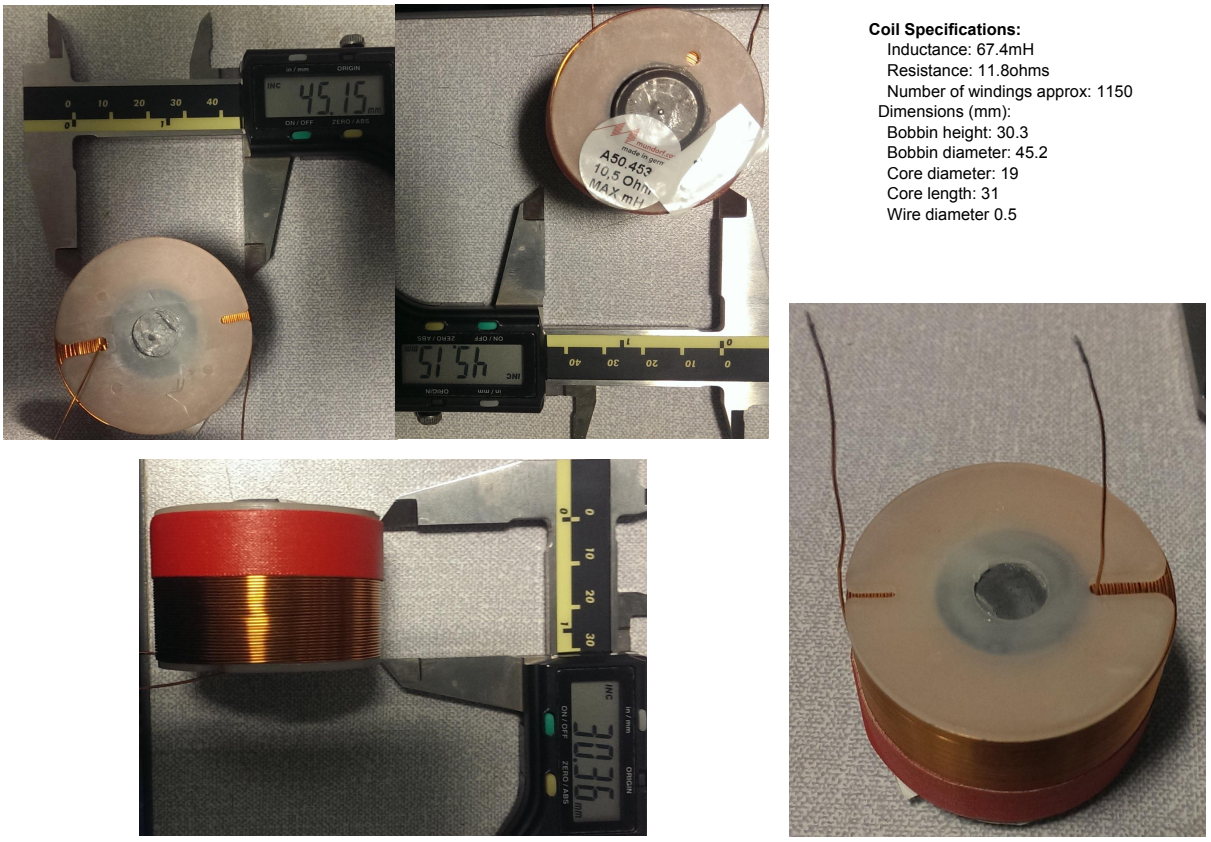

FIGURE 3.1: Induction coil magnetometer, with the specifications on the image top right. It includes inductance, resistance number of windings, dimensions,core diameter and core length

A differential inductive magnetometer (two coils with the opposite orientation wired in series to reduce common mode noise) was capable of detecting the magnetic field created by electrical excitation of the heart. Therefore, our first try used one coil as a magnetic sensor and the other as noise cancellation, wired in the opposite orientation in series. These were placed in a plastic tube made from Delaware's plastic for speciality and protective applications, Fig.3.2. The MCG scan was taken only at one location on the chest, whilst the ECG was simultaneously taken by holding two brass bars in the hands, Fig.3.3.

However, this setup was not successful. We found that by only using two coils with a two lead ECG as a trigger signal we would not be able to produce high resolution images, as it only covered one point by particular alignment on thorax. Therefore, we intended to increase the number of coils, place them differently. In addition, the two bars were our preliminarily ECG that made by ourselves in the lab just to trigger the signal.Then we found out to trigger the heart signal, 3-lead ECG is a minimum requirement, hence we changed it to 3-lead ECG.

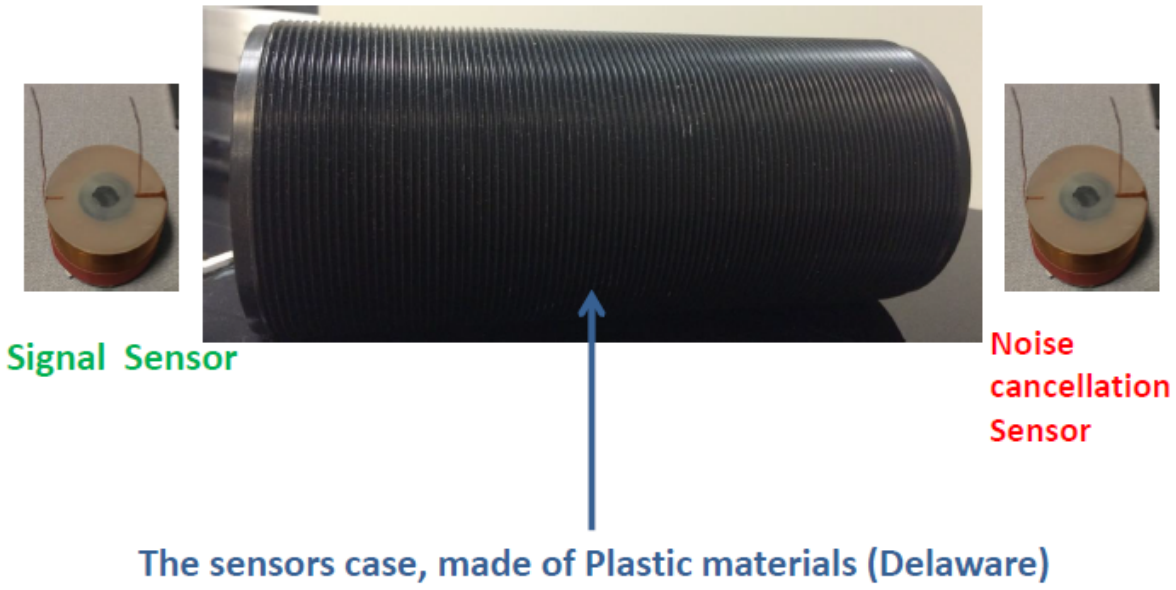

FIGURE 3.2: Two-channel MCG. Two coils were used with entirely equal features; one as a signal sensor and the other as a noise cancellation.

3.1.2 Four-channel MCG-Test 2

Although we have designed a coil sensitive enough to receive the heart's magnetic field, understanding the number and location of the sensors on the body, as well as how to set the coils next to each other, are critical. We constructed a 4-channel MCG using the same coil as before. To receive a signal from the coils with minimum interference, a 1000 preamp was placed immediately above each sensor coil, which were situated in a square co-planar arrangement. The first use of the 4-channel MCG is displayed in Fig.3.4. As it can be seen, the volunteer seated in a reclining chair, with the 3-lead ECG attached to each wrist. The device positioned the sensor in various locations around the chest. At this stage the scan took 30 minutes to complete. It was found that still more sensors were required to be able to map the heart's magnetic field. Therefore, we added 5 more coils, all with amplifiers on top of each, to create MFM of the heart with high resolution. The scan configuration is shown in Fig.3.5. We used labview software to process the MCG scan. To ensure we were capturing purely the heart's magnetic field, we had an opportunity to run the 9-channel MCG in a shielded room at York-YNIC. The MCG raw data recorded from 9 sensors in the shielded environment is displayed in Fig.3.6.

FIGURE 3.3: Shows the bars we used as an electrocardiogram.

The raw signals taken were averaged over 30 minutes and are displayed in Fig.3.7.

Up to this point we were able to see the heart's magnetic field signals from healthy volunteers as shown earlier, but we were still unable to create the MFM to see the dipoles. In order to achieve this, further developments in software in addition to increasing the number of sensors were required.

3.2 Technical Description of Measurements

The following states present a designed coil and number of channels needed to meet the MCG characteristics, which has a surprising and significant outcome over previous tests and allows the manufacture of an MCG imaging apparatus using an inductive coil pickup.

3.2.1 Experimental Apparatus

With the information obtained from the previous tests in hand, we started rebuilding the apparatus with the number of sensors increased to 15. This was sufficient

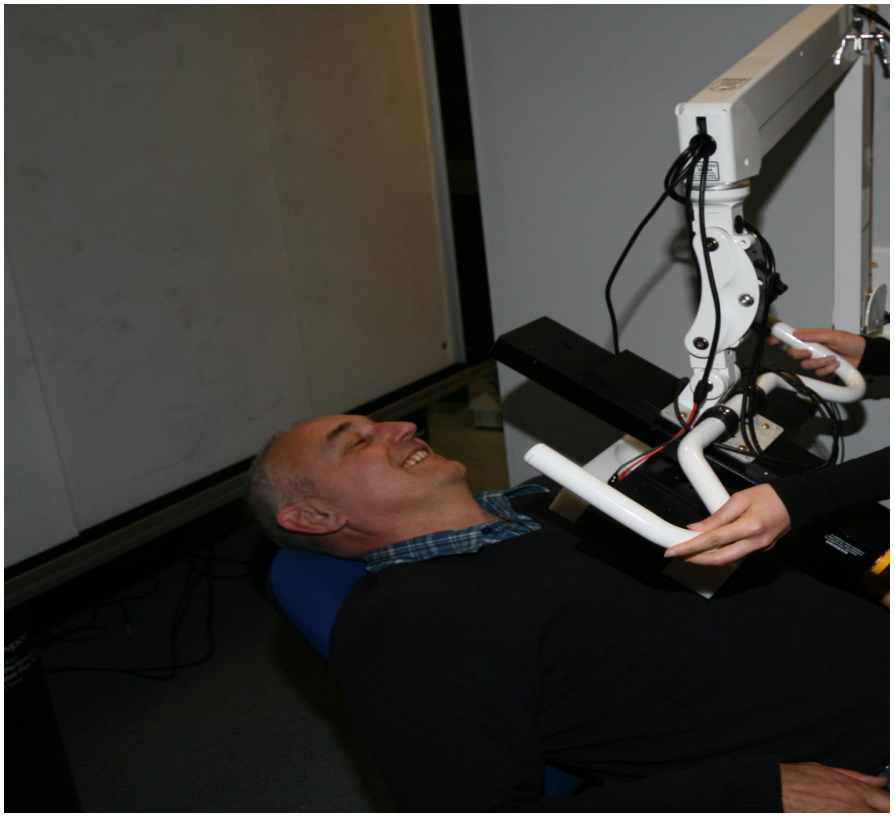

FIGURE 3.4: Four-channel MCG. It is placed as close as possible to the chest.

to get the whole picture of the heart. The sensor holding plate was also modified from square to hexagonal as this can cover the thorax and chest area with significantly higher resolution.

The schematic layout in Fig.3.8 illustrates the apparatus used in the experiment. It briefly consists of magnetic pickup sensors which are made of 15 inductive coils, an ECG trigger, an Analogue to Digital Converter (ADC) and a data processing stage where the signal is extracted from the background. More details will be presented in the following sections.

3.2.2 Electrocardiogram-ECG Recordings

At the very start of the experiment, we used 2 bars made from brass as our ECG tool. It was found that to capture the heart signal, 3-lead ECG is a minimum

FIGURE 3.5: Nine-channel MCG, scanning configuration.

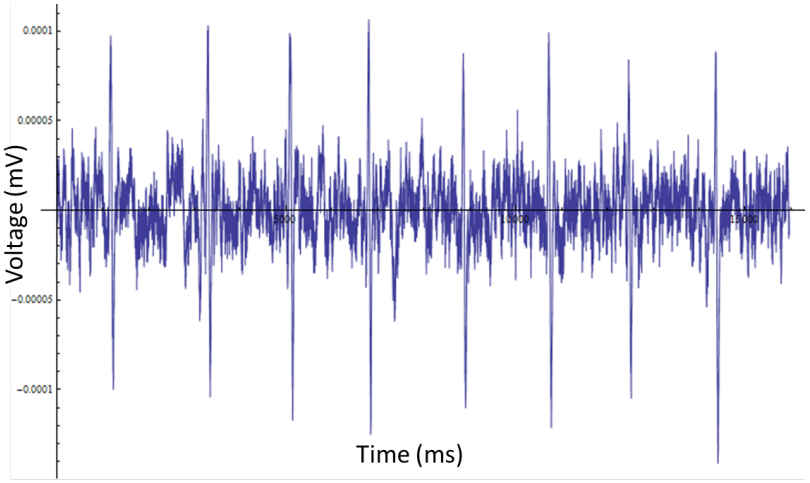

FIGURE 3.6: Shows the 9-channel MCG raw signal in a shielded room. The scan was taken from a healthy volunteer.

requirement. Hence, we changed it to the 3-lead Electrocardiogram as shown in Fig.3.9 that was only used for the purpose of triggering the MCG signal.

However, after several tests on patients, we found that this ECG struggled to trigger with some patients with heart conditions due to their low voltage level. Therefore we changed it to a more updated one which is manufactured by Accusync, Fig.3.10. The new ECG has a specific connector that is capable of triggering the signal for all types of patients, it is called R-trigger gate and enables the device to

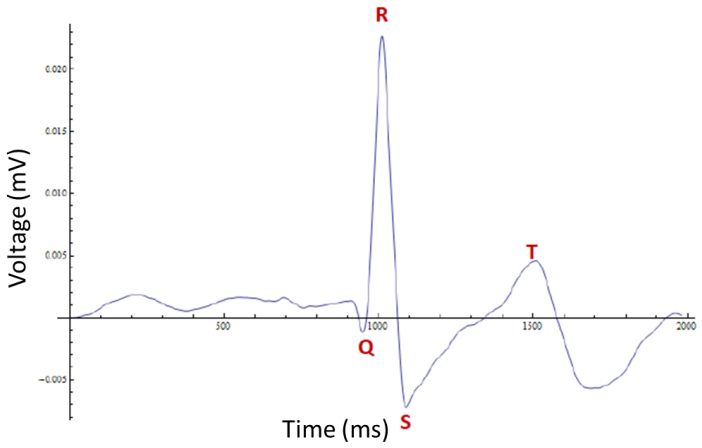

FIGURE 3.7: MCG signals averaged over 30 minutes in a shielded room, with the representation of P-QRS-T complex in a cardiac cycle.

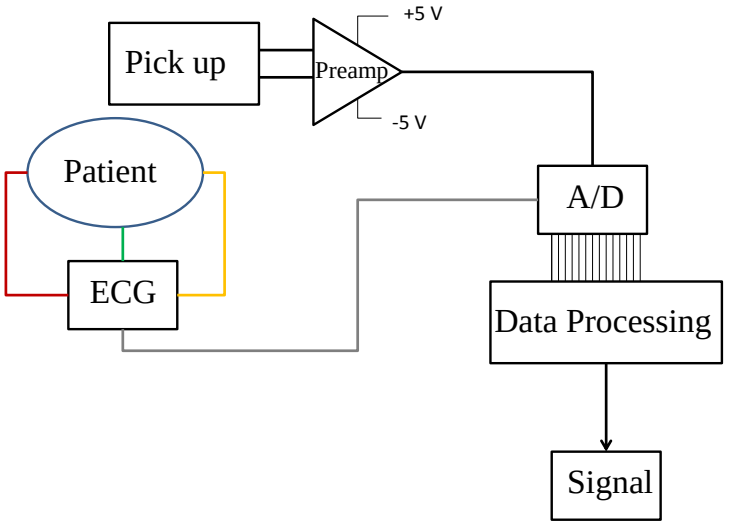

FIGURE 3.8: Scan arrangement, schematic of data processing.

be more useful for different applications.

3.3 Design of the Cardiac Magnetometer

Our design for an inductive cardiac magnetometer is motivated by the desire to create a coil for magnetocardiac imaging. Fifteen channels are the minimum number required for a valid diagnostic depending on the assembly of an imaging system.

FIGURE 3.9: Shows the old ECG used for triggering data, manufactured by HP.

FIGURE 3.10: Shows the new ECG used for triggering data (for high and/or low voltages), manufactured by Accusync.

Fig.3.11 displays the 15 MCG sensors that are placed in hexagonal shape to increase the resolution. Based on the Magnetocardiography literature, in order to get a high resolution image, the number of scan points on the body should be high. Based on our experiments,as explained earlier in this chapter, the more sensors the better the resolution, therefore we moved on to 15 coils, as this was the maximum number of sensors we could fit in our device at that time. The finite size of the chest limits the maximum diameter of a coil to around 5 cm. The frequency of the relevant magnetic signals of the heart is between 1 Hz and 40 Hz and hence the aim is to optimize the coil dimensions for this application. Loop coil receivers are widely used in Extremely Low Frequency (ELF) radio reception[90].

However, the coils used are typically very large in order to increase the flux linkage with the circuit. Typically the coil dimensions are a radius of r = 0.5 m and a winding cross section of A = 1 cm^2. This is too large to be useful for a medical magnetometer, however as we follow the formula for coil design, this coil will have an output voltage determined by the text book formula:

$$V = AN\frac{dB(t)}{dt} = ANB2\pi f, \tag{3.1}$$

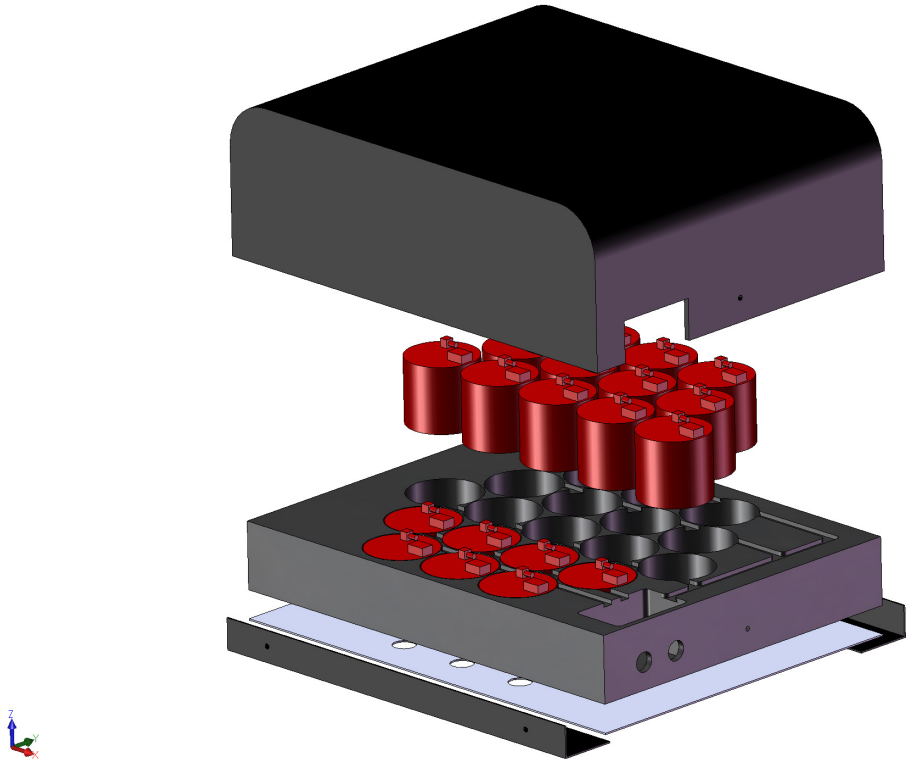

FIGURE 3.11: 15-channel MCG sensor construction.

where N is the number of windings, A is the effective cross sectional area of the coil, $B(t)$ is the time varying magnetic field with a magnitude B and f is the frequency of oscillation of the field. Setting B=1 pT (the smallest field we wish to measure accurately) and f=30 Hz we can find the conversion rate for the signal frequencies that are of the greatest interest for any coil design.

We are free to choose the wire radius to determine the voltage output: a smaller wire increases the voltage output at the expense of increased coil resistance. For any given length of wire, the coil with the highest inductance is given by the Brooks configuration [91]. A Brooks coil is known as having specially adjusted dimensions, which achieve the maximum inductance for a given length of wire. As can be seen from Fig.3.12, the cross section of the coil has been designed as a square and the inner diameter is equal to twice the height of the coil winding. The inductance for a Brooks coil can be found from the following equation:

$$L \cong \ 0.016994 \ a \ N^2 \ \mu H, \tag{3.2}$$

where a is the mean radius of the inductor (in cm), and N is the number of turns.

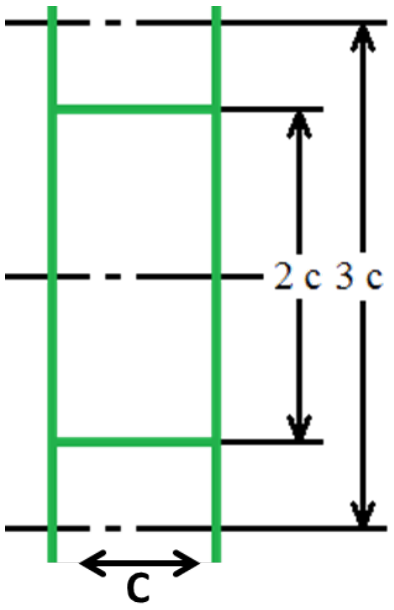

FIGURE 3.12: Illustrates Brooks coil configuration, which has a square cross section and the inner diameter is twice the height of the coil winding.

However, Table 3.1 shows that the coil design presented here has significant improvements over the Brooks coil of the same outside dimension. At all levels this coil design has a higher voltage and lower noise figure at the target frequency of 30 Hz.

	D	Di	l	V(1pT)	S
New Coil	12	5.1	8.28	616nV	57fT
Brooks Coil	12	6	3	211nV	96fT
New Coil	8.5	3.6	5.87	155nV	136fT
Brooks Coil	8.5	4.25	2.125	53nV	227fT
New Coil	4.25	1.8	2.9	9.5nV	773fT
Brooks Coil	4.25	2.125	1.0625	3.3nV	1.3pT

TABLE 3.1: Comparison of the coil described in this work with the Brooks coil. Unlabeled dimensions in cm. The coil parameters are, coil outer diameter (D), coil inner diameter (Di), length (l), voltage pk-to-pk (V), Johnson noise (S) and wire radius is defined as a = 0.23 mm

To extract a signal from the coils with minimum interference, a 1000 preamp was placed immediately above each sensor coil. The coil signal is fed to the preamplifier using a low impedance audio amplifier with a factor of 1000 and the signal is detected using a 24-bit ADC with a $\pm 0.1\,V$ range. A flow chart indicating the major components of the data collection scheme is presented in Fig.3.8.

The signal was then digitized using a multichannel $2000KS/s$, 24-bit and AC-Coupled with a rail-rail voltage of $\simeq 0.3\ V$. A "rail" here is a power supply. Rail-to-rail just means the full range of voltages between the most positive and the most negative power supply voltages present. Most op amps, for example, if powered from $+0.3\ V$ and $-0.3\ V$ rails, cannot make outputs that go through all the way from $+0.3$ to $-0.3\ V$. They usually lose a millivolt or two on each end. A r-r-output op amp can output almost all the way. This gives a minimum resolvable voltage of 17 PV from the coil signals which were reached at 2 KHz sample frequency. All filtering and other noise reduction was performed digitally. The final condition that we require for a useful diagnostic is to remove the background noise. In the normal mode of operation it is considered necessary to have extensive shielding or closely matched gradiometer coils. We use a dynamic coil matching algorithm that uses a global noise source (e.g. 50 Hz line noise) to dynamically match the coil output and subtract the signals.

3.3.1 Noise Cancellation

High sensitivity induction coil magnetometers can be constructed [52] and in fact they were the first sensors used in bio-magnetic sensing. However, creating an induction coil gradiometer requires that the gradiometer coils are sufficiently well matched to eliminate large background fields. Commercial developments have therefore focused almost entirely on SQUID systems, where precision manufacturing techniques are available and gradiometer noise suppression is well understood. Induction coil magnetometers are inexpensive and somewhat more portable than the alternatives hence a noise reduction technique that can enable bio-magnetic sensing using this apparatus would be a significant development. The sensitivity limit of an induction coil magnetometer is given by Johnson noise, which is the electronic noise generated by the thermal agitation of the charge carriers inside an electrical conductor at equilibrium, in the coil:

$$S = (4k_B T R_a)/2\pi f N A, \tag{3.3}$$

where k_B is Boltzmans constant, T is the temperature, R_a is the antenna wire resistance given by

$$R_a = N 2\pi^2 a^2 \rho r_{coil}, \tag{3.4}$$

where a is the radius and ρ is the resistivity of the wire used in the windings on a circular coil of average winding radius r_{coil}. Coil parameters are the length l, the coil outer diameter D and the coil inner diameter D_i. Therefore Johnson Noise can be as small as 100 fT for a few cm scale coil compared with 10-100 pT for a magnetic signal from the heart. The problem is therefore not necessarily sensor noise, but environmental noise. Treating the sensor as a low frequency aerial over the frequency range relevant to cardiomagnetometery (0-50 Hz) the wavelength of background EM radiation will be orders of magnitude longer than the size of the array. Hence, as the wavelength of electromagnetic radiation at this frequency is much longer than the size of the array, interference in the sensor elements will be correlated.

3.4 Data Acquisition

We constructed an array of 15 sensors. Each sensor had a low noise preamplifier attached with minimal length of wire to reduce additional noise coupling. The dimensions of the coils were optimized for signals in the range of 1-40 Hz and for magnetic fields aligned to the axes of the coil.

A preamplifier was placed immediately above each sensor coil. All filtering and other noise reductions were performed digitally in a post processing stage. A PXI 4498, 16 channel, 24-bit with samples obtained at $2KS/s$ with a rail-rail voltage of $\simeq 0.3\ V$ was used, Fig.3.13.

The 15 coils and a 3 lead ECG output was recorded and was also digitized in the Analogue to Digital Convector (ADC). The ECG was attached to left and right hand wrists and one to the left ankle, to gate and window the data stream into individual heartbeats which can be averaged over the duration of the scan. The QRS feature on the ECG is detected when the signal rises above the indicated threshold voltage Fig.3.14. A window extending from 0.5 s before the QRS complex to 0.5 s after the QRS complex was selected from the magnetic field data for each heart beat.

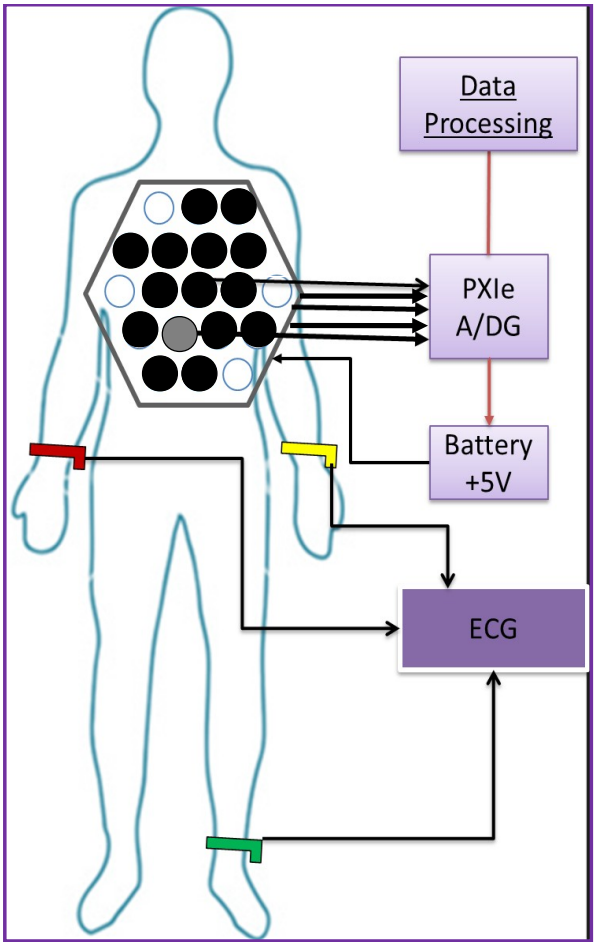

FIGURE 3.13: Shows the experimental setup used for the current study. Filled circles show coil sites. The grey coil is used for centralising the array between the 4th and 5th INTERC Space.

3.4.0.1 Array and Patient Alignment

The sensor array was arranged in a hexagonal configuration with a lattice spacing of $\sim 7cm$. This is consistent with other MCG devices both in overall dimension and sensor spacing [92, 93]. The array pallet is positioned as close as possible above the chest without touching the scan participant (who is lying supine). Because the body mass differs for each person, there is no specific distance. To maximize signal (field strength) our principle aim was to avoid transferring vibrations from the patient to the array. The gray coil in Fig.3.13 was positioned above the xiphoid process between the 4th and 5th intercostal space.

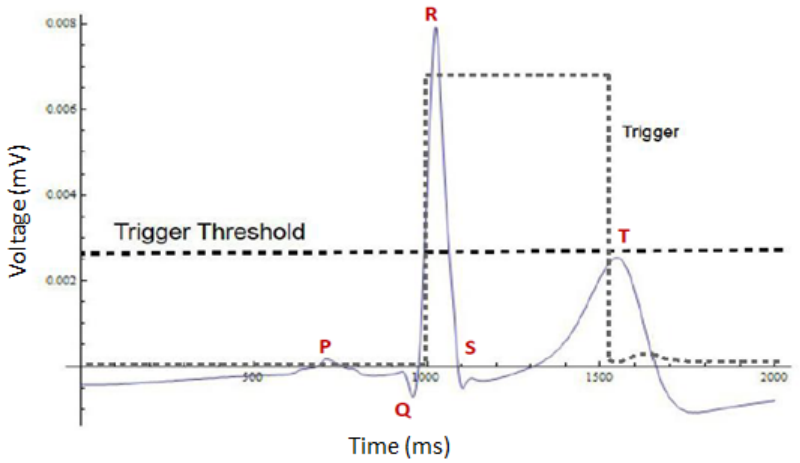

FIGURE 3.14: A sample ECG trace showing the typical P-QRS-T complex. The trigger voltage was set at mid point of the Q-R wave transition. The resultant trigger signal is also displayed.

3.5 Preliminary Results

The Magnetometer signals were recorded simultaneously with an ECG (contact). Fig.3.15 examines a novel MCG device that has been developed at the University of Leeds. This device doesn't require a shielded room, special bed,or specialist staff. The image also demonstrates positioning and alignment. All the results in this chapter and the following chapters were obtained from V_1, which is our first MCG version at the university of Leeds. The device technical specifications were introduced in Table 3.2. As the device is a portable magnetocardiogram, it needs a battery charge to be able to work unplugged from the mains. The cardiac field signal was presented in the raw coil signals (passed through a preamp), even prior to averaging. More details about data extraction will be explained in this section.

Technical specifications

Model	1.0 [17/8/2012]
Dimensions(W×H×L)	1140 mm × 1275 mm × 900 mm
Operating temperature	15°C - 30°C
MCG bandpass (High/Low)	44- 1
ECG bandpass (High/Low)	100-90
Input Voltage	240 V mains (Base unit)
Output Voltage	5v Battery (Sensor unit)
Fuse Rating	Medical class-7A Breakers
Battery life period	4 hours

TABLE 3.2: The table shows the MCG device technical specifications.

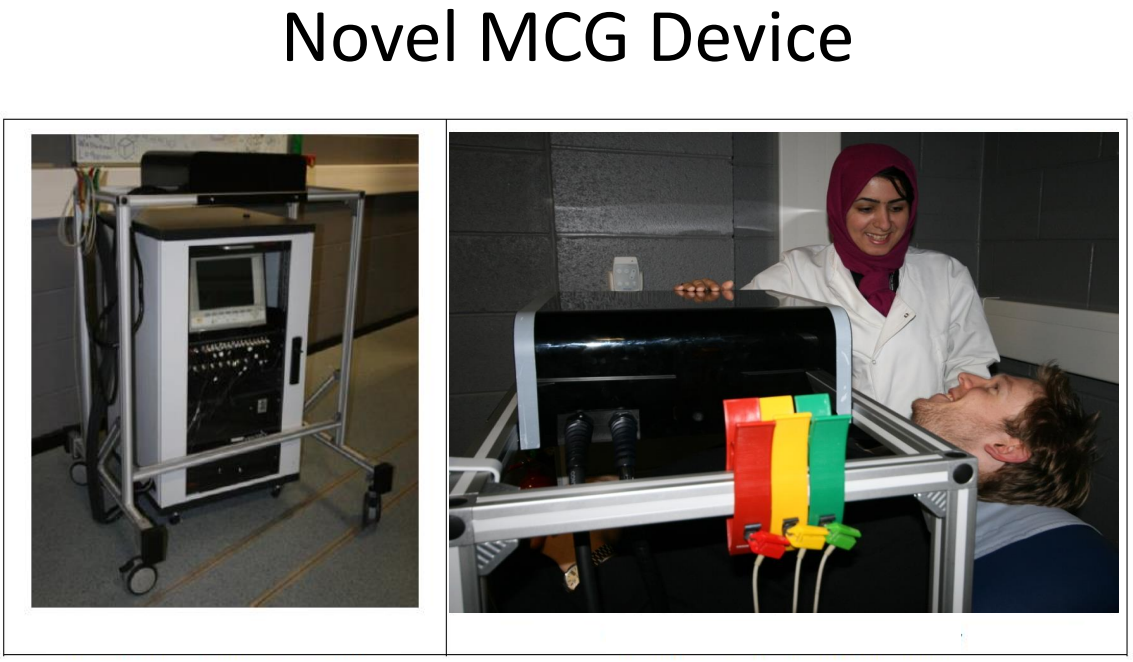

FIGURE 3.15: Shows the MCG device for the current study at Quantum lab of Leeds university. As it can be seen, it is completely portable, easy to use and with no need for specialist staff. The MCG scan can also be done in an unshielded environment.

3.5.1 Coil Correlation

The result of windowing and averaging the data from two coils is shown in Fig.3.16, for a 10 minute scan ($\simeq$ 600 heart beats).

As noted above, noise sources distant to the array will offset all coils equally, hence subtracting the two reveals local differences. The subtracted signals are shown in Fig.3.17, where the small MCG signal has been recorded. The noise is 1-2 orders of magnitude bigger than the signal, but it is highly correlated and therefore subtraction reveals the smaller uncorrelated component related to the local MCG. This shows that the noise is entirely correlated extracting a signal that is several orders of magnitude below the noise. As the coil sensors detected $^{dv}/_{dt}$, the derivative of the associated ECG is also shown for comparison.

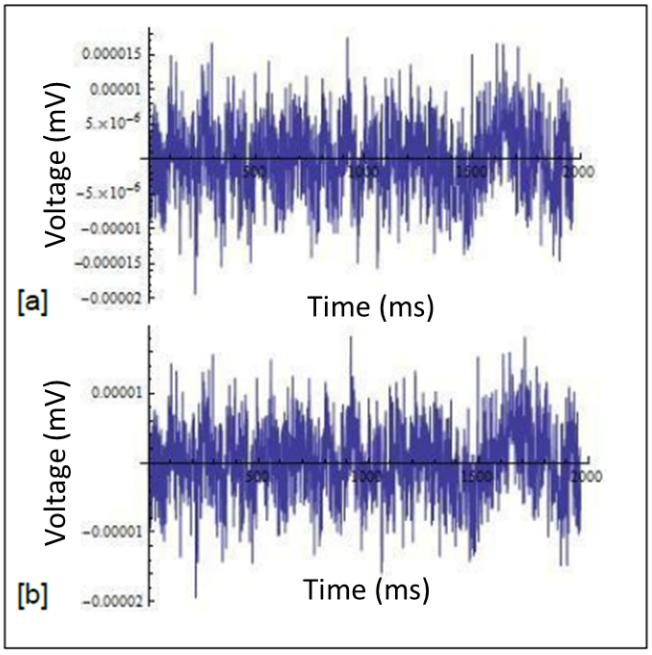

FIGURE 3.16: shows averaged traces obtained from the background pick up coil (a) and the signal coils (b). This shows a high degree of correlation in the quasi-periodic noisy background.

3.5.2 Image Reconstruction

To produce the magnetic field map on a larger scale (across the measurement array) we establish a correlated background extracted form all of the sensors. Fig.3.18 shows the individual traces obtained from all coils (with a low pass filter having been applied) without noise subtraction.

Fig.3.18 demonstrates the average correlated background through which the real signal can be seen. Fig.3.19 shows the MCG signal plot of coil traces produced by subtracting the average correlated background from the traces. Fig.3.19, reveals the Local MCG data. The MCG signal shows some differences to the ordinary MCG trace [94]. This is due to the fact that the coils are measuring $^{dB(t)}/_{dt}$ rather than the magnetic field B.

This stage can lead us into the heart dipole. Fig.3.20 shows the magnetic field map in the region of the QRS complex, where the strongest signals are obtained and also is a region of particular interest for cardiologists [39, 95]. As it can be seen the dipoles are clearly visible and placed in the centre of the heart.

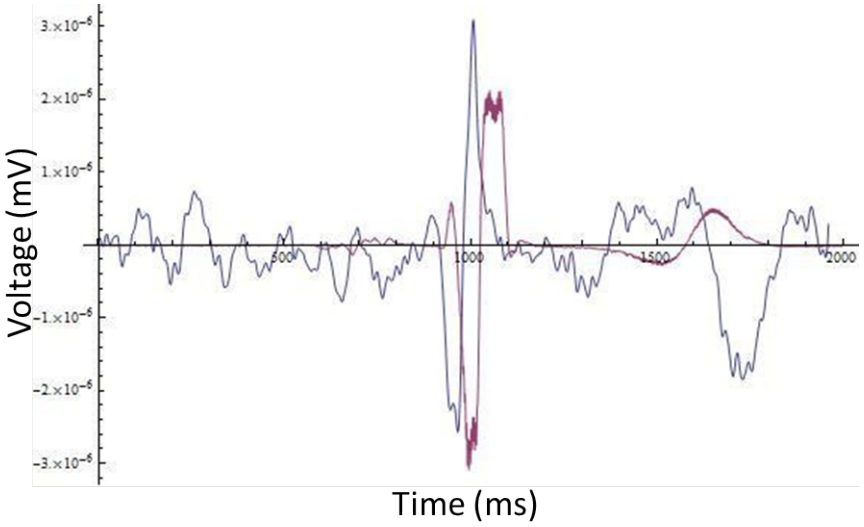

FIGURE 3.17: Subtracted MCG signals, averaged over a 25 minute scan in an unshielded room. The black color represents the MCG signal in an unshielded room and red is for the ECG, at same time and with the same person.

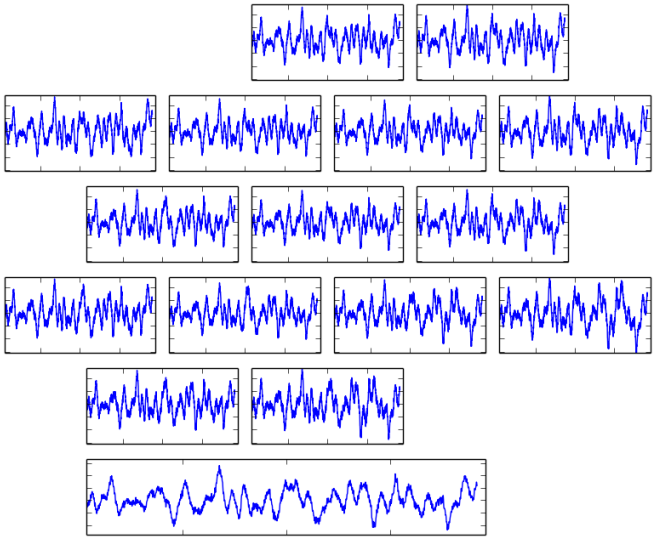

FIGURE 3.18: The traces gained from a healthy participant without noise subtraction. It illustrates fifteen MCG channels in different regions.They are correlated and averaged over a period of scanning time. The X and Y axes represent, Time (milliseconds) and Voltage (millivolts), respectively.

3.6 Conclusion

Using correlated noise elimination, we have demonstrated the operation of an induction magnetometer with sufficient sensitivity to detect the magneto-cardiac

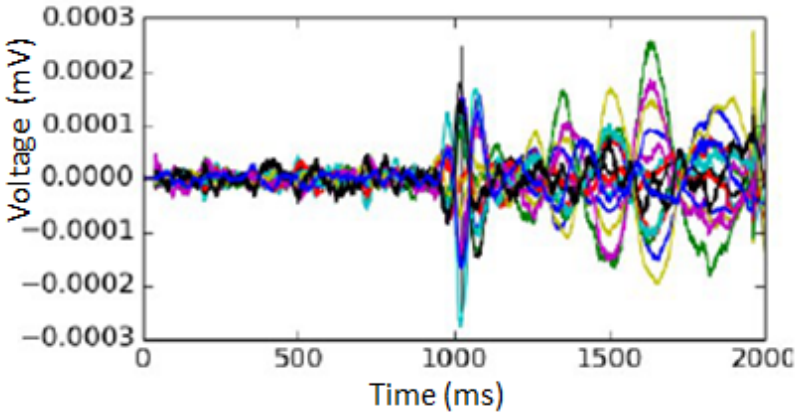

FIGURE 3.19: The traces gained from a healthy participant without noise subtraction. It illustrates fifteen MCG channels in different regions.

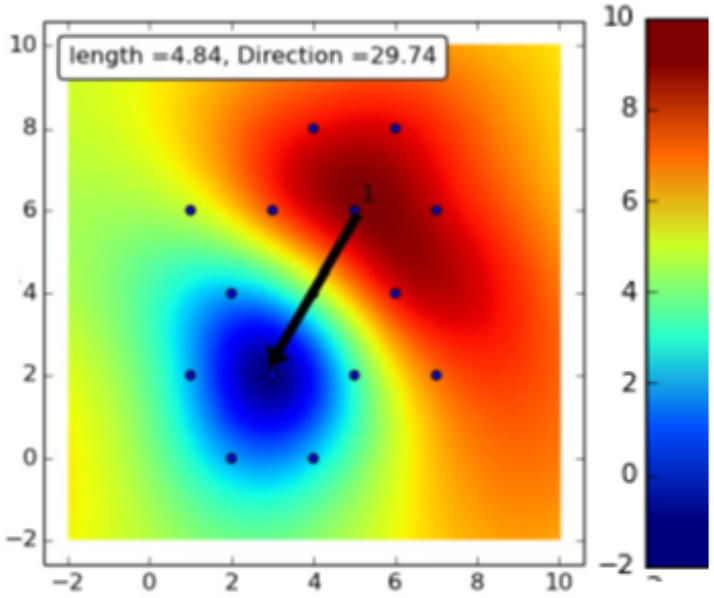

FIGURE 3.20: The image shows the heart MFM from a healthy participant. The MFM illustrates positive (red) and negative (blue) poles. The units are arbitrary, as our device measures the magnetic field changes over a period of time, (more details about the images are details in chapter 6).

field. We have also demonstrated a mechanism for noise reduction which allows the sensors to be used in a noisy lab environment. Importantly the noise cancelled signal is practically identical to the signal taken in a low noise environment making this a device with practical clinical applications. This leads to a cost effective solution for measuring the magnetic field of the heart. Imaging works in unshielded environments and delivers result in 5 minutes. This device therefore potentially paves the way for cost effective MCG in the near future and has been designed

in such a way to detect the magnetic field of the heart with a sufficiently high resolution to be medically useful. The solution is also highly scalable. The array can be any size, with dimensions purely determined by mechanical limitations.

Moreover, a sufficient level of coil matching has been achieved to operate in an unshielded environment. The coil design that has been selected has properties that are optimized to detect the magnetic field of the heart with a sufficiently high resolution to be medically useful. The design minimizes the noise and optimizes the signal detection, while operating within the size parameter constraints. This gives the somewhat remarkable results that an induction coil magnetometer can perform sufficiently well for Magnetocardiography. What is astonishing is that this development does not attempt to optimize the inductance of the coil and is in fact a significant departure from a design that delivers the optimum inductance. The gain achieved is relatively small, a factor of 2 in signal to noise and a factor of 3 in output voltage. However, in obtaining a signal, reducing signal to noise ratio by a factor of 2 means increasing the collection time by a factor of four, which is the difference between a scan lasting 30 minutes and a scan lasting 2 hours. A factor of 3 increase in signal strength leads to a factor of 9 increase in data collection time for the same signal output (this is because digitizing errors grow with smaller signals, when the signal size is within an order of magnitude of the digitization step). The overall impact of these gains is a factor of 36 improvement in data collection time. Hence very small gains make the difference between having a useful medical device or not.

Chapter 4

Magnetocardiography Study Protocol

In the following chapters, where some parts of the work were undertaken in collaboration with other people, appropriate acknowledgment has been given. All other work was carried out by myself.

Magnetocardiography (MCG) magnetic field map technique is in its infant stages and the data is understood by few in the clinical sphere. Several groups [2, 10, 31, 42, 43, 45], today are working on the development of MCG imaging but there are no diagnostic protocols for the images produced by the various devices around the world. This means there are no clinically based cardiologists, who are not connected to the study that can interpret our images. Hence, the study solicits exceptional considerations regarding the assessment of the results.

No clinical diagnoses will be delivered by our MCG testing, we are checking that this device gives a signal that is consistent with the consultant cardiologist's diagnosis.

The design of the study was chosen to assess the differences in data parameters between cardiac images obtained from healthy volunteers and patients with existing ischemic heart conditions. For this we evaluate the device in an NHS clinical setting on patients who have already been diagnosed with ischemic heart conditions. In this chapter the study protocol of our first trial will be detailed.

4.1 Aims and Objectives

The aims of the current clinical study are to characterize the outputs generated by the new coil-based magnetometer device and to assess the technical performance of the device. In the following subsections the objectives of the study will be described.

4.1.1 Primary Objective

A preliminary review of the data indicates that there are differences between the images from healthies and patients which will be demonstrated in the end of this chapter. These differences can be objectively distinguished using an unique innovative analysis method in magnetocardiography, called an image correlation algorithm, which compares each image against a "Standard Normal" image. The results of the image correlation comparisons have been graphically presented in Fig.4.1. It can be seen there is a magnetic imaging Receiver Operating Characteristic or ROC curve, which illustrates the performance of a binary classifier system. The curve is designed by plotting the true positive (sensitivity) against the false positive rate (1-specificity) for the different possible cut-points of a diagnostic test.

From this we can also derive estimates for the True Positive and True Negative rate which are presented in Table 4.1.

Tests	Post MI	Normal
Test Positive	98%(±2)	10%(±3)
Test Negative	2%(±2)	90%(±3)

TABLE 4.1: Preliminary results for the magnetometer assessment. Ranges indicate likely experimental error. Sensitivity= $95.4 - 100\%$, $Specificity = 87.5 - 91.6\%$.

4.1.2 Secondary Objectives

The following list outlines the secondary objectives of the study:

- To identify characteristics (markers) of the images that clearly and objectively differentiate between normal and abnormal images

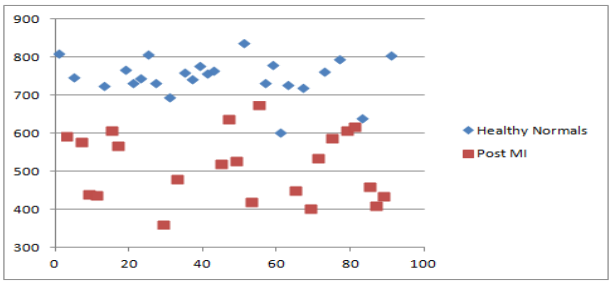

a)

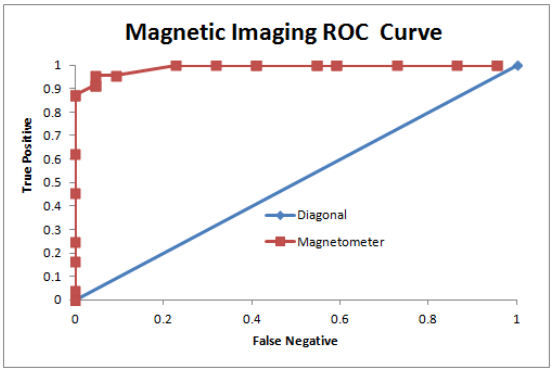

b)

FIGURE 4.1: a) Image correlation index, showing clear banding between Healthy Normal and Post MI populations. b) ROC curve for the first 10 participants (5 Post MI, 5 Normal) each of which have had 4 scans (an assessment of 40 scans in total). Preliminary MCG study at Leeds General Infirmary. The X and Y axes are binary and don't have units. The correlation index values were computed in Python code and then plotted in an excel spread sheet.

- To characterize the markers in a subset of patients who have had a recent myocardial infarction
- To determine if there are marked differences between normal and abnormal images in an early subset of participants
- To estimate inter-operator and intra-operator reliability

- To estimate inter-rater and intra-rater reliability
- To estimate reproducibility of the device
- To evaluate procedural aspects of the device including ease of use/handling, timing of the procedure.
- To evaluate the participant's experience of the procedure

4.2 Study Design

The study was a single-center study of 120 participants (60 patients and 60 age gender-matched healthy) conducted at the Cardiology clinic at Leeds General Infirmary. The design was a technical performance study.
Scanning procedure: On day one, the participants were scanned twice by one operator. Follow-up sessions were held one week later on day 8 $(-2; +7$ days) at which two MCG scans were taken; one from the same operator as on day 1, and one by a second operator. The follow-up time point was standardized across participants, and chosen such that the condition of the patient was sufficiently stable so that any changes in the image represent a difference in technical performance rather than deterioration (or improvement) in heart condition

4.3 Eligibility

Leeds General Infirmary cardiology clinic has recruited patients with ischemic related heart disease to be scanned by the device. The research nurse and I then recruited a healthy control group index matched on gender and year of birth $(\pm\ 3\ years)$. A subgroup of 20 patients, who have experienced a recent myocardial infarction (post-MI patients from cardiac wards) within the patient group have also been recruited.

4.3.1 Eligibility Criteria for Patients

Inclusion criteria

Anybody able to understand the study objectives and willing to provide informed consent form with an age of 25 years or above and have a diagnosis of ischemic related heart disease also willing to return for follow-up assessment one week later. Additionally we considered a subgroup of 20 in-patients suffering a myocardial infarction within 3 days of the clinic assessment.

Exclusion criteria As we are at the stage of testing the device, preferably patients with a pacemaker or who are pregnant or lactating were excluded from the study.

4.3.2 Eligibility Criteria for Healthy Volunteers

Inclusion Criteria Anybody able to understand the study objectives and willing to provide informed consent form with an age of 25 years or above with no history of cardiac disease as confirmed by ECG scan or ECHO cardiogram. Also willing to return for follow-up assessment one week later.

Exclusion Criteria Anybody pregnant or lactating or taking concomitant medications relating to cardiac disease were excluded from the study.

4.4 Recruitment

The research site was required to have obtained local ethical and management approvals prior to the start of recruitment into the study. The recruitment target requires 120 participants (60 patients and 60 healthy volunteers) over a 10 month period. Recruitment began on September 2013 and completed uneventfully 5 months later than anticipated on the 15th September 2014. This delay was due to difficulties identifying suitable subjects as scheduled for urgent angiography. Posters advertising recruitment to the study were displayed in the Cardiology clinic, and in selected departments at the University of Leeds for healthy subject recruitments. Healthy volunteers were identified and matched to the patients recruited by gender and year of birth (within ± 3 years).

Recruitment of Patients

Potential participants were identified from medical records by the research team and approached by the attending medical team during a clinic appointment or on the hospital ward if the patient was an in-patient. Patients were given an invitation letter and had the opportunity to ask questions on the study at the appointment and afterwards with the research nurse.

Assenting participants were formally assessed for eligibility and invited to provide informed, written consent which was obtained prior to attending the study for the MCG scan.

4.4.1 Procedure Details

Electronic MCG imaging was undertaken by the research nurse and/or research physiologist. On day one, each participant will have two MCG scans by one operator. A follow-up session will be held one week later on day 8 $(-2, +7 days)$, at which two MCG scans will be taken; one scan by the same operator as on day 1, and one scan by a second operator. To minimize the possibility of metals from clothing and underwear interfering with the natural magnetic field of the heart, participants will change into a hospital gown prior to scanning. Only clothing covering the top part of the torso will need to be removed, trousers, skirts or shorts can be kept on during the scan.

4.5 Development of the Manual of Image Markers

A sample of 30 data from 30 patients with ischaemic heart disease and 30 healthy volunteers are being used to identify and characterize the markers of the images (training cohort). Data were collated at the Experimental Quantum Information group (QIX) laboratory and reviewed to characterise the image markers, based on a number of analytical and observational parameters in order to produce a manual of summary features for ischaemic heart disease that will allow training of the "raters". The remaining data from 30 patients and 30 healthy volunteers were used to evaluate the technical performance of the device (validation cohort) using the information generated from the set of data used to characterise the markers.

4.5.1 Rater Assessment

The technical performance was evaluated using the manual of image markers on the images from the sample of 30 patients and 30 healthy volunteers (validation cohort). Inter- and intra-operator reliability, reproducibility, and inter- and intra-rater reliability were also evaluated. The second image from each participant, taken on day one, was assessed twice by two "raters". The second rater assessments were conducted at a later time point, after which there was not expected to be recall of the images from the first rater assessment. Assessments of images were conducted blindly, such that the raters are not aware of whether an image was from a patient with IHD condition or a healthy volunteer. Data from the first five patients and first five healthy volunteers were reviewed to determine if there are large differences between normal and abnormal images and will be presented later in this chapter.

4.6 Intervention Details

The study is a technical performance study using an in-house manufactured Magneto-Cardiogram imaging prototype.

Contact with participants were limited to two assessments, at which two scans were conducted. The scan uses a non-invasive, non-contact sensor which is emission-free. The participants will lie on a hospital bed/trolley and will have the non-contact scanner positioned as close as possible above the chest and aligned to the position of their heart to enable an image of the natural magnetic field created by the normal processes of the heart to be obtained. Each scan lasts for approximately 10 minutes. The device arrangements are displayed in Fig.4.2.

4.7 Preliminary Outcome

Preliminary outcomes are positive showing a high reliability of the apparatus as can be seen in Fig.4.1. The results from both intra-operator (intra-patient) and inter-operator (intra-patient) reliability are shown in Fig.4.3. It is interesting that there is more variation within patients than there is between operators, indicating

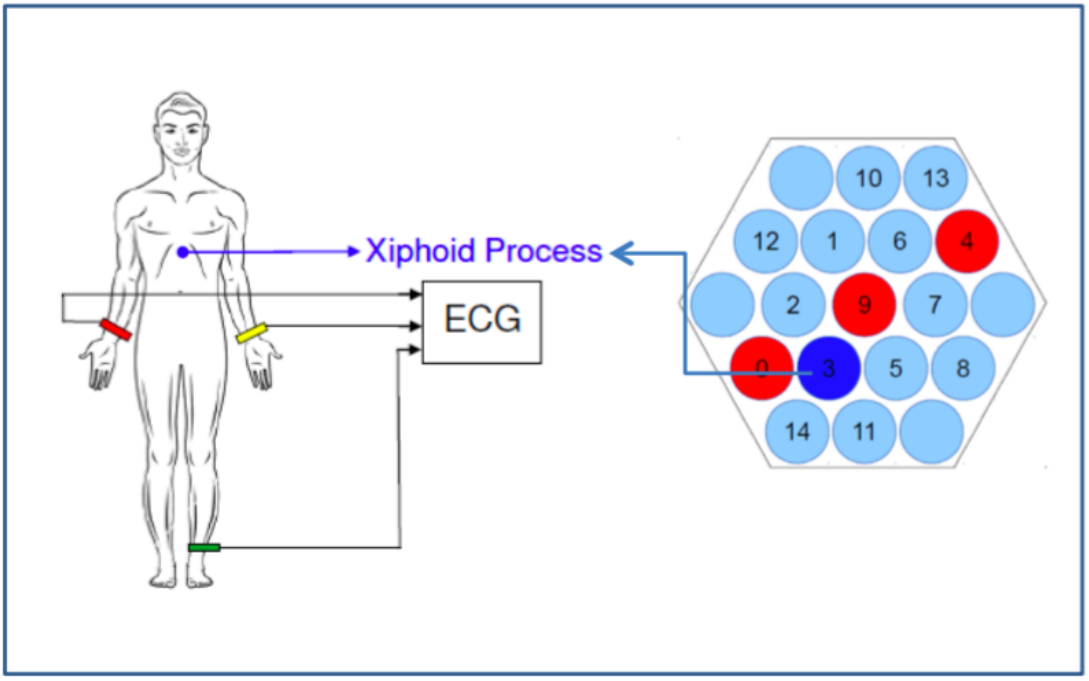

FIGURE 4.2: Device arrangement, initial magnetometer sensitivity measurement was carried out using the numbered coils.

that this is a patient variability rather than operator variability. The inter-operator and intra-operator reliability is very high Fig.4.4, however this needs to be measured against the very small number of comparator scans particularly in the case of inter-operator reliability. Nevertheless, this is very positive with no obvious trend emerging.

4.7.0.1 Reproducibility

Proving the ability of the magnetocardiography study to be reproduced by the nurses, study subjects or anyone else involved and working independently, such as raters, is significantly important. It is also one of the main principles of the scientific method and relies on other things being equal. Fig.4.5 shows all four scans from the first five participants from each participant grouping, healthy and patient. Within a group, visually, there is an outstanding level of agreement between the images. For instance, the magnetic field map of the first row of patients in the image shows an unhealthy map with respect to the dipole angle and distance. Likewise reading methods for the healthy group are applied.

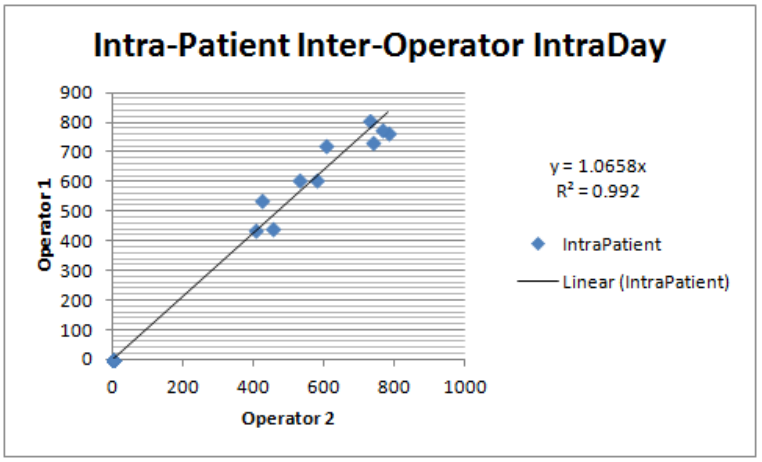

FIGURE 4.3: Comparison of images taken by two operators on the same day of the same patient. The slope is 1 indicating that on average there is no difference between scans taken by the same operator and the spread in the data is small with a high degree of correlation, (the numbers are correlation quantity and they are unit less).

Furthermore, evaluating the operators can show the stability of the images, along with whether or not the outcome would show equality when comparing MFM day 1 with the follow up session, day 7, if they were both taken by the same operator. Fig.4.6 indicates the stability of images taken by the same operator on day 1 and day 2 (taken 7 days after).

Operational Definitions and Procedures

4.7.1 Expected AEs / SAEs – Not Reportable

This is a study in a patient population with high levels of morbidity and co-morbid diseases, and as such in this patient population acute illness resulting in hospitalization, new medical problems and deterioration of existing medical problems are expected. In addition, participants will be seen only twice at the

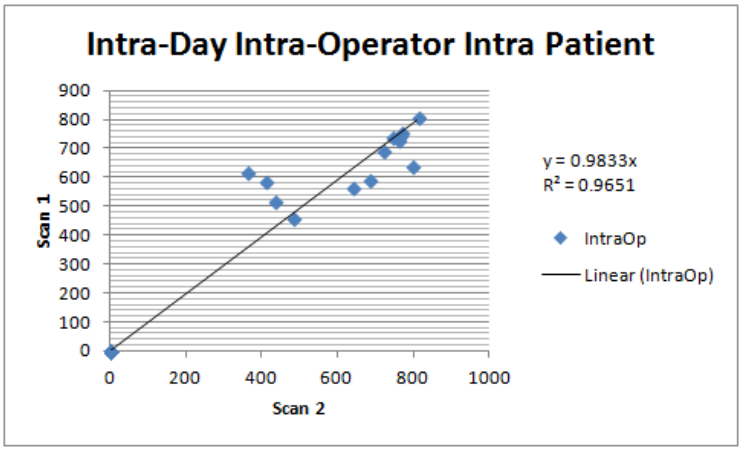

FIGURE 4.4: Comparison of images taken by the same operator on the same patient on the same day. The slope is 1 indicating that on average there is no difference between scans taken by the same operator and the spread in the data is small with a high degree of correlation, (the numbers are correlation quantity and they are unit less).

initial assessment on day 1 and then at the follow-up assessment on day 8. In recognition of this, events fulfilling the definition of an adverse event (AE) or serious adverse events (SAE) will not be reported in this study unless they are classified as 'related'.

4.7.2 Related and Unexpected SAEs (RU SAEs)

Any SAE which is considered as 'Related' to the research and is Unexpected must be recorded on the Related Unexpected Serious Adverse Event Form. For each RU SAE the following information will be collected:

- full details in medical terms with a diagnosis, if possible
- date of SAE

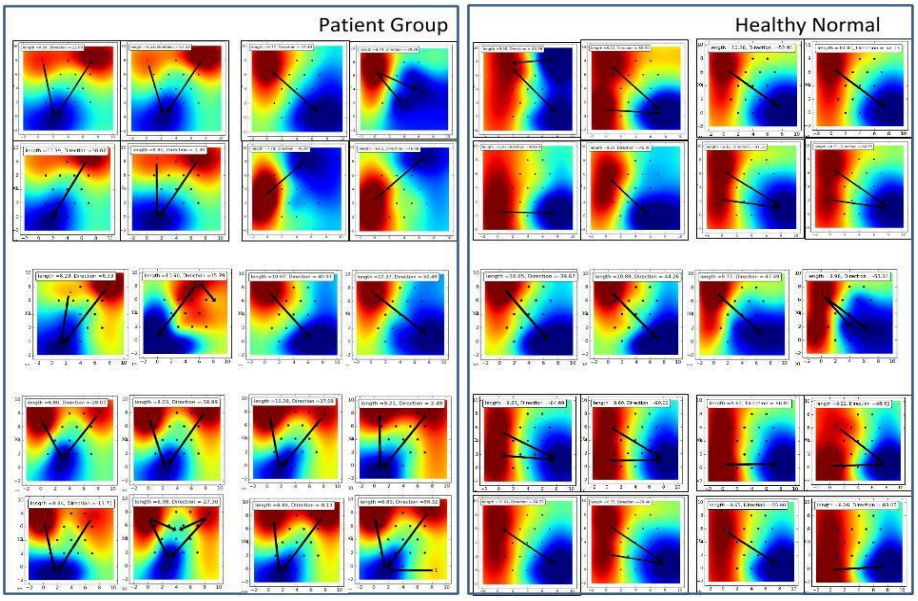

FIGURE 4.5: Current MCG Scans from the first five patients and first five healthy participants. They were grouped into blocks of four representing two scans by two operators on two days. The MFM clearly distinguishes abnormal from healthy participants (they are grid positions and each number is placed with a sensor, the units are arbitrary)

- its duration (start and end dates; times, if applicable)
- action taken
- outcome

Events will be followed up until the event has been resolved or a final outcome has been reached. All Related / Unexpected SAEs will be reviewed by the Chief Investigator and subject to expedited reporting to the main REC and Sponsor by the Research Nurse on behalf of the Chief Investigator within 15 days.

4.8 Reporting

Safety issues will be reported to the Main REC in the annual progress report. An annual summary of all events will also be reported to the Sponsor. Expedited

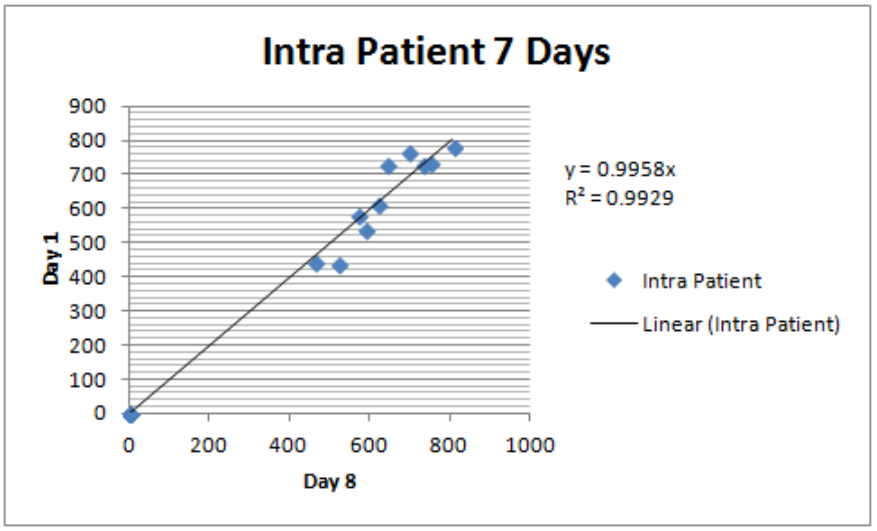

FIGURE 4.6: Comparison of images taken by the same operator on the same patient between the first and second visits (images taken 7 days apart). High correlation between visits (slope =1) and low spread in the data indicates a high reliability. The graph shows correlation quantity, being in patient region, X axes their second visit (day 8) and Y axes shows their first visit (day 1) and they are unit less.

reporting of events to the main REC and the Sponsor will be subject to current NRES guidance and Sponsor requirements.

4.9 Sample Size Calculation

We plan to use a total of 60 patients with ischemic heart disease and 60 healthy volunteers. As this is a "first in patient" study there is no existing information on the device to inform a formal sample size calculation. Thirty participants per parameter is recommended for a pilot study [96], which corresponds to 30 patients and 30 healthy volunteers in each of the marker characterization and technical performance evaluation phases of the study.

4.10 Statical Analysis

Early review

The first five patients and first five healthy volunteers recruited were analyzed in an early review of the images, in order to determine if there were marked differences between images taken from patients and those from healthy volunteers. At the end of recruitment, the images from these ten participants were included in the characterization of the image markers.

Characterization of image markers

Markers of the images were characterized in order to objectively differentiate between normal and abnormal images, and to assess consistency within and between operators (on same day and over different days) and within and between raters, e.g. angle / distance between two distinct areas on the image.

Summary statistics (mean, median, standard deviation, minimum, maximum) will be generated on the summary features, and presented by operator, rater and normal/abnormal scans. In addition, summary features will be presented by gender and age group, explained in more detail in the results chapter.

4.11 Monitoring Data Collection

All record keeping will be in accordance with the Data Protection Act 1998 and the NHS and University of Leeds data security policies. Personal data were recorded and stored by the research team. The University of Leeds will permit monitoring, auditing and reviewing and allow direct access to any data collected and consent forms. Data will be monitored for quality and completeness by the research fellow. The electronic database is password protected and accessible only to members of the research team.

All the information obtained about a participant will be anonymized. The scan and data will be linked by a unique anonymised code. The scan data is in the form of digital cardiac images. The images are stored only temporarily on an encrypted hard drive once I have transferred them from the device imaging memory stick and then the information on memory stick will be deleted. These were uploaded into

the secure University server, which allows access only to the immediate research team and on entry of a password.

Should the research team wish to publish sample images there will be no personal data connecting the participant to the image. These will be kept for a minimum of three years, keeping within the Data Protection Act 1998 guidelines, as well as the NHS and University of Leeds data security policies. All anonymised data will be accessible via peer reviewed publishing.

Quality Assurance and Ethical Considerations

4.11.1 Ethical Considerations

The study was performed in accordance with the recommendations guiding physicians in biomedical research involving human subjects adopted by the 18th World Medical Assembly, Helsinki, Finland, 1964, amended at the 52^{nd} World Medical Association General Assembly, Edinburgh, Scotland, October 2000. Informed written consent were obtained from the participants prior to recruitment into the study. The right of a participant to refuse participation without giving reasons must be respected. The participant must remain free to withdraw at any time from the study without giving reasons and without prejudicing his/her further treatment. The study were submitted to and approved by a Main REC prior to entering participants into the study. A copy of the final protocol, participant information sheets, consent forms and all other relevant study documentation were provided to the Main REC.

4.12 Statement of Indemnity

The sponsor, University of Leeds, was to provide insurance with indemnity to meet the potential legal liability for harm to participants arising from the management and design of the research. To meet the potential legal liability of investigators/ collaborators arising from harm to participants in the conduct of the research, the participating NHS organization is responsible for providing insurance and/or

indemnity. The sponsor did not make arrangements for payment of compensation in the event of harm to the research participants where no legal liability arises.

4.13 Reporting and Dissemination

As this is an early stage study there was no public registration of the recorded waveforms or any magneto-cardiograms produced. We intend to publish and disseminate the results and quantitative data via peer reviewed scientific journal, internal University of Leeds report, conference presentation and University website publication. Credit for the main results will be given to all those who have collaborated in the study, through authorship and by contribution. Uniform requirements for authorship for manuscripts submitted to medical journals will guide authorship decisions. These state that authorship credit should be based only on substantial contribution to:

- conception and design, or acquisition of data, or analysis and interpretation of data
- drafting the article or revising it critically for important intellectual content
- final approval of the version to be published
- and that all these conditions must be met (www.icmje.org). Any data that is published will be void of personal data and have no link that might identify the participants.

4.14 Conclusion

To summarize this chapter, the study carried out under ethics approval with the REC Reference Number,12/YH/0562 in Leeds General Infirmary, recruiting 60 myocardial ischemic patients vs 60 from a completely healthy age matched group. The results of the first 5 healthy and 5 patients, as presented earlier in this chapter, were reviewed at the start of the study to ensure the operators were comfortable and competent using the MCG scanner as it is a novel technique. Also from the rater point of view looking at the differences between normal and abnormal images for the first time ever helped us to structure our data analysis format for the study.

Taking reproducibility into account can enhance the accuracy of the study and to evaluate image quality, within 7 days with different operators. The 10 presented data revealed that the image group including patient and healthy have completely distinguishing features in terms of diagnosis; patients show as abnormal and healthy show as normal. Therefore, it is suggested that the scan results do not depend on operators or timing (as long as the participant's circumstances stay stable).

More subjects were recruited after this review, taking more than a year to find 120 subjects. This will be explained in detail in the results chapter.

Chapter 5

Testing, Extracting Field Maps and Analyzing Data

A fully functional design of the MCG device has been achieved but noise interference to the signal is a challenge. Whilst the outcome is readable, it is not sufficient for the purposes to which we will be applying it. The aim is for the MCG signals to be useful for the medical diagnosis of the images.

In order to begin to optimize the MCG signals to make them medically useful, it was necessary for us to understand the sources of signal interferences that are involved, along with other factors that increase the image resolution. This requires performing several tests. All the tests in this chapter have been formally done on a young healthy volunteer at rest and supine position in an unshielded environment, under ethics approval. In this chapter, I am going to describe several sources that affect the signals and possible solutions to avoid them.

5.1 Patient Alignment

It is important that MCG sensors be able to cover the whole the chest area in order to provide a diagnosable magnetic field map. Hence, positioning the sensors on the body (chest area) is the key issue in the scan procedure that needs to be done very carefully.

To get the best understanding of how different points on chest produce different MFM features in terms of pole distance, vector and angle, we followed Cohens

findings [37]. He presented several possible points with their MCG signals that could be captured by a magnetic sensor, Fig.5.1. It is expected that centring at point H5 results in a very large QRS-complex compared to other points.

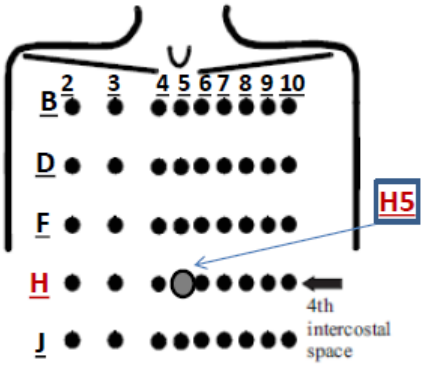

FIGURE 5.1: Shows point H_5, MCG centring position.

We are using a 15-channel MCG to produce a MFM with sufficient resolution for diagnostic purposes and it requires a precise location to be chosen to place the sensors, in order to get the best fit of the array over the chest. Therefore, we considered testing points J_5, F_5 and H_5. Fig.5.2 shows the results of the MFM in different positions. These are different points on the thorax that a sensor can be lined up to. This figure shows the differences between 3 main points. More details for locations can be found in, Fig.5.1.

The results obtained from the test suggested point H_5 is the best place to situate a sensor of the magnetocardiogram and it shows the recordings in xiphoid process. H_5 is chosen as our positioning scan point, because by centralizing at this point the 15 MCG sensors can sufficiently cover the chest area, resulting in high resolution MFM, making them suitable for medical diagnosis.

5.2 Interferences

There are several sources that can have a massive impact on the MCG signal quality that can be removed easily. By avoiding them, scan duration could be shortened, which benefits both patients and clinical staff. Therefore, this method may have potential as a non-invasive tool to investigate cardiac abnormalities at a very early stage.

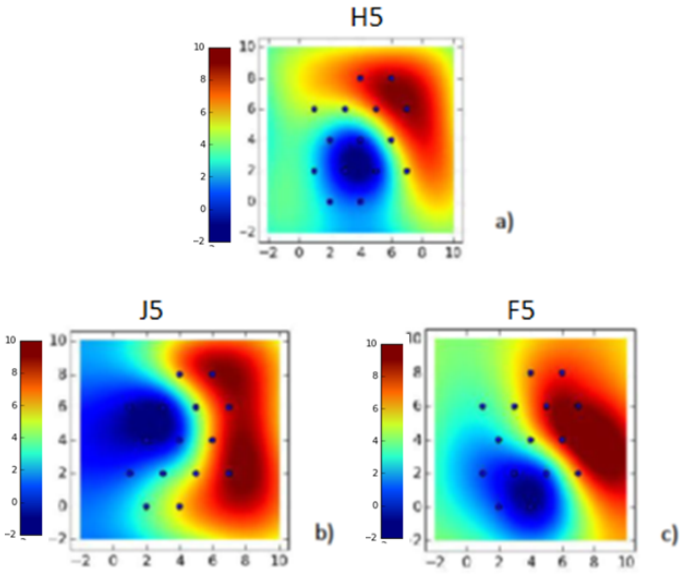

FIGURE 5.2: Magnetic Field Map of a young healthy subject at different positions on the chest. a) MFM at H_5, b) MFM at J_5, c) MFM at F_5. The X and Y axes are arbitrary numbered, dependent on the coil spacing in the sensor head.

Although our MCG device is not sensitive to DC, some sources clearly have strong effects on the signal and make the results difficult to read. Therefore, we tried to minimize the interference from any existing sources causing disturbance in magnetic field and MCG signal. For instance, vibrations caused by the bed, 12-lead ECG interferences during operation, stents and metal objects around chest area, are some possible factors that can distract signals.

5.2.1 Bed Noise

Vibrations from the electric bed, while plugged in, is one of the cases that resulted in distributing noise into the scan. Two phantom scans have been taken, when the bed was plugged in compared to the unplugged bed. Measuring the noise level is very important and can help us to minimize it. Allan variance is best to define the variance over a period of time. It is the measurement of frequency stability over time. These measurements were taken by 15-channel MCG, Fig.5.3. The data in this figure is the Allan variance for measuring noise, while the bed is off compared to the time the bed is on.

Although the current MCG device, unlike SQUIDs, does not require a special bed, the results revealed that keeping the bed unplugged during the scan can improve

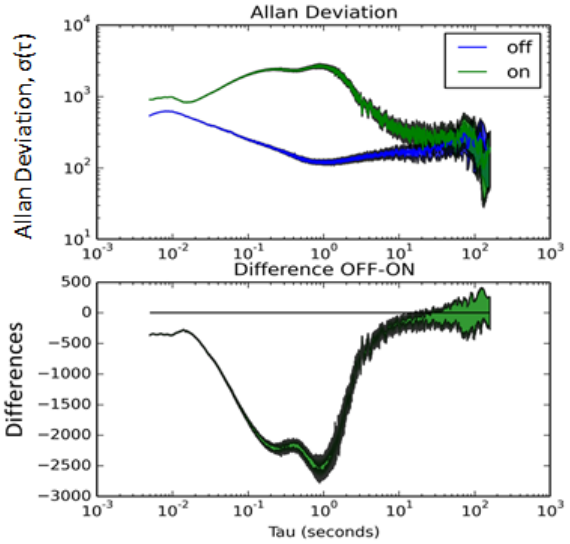

FIGURE 5.3: The graph displays Allan Variance to evaluate noise level of bed while the MCG scan was taken. Y-axes show the Allan variance result, which represents the quantity of variances over time.

the scan results by reducing the noise level and producing an MFM with sufficient resolution.

5.2.2 Metal Objects

The existence of metal objects during the MCG scan on the chest area causes interferences which reduce the MFM resolution and makes the outcome devoid of value. Here are some results from testing different metal objects during the MCG scan to clarify how metal objects effect the results.

Metal-interferences

Fig.5.4 clearly shows the distribution of interferences in the signal that makes the results completely impossible to read and not suitable for diagnosis purposes.

Stents

There are many different type of stents and pace-makers. Unfortunately, we weren't able to test all of them and report their results. Hence, it will be part of our future research, using magnetocardiography on patients with stents and pacemakers.

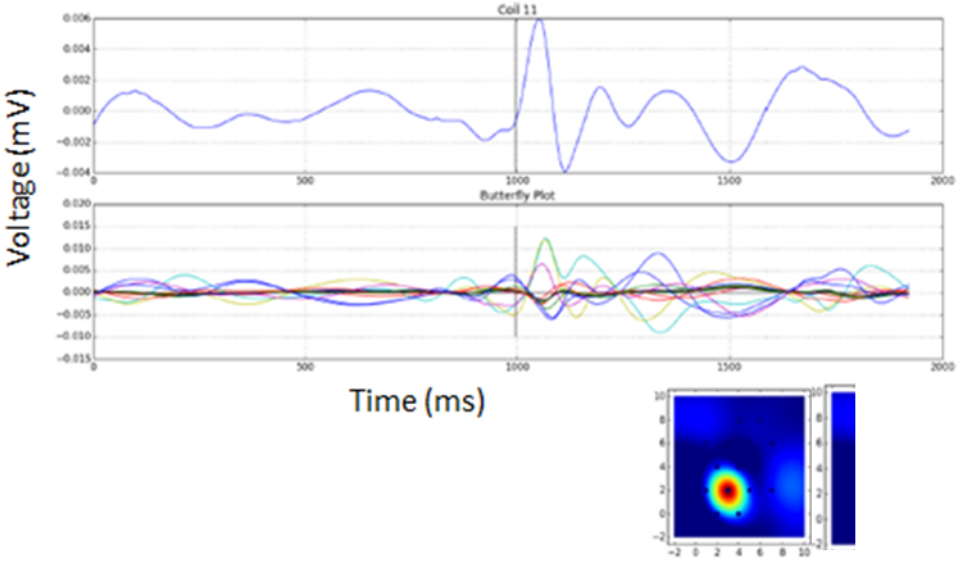

FIGURE 5.4: Shows the results of the MCG scans while the participant was wearing underwear containing metal elements around the chest area.

In general, magnetocardiography does not harm people with stents and/or pace-makers. From our experience, from the MCG scan with an underwired bra on, having metal characteristics can impact the signals. However, this does not mean to exclude people with pace-makers and stents from the MCG scan. Hence, it will be part of our future research, using magnetocardiography on pregnant woman and patients with stents and pacemakers.

5.2.2.1 12-lead ECG Pads

Interferences from 12-lead ECG was another noise source that affects the MCG result. As our future aim is to increase the usability of the MCG in different parts of hospitals, in particular the A&E department, we were interested in the level of interference that would be shown during the MCG scan on a patient with all 12 ECG leads connected to the chest. The results obtained from the previous test reveal that if the 12 lead ECG consists of metal objects on the chest area this can have an effect on the MCG signal and result in misinterpreting the outcome. However, there are some types of ECG electrodes without any metal material and with very thin wires covered by plastic, being used in some A&E departments. Nevertheless, while we have not tried this type with our 15-channel MCG, we believe that it shouldn't have any impact on the MCG signals. We are planning

to test them as this will be very useful in A&E departments on cardiac chest pain patients immediately after arrival.

5.3 Distance

The purpose of this test is to identify whether MCG signals and MCG parameters change with the distance of the MCG sensors from the body. It can bring vital information to the standard measurements. A healthy volunteer was chosen for the test. The distances between the chest surface and the MCG sensors were 2,4, 6, 8 and 10 *cm*. Recordings were made using the 15-channel MCG device system.

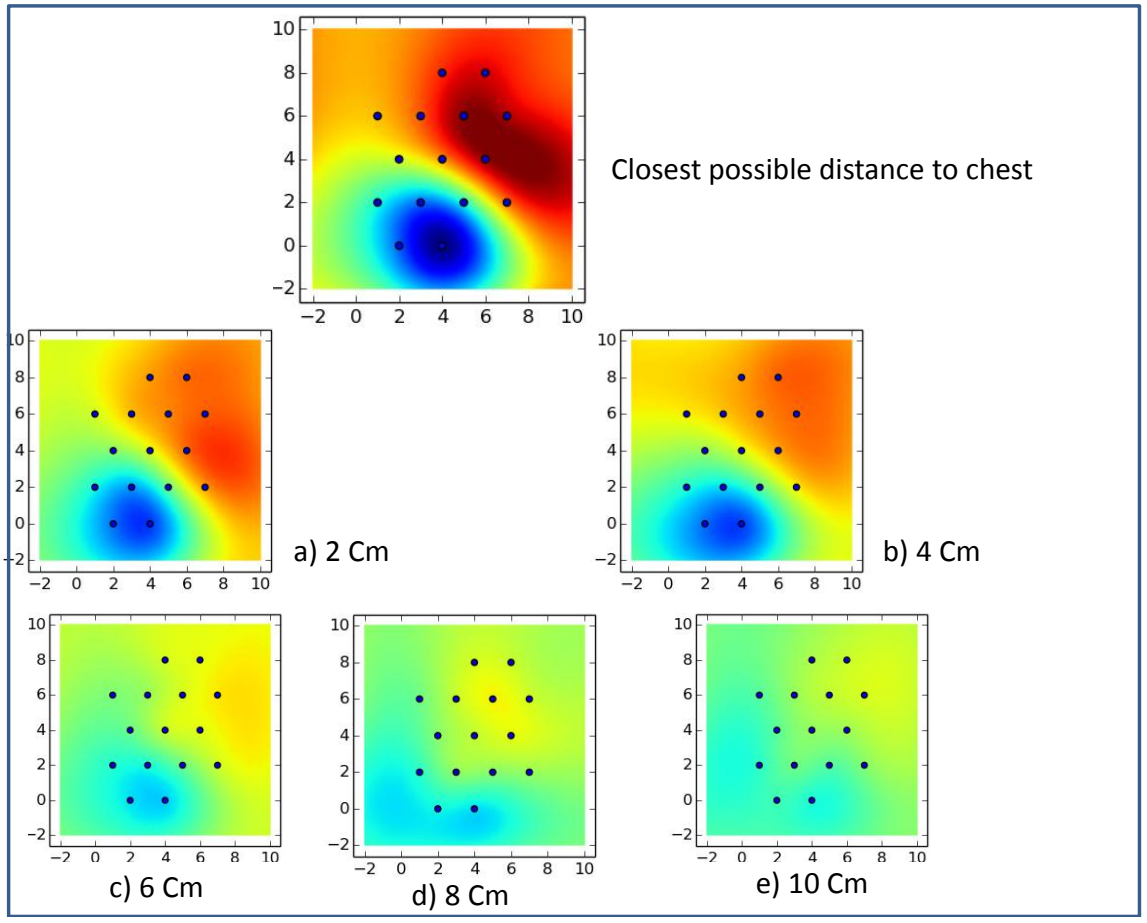

FIGURE 5.5: Shows the MCG scan results of a healthy volunteer at R wave. The top one is demonstrating R peak dipole as close as possible, and the rest show the distance from the chest in increments of 2 *cm*, up to a total of 10 *cm*. They are grid positions. Each number is placed with a sensor (it does not have specific unit).

Since MCG is a non-contact and non invasive device, the positioning and distance between the sensors and the body is significantly important. In order to produce MFM with high resolutions and which are medically diagnosable, we have tested and measured MFM at different distances. The test results show which distances produce images with the most diagnostic value. We have found that up to 10 *cm* further away from the chest we are still able to obtain a MFM. However, as can be seen in Fig.5.5, the lower the distance, the higher the resolution. Therefore, the closer to the chest the better.

5.4 Conclusion

In this chapter we examined the effect of several sources of noise on the MCG signals. We have considered reducing the noise level by unplugging the bed from the mains. We have shown that having metal objects around the chest area can affect the MCG signals.

We have also tested the MCG at different distances from the body. Overall, the further the distance, the more growth on the magnetic field. Therefore, considering the information layout of the 15 sensor array the MFM is no longer suitable for diagnosis. The distance between the sensors and body during positioning must be chosen very carefully and ideally should be as close as possible.

Chapter 6

Magnetocardiography Clinical Tests

Magnetocardiography is known to be very useful in clinical aspects. However, it is not easy to find a magnetocardiography (MCG) system in the clinical field. There are several factors behind the absence of magnetocardiography. One of the reasons is that the interpretation of the results is not immediate to clinicians compared with the results of other competing diagnostic imaging modalities such as, electrocardiogram, echo-cardiogram, magnetic resonance imaging (MRI), computed tomography (CT), positron emission tomography (PET), single-photon emission computed tomography (SPECT), etc. Another contributing factor for the absence of MCG is the non-portability of the MCG and the cost of the apparatus that make the clinicians avoid using this valuable technology. Following our recent development of a novel 15 sensor MCG within an unshielded room for the source visualization, may cardiologists expressed their interest in the practical usage of MCG.

The study will test the science and concept behind this new technology, which can be used to detect cardiac conditions by collecting and measuring the natural magnetic field emitted during the heart beat. The device allows us to map a waveform associated with an ECG [39], which has been demonstrated to contain more useful diagnostic information than the ECG alone [2].

During the trial process, MCG data were recorded from 60 healthy (age-matched group) and 40 patients with IHD history as well as 20 post MI patients. A standard 12-lead ECG was obtained in all subjects. The MCG recordings were contact-less

and taken from 15 sensors under resting and supine position. From these, magnetic field maps were generated during the cardiac cycle.

For interpreting and analysing the results we found several key parameters that can have significant impact on the diagnostic. Therefore, these parameters will be known as diagnostic parameters. The predictors in magnetocardiography will be explained in the following states.

6.1 MCG Overview and Terminology

The device measures the rate of change of magnetic field in the anteroposterior axes with a hexagonal array of 15 sensors (7 *cm* spacing) placed above the chest of a supine human. The output of the MCG is a set of 15 magnetometer and ECG time series, 2000 samples per second coil raw data signals, for a duration of 3 to 10 minutes plus a single ECG waveform Fig.6.1.

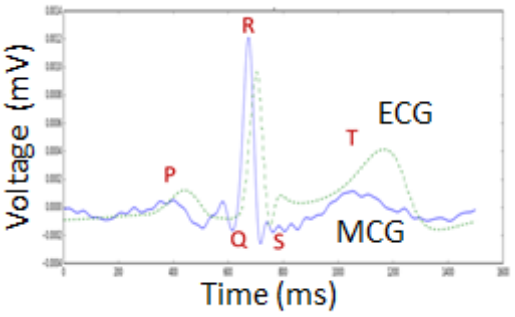

FIGURE 6.1: The similarity within the MCG waveform morphological features to that of ECG such as a P wave, QRS complex, and a T wave.

Using the ECG R-wave as a trigger position, the magnetometer time series are divided into chunks of $\pm 500ms$ about the trigger position. These chunks are then averaged together to produce 15 average cardiac cycle time series, which are stored in a 15×2000 array called Coil-Data. As both waveforms originate from the same source they each have space-time features or parameters that can be measured and quantified in a similar way (i.e. deformation or alteration of the vortices, current vectors, wave angles and time intervals). As with ECG, the MCG parameters of a normal healthy heart are well documented. From a registry of over 400 healthy subjects Kandori and co-workers [97, 98] were able to measure and quantify the MCG parameters of normal healthy subjects (The

standard normal template). These data are particularly useful as they can be used to differentiate a normal MCG from abnormal one. Furthermore, another group [99] compared the images derived from normal healthy subjects with those of patients with clinically significant coronary artery disease (CAD). The authors concluded that the MFMs of the CAD patients differed markedly from those who were healthy, Fig.6.2. Where the CAD patients had more than two vortices with no clear maximal vector orientation, the healthies had two distinct vortices and a maximal vector consistent with other normal healthy subjects.

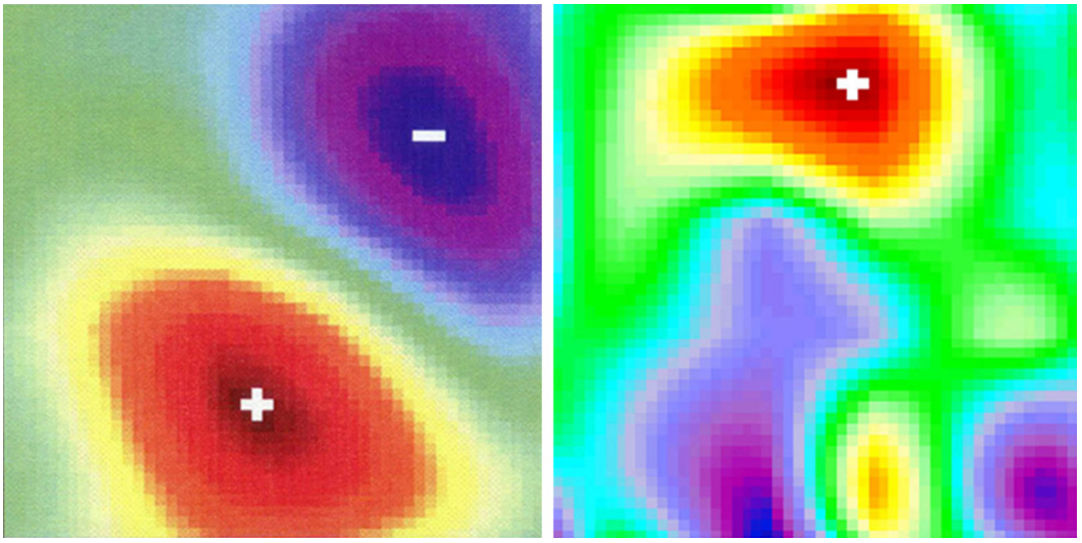

FIGURE 6.2: Magnetic field maps of healthy person (left) and CAD patient with triple-vessel disease (right) (At the moment of T-wave apex) [99].

To fully understand the analysis, it is important to test all possible cardiac features. One way to visualize MCG data is in the form of a butterfly plot which consists of 15 MCG waveform segments superimposed one on top of the other, simultaneously, Fig.6.3. It too has morphological features that correspond to its associated ECG. A notable feature of the MCG is that it provides additional data to that of conventional ECG. For example, the device produces magnetic field maps (MFMs), which are similar in appearance to those of geographical maps in which areas with similar values are similarly colour coordinated. However, whereas the geographical map represents undulation in the earth's surface the MFM shows the signal strength (amplitude) of the magnetic field at specific measurement points (i.e. at the peak of the T wave) and at precise moments within the cardiac cycle.

By doing so each map then reflects the average of all measurement points and the natural projection of the electromagnetic phenomena registered above the thoracic

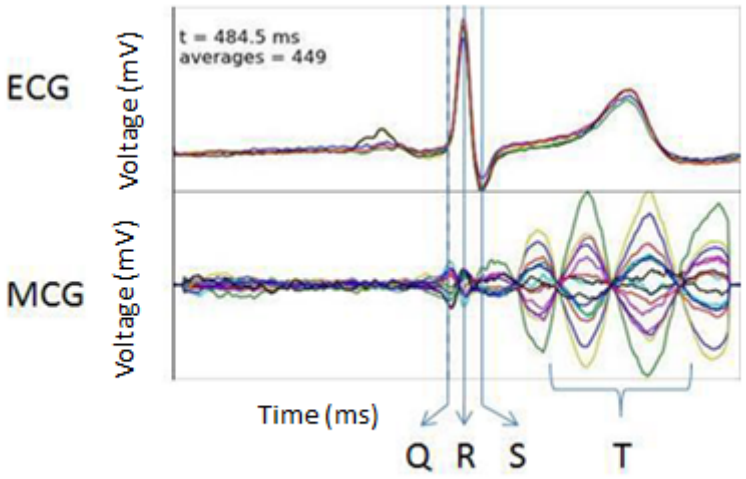

FIGURE 6.3: Cycle averaged ECG and Magnetometer signals. Showing cardiac standard features, P-QRS-T

surface of different parts of the heart. The most informative characteristics of a MFM are the following:

1. The number of magnetic field extrema (points of maximum value), these reflect inhomogeneity in the map

2. The arrangement or position of these extrema relative to each other. As the map simultaneously permits visualization of the magnetic fields minimum and maximal values, it is possible to determine the orientation of the equivalent current dipole (i.e. the excitation wavefront) by drawing a line from the minimum and maximum vortices's and by rotating this line counterclockwise through 90 degrees Fig.6.4

6.2 Standard Features and Space - Time Parameters

Within each magnetocardiogram there are standard features or "lobes" which are common to all healthy normal subjects. For the purpose of evaluating the diagnostic performance of our 15 channel MCG these are referred to as cursors. From the cursor position there are 6 parameters that can be estimated and defined as the following: QR cursor, RS cursor, T_1 cursor, T_2 cursor, T_3 cursor, T_4 cursor,

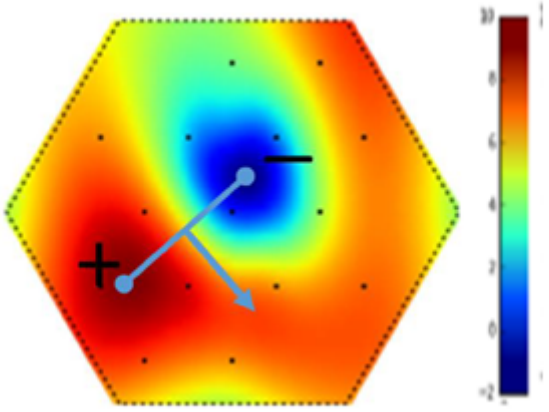

FIGURE 6.4: The figure shows a MFM and the orientation of the equivalent current dipole by drawing a line through the magnetic fields minimum and maximal vortices and rotating this line clockwise through 90°.

shown in Fig.6.5. These are based on the principle that each lobe in MCG corresponds to a rising or falling wave slope in ECG. For instance,the T_1 lobe has a peak corresponding to the rising edge of the ECG T-wave and the T_2 lobe has a peak corresponding to the falling edge of the ECG T-wave.

The absence of one of these features could be a diagnostic in itself, or caused by a low signal to noise ratio (SNR), e.g. A missing or underdeveloped T_1 is not uncommon.

At each of these cursor positions a magnetic field map is generated. A dipole vector is fitted to the map, and its angle and length are recorded in the data-frame, e.g. Q_angle, R_length. An image correlation algorithm is applied, outputting the maximum possible correlation between the MFM and a match template, e.g. Q_corr, R_corr, etc. Fig.6.6 shows dipoles of Q, R and $T_{1,2,3,4}$ correlations. For instance, QR_ corr is defined as a numeric value derived by placement of the cursor over the highest correlation peak in the Q wave correlation dot plot. It expresses the similarity of the R wave with that of the corresponding wave in the standard normal MFM. The higher the value, the greater the correlation. Likewise RS_corr is defined where the cursor is set over highest correlation peak in the S wave.

It defines angle and length of and each dipole. Further details on the dipole and correlation algorithms will be explained in the following subsections.

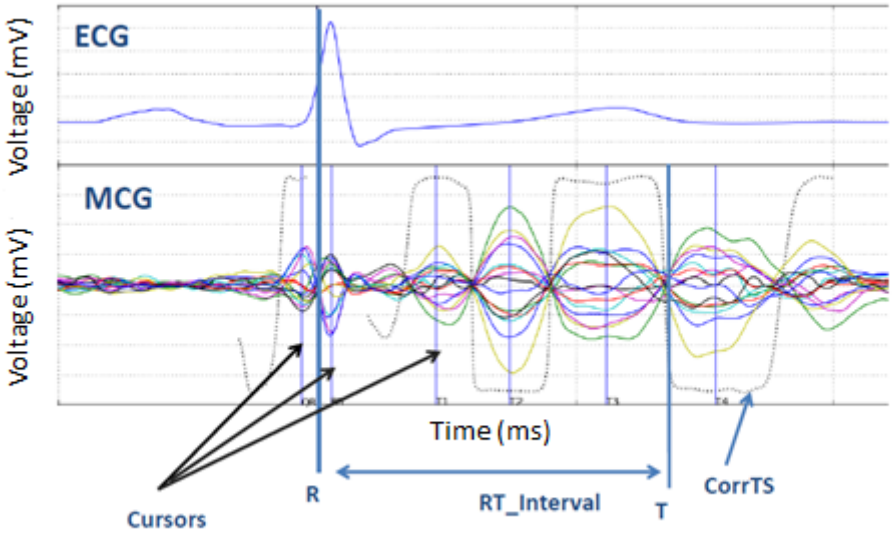

FIGURE 6.5: Cycle averaged ECG and Magnetometer signals. Showing cursors R-trigger, RT_Interval and corr-Ts.

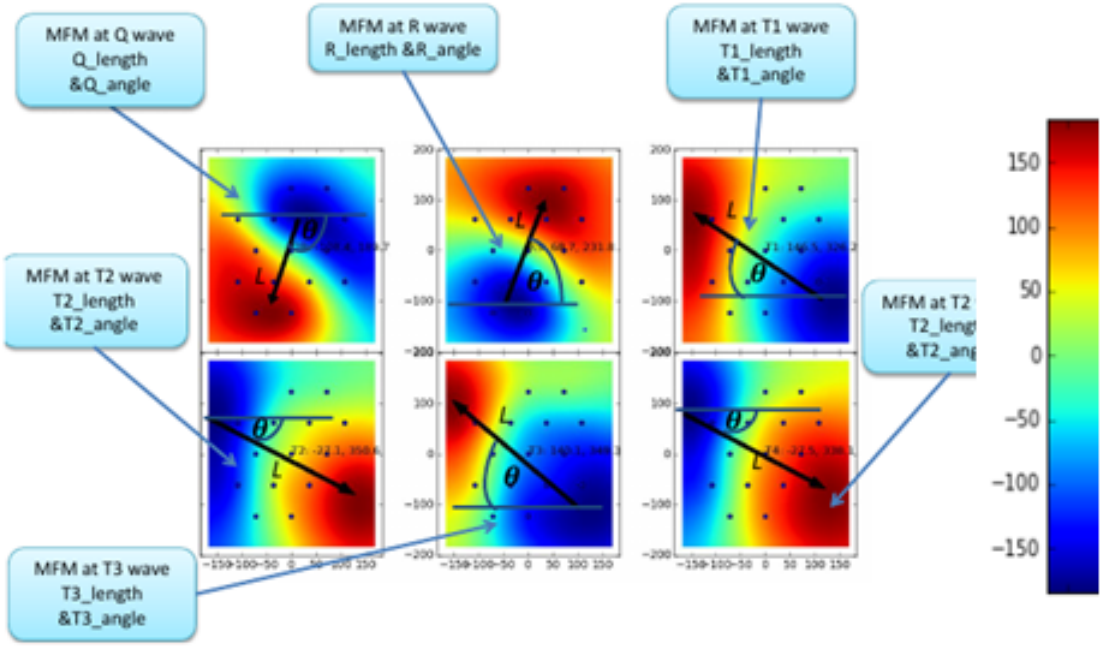

FIGURE 6.6: The image shows magnetic field maps of Q, R and $T_{1,2,3,4}$ based on correlations. They are grid positions. Each number is placed with a sensor.(it does not have a specific unit).

6.2.1 Interval Analysis

The absolute and relative positions of the cursors are potentially diagnostic. However, lobes are often noisy and not symmetrical, with no clearly defined single peak to choose. Therefore, for interval analysis we use the zero crossing (ZC) positions. Since our magnetometers measure $\frac{dB}{dt}$, these ZC's correspond to peaks of action potential activity. A lobe is defined as the region between two ZC's; 5 ms are trimmed off each edge to reduce the variance contribution from the lobe transitions, we are interested in variance within the lobes, not between, as variance within the lobes is a more effective measure of dipole stability.

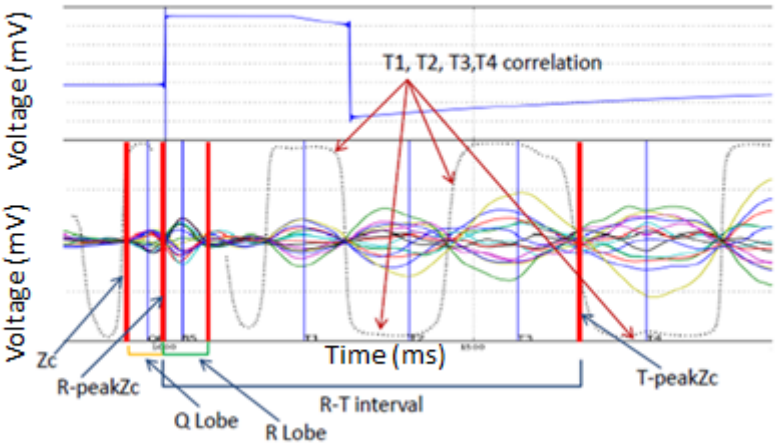

FIGURE 6.7: The image shows the calculated MCG parameters in the butterfly signal.

The mean and standard deviation of the correlation across the lobe is calculated. The average of the lobe means is R_corrmean and T_corrmean. The average of the lobe standard deviations is R_meancorrvar and T_meancorrvar. The standard deviation of the lobe standard deviations is R_stdcorrvar and T_stdcorrvar.

RT_Interval

The R wave is defined as the zero crossing between the QR and RS lobes; **R-peakZC**. The T wave is defined as the zero crossing between the T_3 and T_4 lobes; **T-peakZC**. RT_Interval is the difference between zero crossings of R and T_3. To clarify the named MCG parameters Fig.6.7 illustrates some MCG terminology definitions in the MCG butterfly signal.

6.2.2 Wavelet Decomposition

In a similar fashion to a Fourier decomposition, a single sensor time series can be decomposed into a wavelet coefficient map over frequency and phase. Searching within a specific freq/phase area for peaks allows the general R and T locations to be found. The R area is defined as -75 ms to +50 ms of the trigger position. The T area is defined as +50 ms to +500 ms, Fig.6.8.

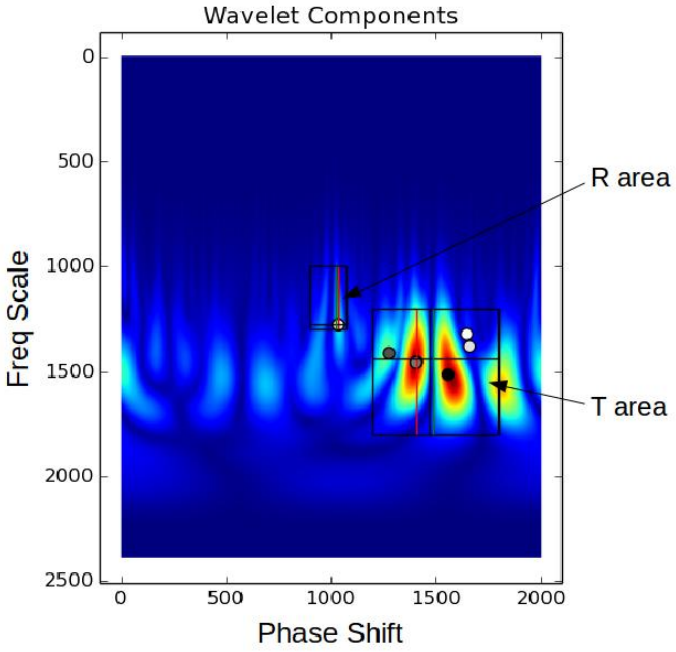

FIGURE 6.8: Wavelet coefficient map with showing freq/phase area to detect R and T locations.

A weighted average is performed for peaks in each area, over each sensor in Coil-Data, to find the average R and T peaks; R_av and T_av (which aren't output for analysis as the positions are imprecise). The min and max and standard deviation of the peaks found within the area give; R_p2p & R_stdev. These can be useful diagnostic parameters as they measure the diffusivity of the sensors time series.

R-T_mean

This is the RT interval as calculated between R_av and T_av. This is not very accurate, and is now superseded by the direct RT_interval measurement between ZC's.

R-T_p2p

The difference between the minimum R peak time position and maximum T peak time. The correlation time series algorithm is used to to find the zero crossings within the R and T areas. The total number of ZC's found are given by R_zc total and T_zc total. The average ZC spacings are given by R_zc mean distance and T_zc mean distance.

6.3 Magnetic Field Map

Another advantage of the MCG is that it provides additional data to that of conventional ECG. A 2D magnetic field map (MFM) is interpolated from a set of 15 magnetometer sensors from a given position in time. This produces a 50×50 pixel image of the cardiac magnetic field at an instant in the cardiac cycle. Generally this looks like a simple dipole (a pair of opposing peaks-one positive [red] and one negative [blue]) as it was illustrated in Fig.6.4. Though in some disease states structures with more than two poles can be seen.

6.3.1 Dipole Vector

The dipole vector is defined as the vector between the maximum positive and negative peaks. For each standard feature a MFM is computed. The dipole vector angle and length are diagnostic features, Fig.6.4.

Because of the small number of magnetometers used, the vector tends to jump into different discrete states, rather than continuously vary with time. This shot noise can be as large as $\pm 30°$, and is amplified by the $atan2$ function (standard cardiology angle mapping, positive angles anti-clockwise to 180°, negative angles clockwise to $-180°$) when the angle is approximately 180°, flipping across the discontinuity.

6.3.2 MFM 2D Correlation

An image correlation algorithm captures not only the angle and length but also the shape of the poles (surface area, fracturing). Effectively, this compresses all of the diagnostic information in a 2D MFM into a single value.

An image correlation algorithm compares two images (the MFM and the match template) by overlaying them, multiplying the overlapping pixels together then summing these products. The match template is translated across the MFM to find the maximum correlation.

The simplest implementation uses a healthy normal MFM for a match template, then finds the maximum correlation with a standard feature MFM. This produces QR_corr, Rs_corr and the rests.

6.4 Young Healthy MCG Results

In early 2013, I completed a study of 40 young healthy volunteers using the V_1 MCG device, which was our first device to use in a clinical environment. It consists of 15 large coils. Fig.6.9 shows the outcomes of the MFM on 40 young healthy volunteers from the University of Leeds. As it can be seen the MFM are identical to each other.

Using the MCG scans from young healthy subjects, we made the following observations:

- The device clearly distinguishes magnetic fields from electric field, whilst generating a waveform that, as expected, precedes in time that of it associated ECG.
- The field maps generated by our MCG device are clearly comparable to published studies of healthy normal subjects [33, 97, 99], and also the field maps generated by other commercially available MCG devices [94].

The controversial issue is whether or not the device could be useful to differentiate cardiac patients with acute coronary syndrome from normal healthy. In this

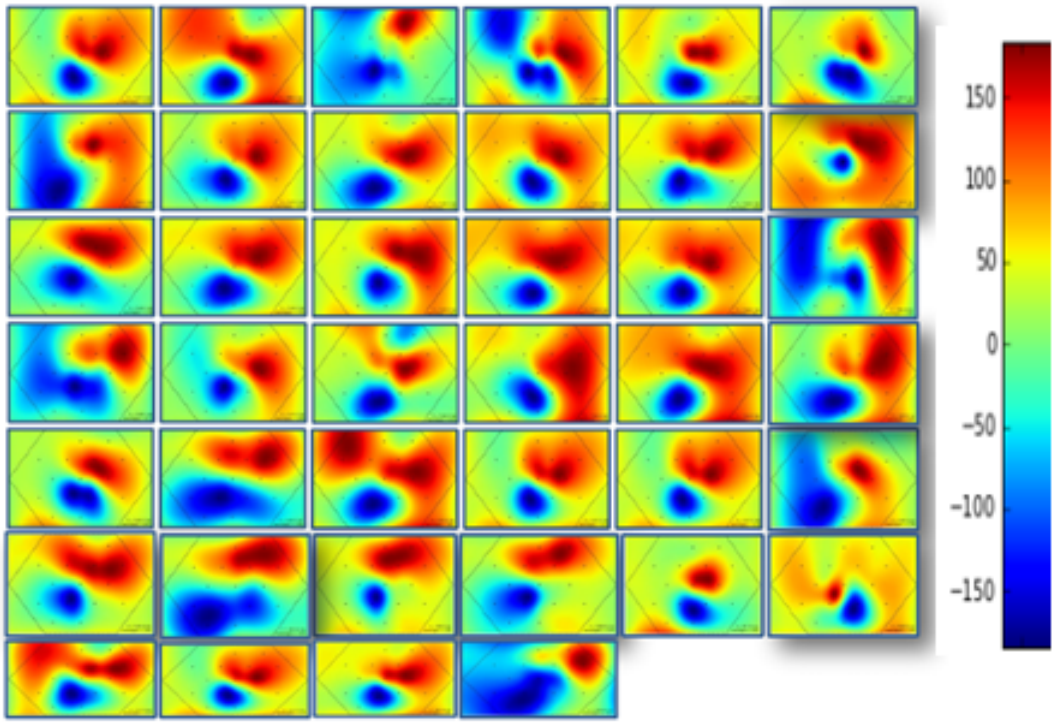

FIGURE 6.9: Scans of 40 young and healthy volunteers that were recorded in a noisy environment (Quantum lab) They are grid positions. Each number is placed with a sensor.(It does not have a specific unit.

context the 60:60 study was conducted to determine the extent to which the device can provide a clear image across a range of test subjects and to determine which parameters from the MCG data are markers for ischaemic heart disease when comparing with healthy controls. A further objective was to establish which of these markers could be used to rule out an acute coronary syndrome in patients presenting with acute chest pain.

6.5 Trial Performance & Study Population

As it was explained in chapter 4 the 60:60 study had an uneventful delay. For this reason, a significant number of patients were excluded on the grounds that they either did not have ischaemic heart disease or were considered likely to proceed to early revascularisation.

6.5.1 Study Allocation, Data Collection and Retention

Patient enrolment and data collection was completed with a few exceptions. This resulted in loss of data from both groups in the final analysis. For example, in the healthy volunteer group, 6 subjects were excluded due to their past medical history of CAD. For 5 other healthy subjects their MCG was either missing completely or could not be evaluated due to position error, therefore 49 healthy subjects were analysed.

In the patient group, 4 scans were lost due to device failure, the operators forgot to switch on the battery power in order to map the magnetic field. Therefore, the amplifiers in the scan head had not been charged. And there is one more scan that was completely missing. For instance in 3 subjects, the scans were clearly abnormal but the computer software used to generate and quantify the parameter estimates was unable to produce meaningful data. This was because the MCG signal was so disordered or of insufficient amplitude for the algorithm to function correctly. Hence, it was decided to exclude them from the final analysis.

6.6 MCG Parameters in Detection of Patients and Healthy

All the analyses described hereafter were conducted on a single scan rather than the average of the first two scans completed on day one. This is because where data were missing from one scan they were also typically missing from the other. Several of the scans could not be used due to misalignment of the scan head or a device failure. As the data had not been fully cleaned yet, the analyst adopted a pragmatic approach, in which the first scan of day one was used unless the second day one scan had fewer missing data points. To enable replication of the results which of the two scans was used is indicated in the data set.

6.7 Statistical Analysis

The following statistics have been done independently by Dr. Paul Wathall. He created some models and tried to fit the data to them. In this way he could find

the most effective predictors used in the study. The interactions were included in a stepwise analysis with other significant predictors. Candidate predictors entered at step 1 include the following; T2_corr by T2_length, QRcursor, QR_angle , T1_angle, T_zcMDIS, QR_length by RS_length, GENDER(1) by T_stdcorrvar, Table 6.1 demonstrates significant differences .

Candidate Predictors	B	S.E.	Wald	df	Sig.	Exp(B)	95% C.I.for EXP(B)	
							Lower	Upper
RS_length*T2_angle	.000	.001	.085	1	.770	1.000	.998	1.001
T2_angle*T2_length	.001	.001	.752	1	.386	1.001	.999	1.002
RS_length*T2_length	-.003	.016	.034	1	.853	.997	.967	1.028
QR_length*RS_length	.029	.016	3.296	1	.069	**1.030**	.998	1.063
RS_length*T3_corr	.000	.000	.711	1	.399	1.000	1.000	1.000
T2_angle*T2_length	.001	.001	.752	1	.386	1.001	.999	1.002
T2_corr*T2_length	.000	.000	5.753	1	.016	1.000	1.000	1.001
AGE*T2_length	-.001	.002	.322	1	.570	.999	.996	1.002
AGE*T3_corr	.000	.000	1.633	1	.201	1.000	1.000	1.000
GENDER*T_zcMDIS	.000	.002	.035	1	.851	1.000	.995	1.004
GENDER(1)*T_stdcorrvar	.020	.008	5.915	1	.015	1.020	1.004	1.037
GENDER(1)*T_zcMDIS	.004	.002	2.853	1	.091	1.004	.999	1.009

TABLE 6.1: Introduces all the possible predictors and highlights (green lines) the most effective variables.

Averaged map class was used to examine sensitivity and specificity in the prediction of CAD. Sensitivity was defined as the percentage of CAD patients classified by the test to the CAD group and specificity as the percentage of the healthy controls classified to the control group. Cut-off value was defined on the basis of the ROC, Fig.6.10.

True positive values define correctly diagnosed disease and False positive values describe incorrectly diagnosed healthy as diseased. True negative value shows correctly diagnosed healthy as healthy and False negative value defines incorrectly

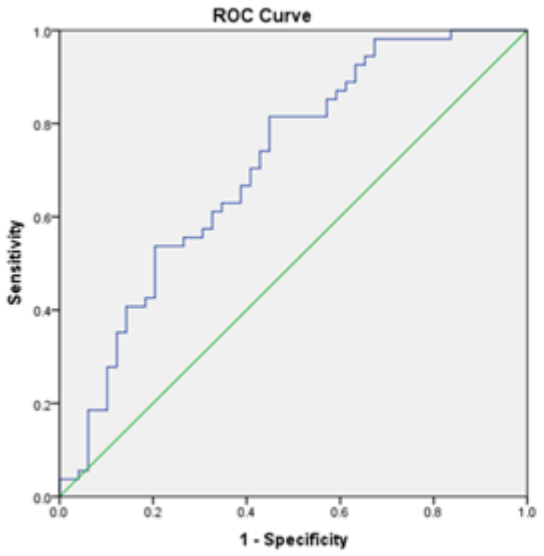

Area Under the Curve

Test Result Variable(s): Predicted probability

Area	Std. Error[a]	Asymptotic Sig.[b]	Confidence Interval Lower Bound	Confidence Interval Upper Bound
.712	.051	.000	.611	.812

a. Under the nonparametric assumption

b. Null hypothesis: true area = 0.5

FIGURE 6.10: Shows the ROC Curve, with the respect of sensitivity vs specificity.

diseased as healthy. I defined these values of the 60:60 study in confusion table, Table 6.2.

	+	-
+	TP	FP
	54	34
-	FN	TN
	1	15
	Prevalence (%)	53%

TABLE 6.2: Shows values for true positive, true negative, false positive and false negative and disease prevalence.

6.8 MCG Capability to Distinguish Ischaemic from Non-Ischaemic Patients

Manual measurement of the magnetic field polarity based on correlation rate of the Q-wave dipole, R-wave dipole and T_1, T_2, T_3, T_4 could be factors to separate the pooled IHD patient group from the control group at rest. Fig.6.11 demonstrates the result of a patient with IHD. The first signal on the top is the outcome from R-gate ECG trigger that is lined up with R-wave in the butterfly signal. The

dashed lines are correlation time series along the signal at each peak. They can also count as a visualizing significant factor to distinguish normal images from abnormals. If the dashed lines at T-wave regions are not square waves then from the correlation point of view the image classifies as an abnormal image.

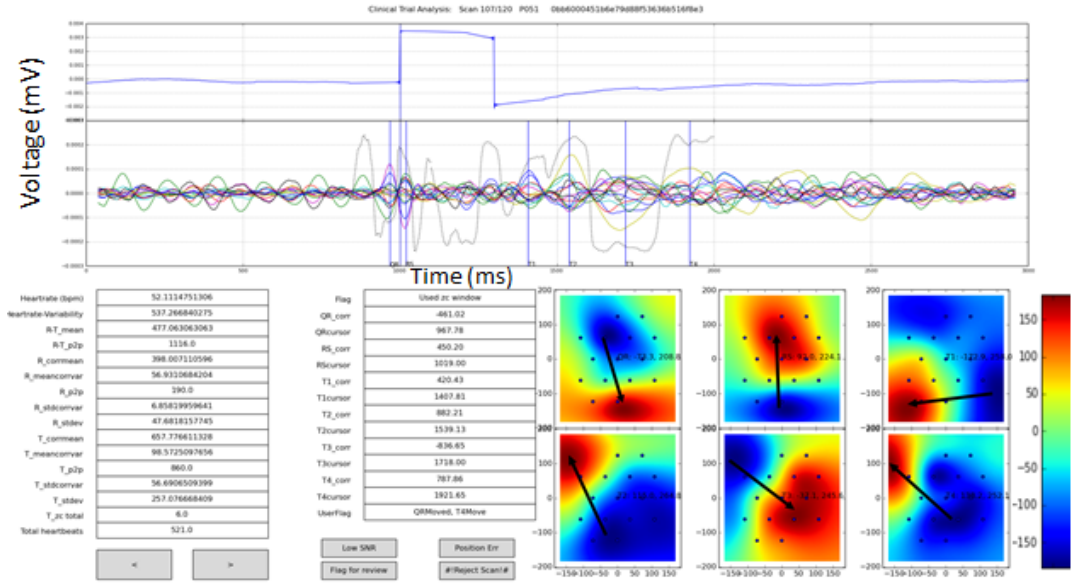

FIGURE 6.11: Shows the MCG scan results of a patient with IHD, produced in post data processing analysis. The top one is demonstrating R trigger ECG and the signal below introduces the butterfly MCG signal averaged over a 10 minute scan. MFM dipoles as close as possible can be seen in QR, RS, and Ts.

The correlation time series plot here (dashed line on top of the butterfly plot) is not a square wave because of the angle of the 'standard normal' match template it was compared with. Therefore, it explains the abnormality on the image and marks it as a patient. This also is a factor, which by looking at the correlation time series plot, can help us to separate normal and abnormal groups.

6.9 Age-matched Control Group

The healthy group of the current study was age-matched control group and Fig.6.12 displays a healthy subject (mean age 54). As it can be seen, the dashed lines in T-wave regions are square waves. Hence, the image is classified as a normal image (without cardiac condition).

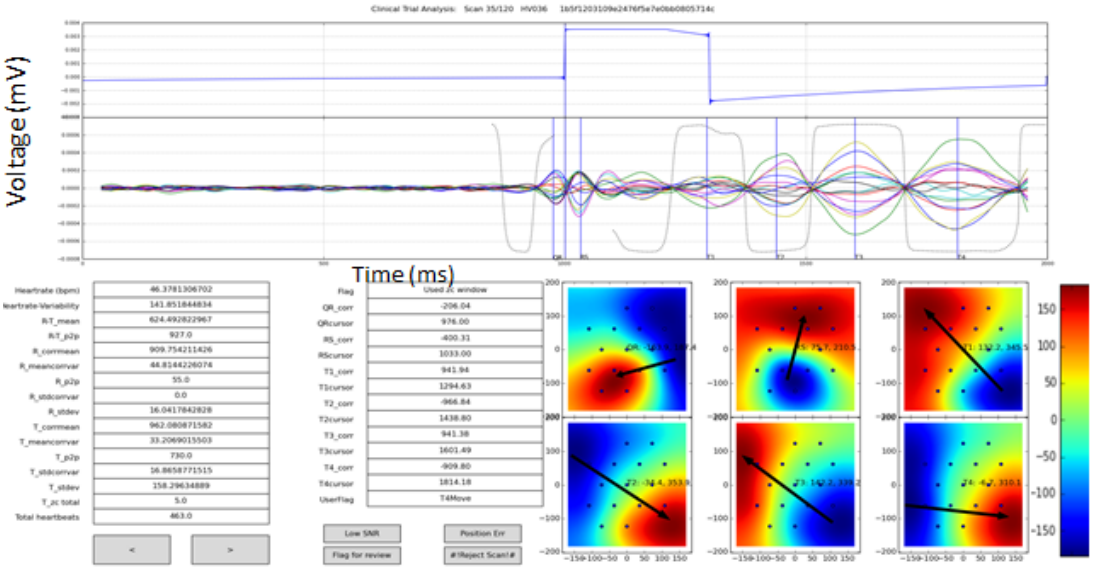

FIGURE 6.12: Shows the MCG scan results of a healthy volunteer. The top one is demonstrating R trigger ECG. The second, a butterfly MCG signal averaged over a 10 minute scan. And at the end MFM dipoles are produced at QR, RS and Ts.

Looking at MFM (dipoles) could be another easy and fast way to distinguish healthy and unhealthy subjects. Considering dipole length and angle could be very vital to separate patients from healthy. The final parameters could be categorized by running several statistics through the data (as explained before).

6.10 Results

Forty-nine healthy volunteers underwent MCG recording. All had at least one MCG recording. Six healthy subjects were excluded due to their past medical history of CAD as well as five other HV as their MCG was either missing completely or could not be evaluated due to position error. Therefore, 49 AMC are included in the present study. Fifty-five IHD patients were examined by the MCG scanner. Four patient scans were lost due to device failure. And there is one more scan that was completely missing. Three subjects were also excluded due to the software inability to produce meaningful data. Hence, in 55 patients, the MCG recording was interpreted as positive for ischemia.

Statistic	Value	95% CI
Sensitivity	98.15%	90.11% *to* 99.95%
Specificity	30.61%	18.25% *to* 45.42%
Disease Prevalence	52.43%	42.35% *to* 62.36%
Positive Predictive Value	60.92%	49.87% *to* 71.21%
Negative Predictive Value	93.75%	69.77% *to* 99.84%

TABLE 6.3: Preliminary results for the magnetometer assessment.

The Fig.6.13 shows MFM at QR wave from 4 AMC subjects vs 4 IHD patients. The MFM can clearly distinguish patients from healthy.

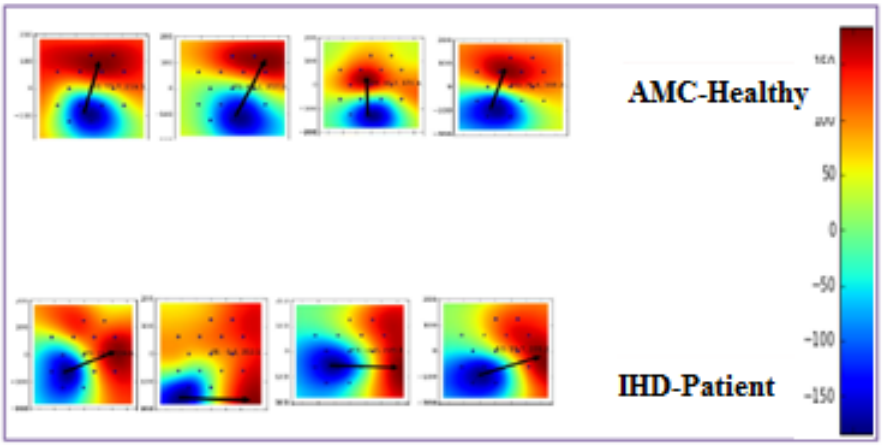

FIGURE 6.13: Shows the MFM results of four healthy age matched control (AMC) versus IHD patients. They are grid positions. Each number is placed with a sensor.(it does not have a specific unit.

However, the most effective parameters to differentiate patients and controls were found when all the MCG parameters were used including the correlations by specialist statistician, Dr. Paul Wathall.

In addition, in the visual interpretation, significant differences between normal and ischemic subjects were noticed, as demonstrated in Fig.6.11 and Fig.6.12. The sensitivity and specificity of the results, presented in Table 6.3, are 98.15% and 30.61%, respectively. The table also indicates NPV and PPv. The positive predictive value (PPV) is the probability that with a positive diagnostic test result the disease is actually present. The negative predictive value (NPV) is the probability that with a negative diagnostic test result, the disease is not present. All are presented in Table 6.3.

Chapter 7

Conclusion

A clinical trial is currently under way at Leeds General Infirmary to determine whether or not the device is capable of detecting recent onset of NSTEMI in patients with high accuracy. There are existing devices in use around the world such as Cryoton Ltd, Moscow [51], Hitachi High-Technologies Ltd., Tokyo, Japan [36], CardioMag Imaging, Inc. Schenectady, NY, USA [42]. However, our device uses an unique innovative sensor arrangement making it potentially smaller and more portable.

The detection of myocardial ischemia could also be enhanced by improving our data analysis and the signals over the S and T waves to the end of the T_4. We have presented a new induction coil based magnetic field mapping device. The device reliably collects cardiac magnetic field signals from study participants. It is compact, portable and low cost, making it suitable for use in the first point of contact for patients with chest pain. In this context under Professor Varcoe's supervision at the University of Leeds, we produced a prototype coil based MCG device which could be deployed freely around a hospital environment. Initial testing of this unshielded device has produced promising results.

Over the period of my DPhil, we have successfully developed and designed a very vital cardiac diagnostic tool, magnetocardiogram. We have done several studies in different cardiac co-morbidities and healthy subjects and implemented a range of new technologies that will help to push Magnetocardiography to the forefront of clinical technologies. My work on MCG has led to a novel technique for detecting cardiac abnormalities. In conclusion, it is very satisfying to see how far the MCG device has developed and functioning well, although the data analysis still requires

more progress and more studies need to be done to complete the understanding of magnetocardiography responses in different cardiac circumstances.

7.1 Future Work

7.1.1 Study in Progress

Although the results presented here have demonstrated the effectiveness of the Magnetocardiography approach in ischemic heart disease, it could be further developed in a number of ways; One way would be to investigate more cardiac conditions in different circumstances. This allows us to expand the use of MCG and make diagnosis fast and easy with high accuracy for clinicians.

A new study is in progress, including 20 subjects with history of chest pain but where there are no symptoms of MI (within 8 weeks), using myoview or stress echo as a reference test, compared with 20 post MI patients based on troponin test (within 48 hours).

Furthermore, we are interested in testing the 15-channel MCG under stress test and compare the sensitivity and specificity with comparators. This test enables us to compete the 15 channel MCG resulted in unshielded environment with other stress test such as stress echo and myoview test.

7.2 Developing Constructions

A future device may want to use more sensors to increase the mapped area and may also consider smaller coils to achieve a higher resolution. Fig.7.1 shows April 2015 magnetocardiogram (alpha-plus), comprising much smaller coils with increasing the array size, including 37 magnetic sensors. The alpha-plus brings enormous benefits to patients and clinicians. It would enable clinicians to approach the test to patient beds and A&E. As a result of this, patients who have moving difficulty can stay in their bed, Fig.7.2. Hence, by making the diagnostic process easier and faster, patients and clinicians time will be saved. Since alpha-plus MCG sensors-head can rotate in an up and down direction, the scan can be taken in a reclined

position for patients in special circumstances, this takes a lot of pressure off of their spine and back muscle.

FIGURE 7.1: Shows MCG alpha-plus device, including 37 small coils with the portability feature.

Although the array size is different to the first version MCG, we are going to use the same algorithm for the analysis. However, some improvements are required to allow us to gain high resolution images. It would be very useful if we would be able to use a De-noised algorithm to clean up the signal from environmental noise. That can enhance the image quality for diagnostic purposes. Also, it would be vital to interpret more cardiac features from the MCG perspective. Because of the MCG characteristics, it produces extra information, I am confident to say it would be worth looking at the waves with different frequencies, finding more diagnostic symptoms.

FIGURE 7.2: Shows the portable MCG alpha-plus, recording an MCG scan at the university of Leeds.

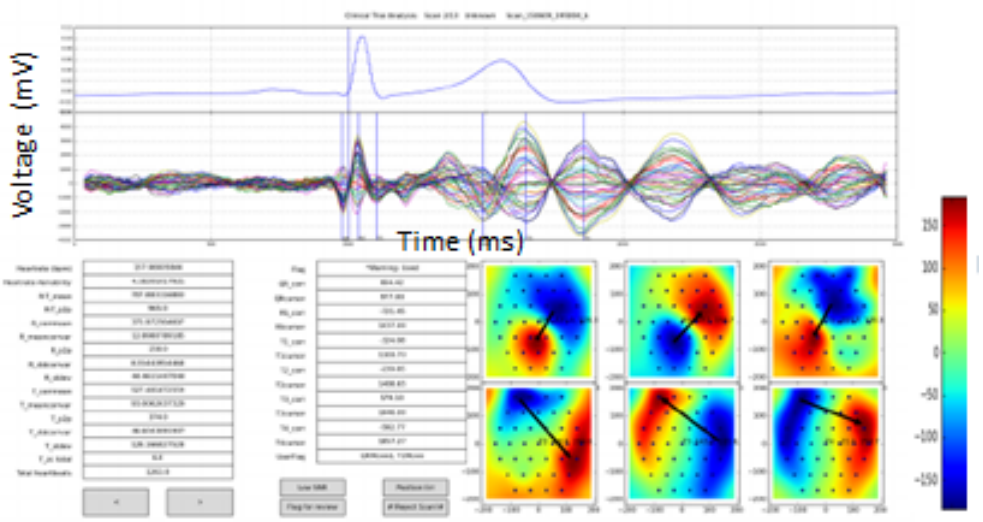

FIGURE 7.3: Shows MCG waveforms and MFM from a young healthy participant in an unshielded environment. Including QR, RS, T_1 to T_4s.

All these improvements require taking more samples and tests. Therefore, after each step of development we need to run a new study and collect data, as much as we can to improve our ability to obtain high quality images, interpreting them carefully and at the end make the software easy for users (e.g. nurses).

Appendices

Appendix A

A Literature Review of Cardiac Conditions

In section 1.3 we discussed magnetocardiography in clinical use and explained its use in detecting CAD and IHD patients. This Appendix covers more details of different cardiac conditions and the outcome of magnetocardiography for each.

A.1 Coronary Artery Disease (CAD)

Single Vessel. Exercise induces alterations (rotation of peak gradient) in the magnetic field distribution of the mean ST-segment and T-wave apex, which can differentiate between different coronary lesions. Changes in the ST segment are most profound immediately after stress, while those in the T-wave emerge later [100]. Also an ST slope increase and ST elevation were found to perform best in single-vessel disease when searching for optimal sites for detecting ischemia induced changes on MCG during stress [39].
Sternickel et al.[101] found that for a 2D map during the ST-T segment, for single vessel blockage the magnetic map is inverted.
Multi-vessel. Increase in lesion areas enhances the residual electrical components or degrades normal electrical activities [36]. For triple vessel disease the magnetic map shows an unstable, falsely oriented and inhomogeneous pattern [101].

A.2 Arrhythmias

Cardiac arrhythmia condition is a group of conditions in which the heartbeat is irregular, either too slow or too fast. There are four main types of arrhythmias; Supra-ventricular Tachycardia, Atrial Fibrillation, Atrial Flutter and Hypertension. These conditions will be detailed in this section. Main successes are in the risk assessment of cardiac sudden death or major heart failure via arrhythmogenic features; localisation of bio-electric sources to guide intervention procedures or diagnose conditions; and visualisation of fundamental arrhythmogenic mechanisms.

Risk assessment- Abnormalities during ventricular depolarization and re-polarization could have been seen in MCG through late fields, intra-QRS fragmentation (a phenomena that polarity changes during a cardiac cycle) and QT dispersion [2] or variability of time durations and magnetic field map components.
Late fields- Of the MCG QRS correspond to the ECG low-amplitude late potentials that detect disturbances [84, 102, 103].
Localization- Many methods have recently been developed to track the conduction propagation with time in 3D mapping. Abnormal current flows from exercise-induced MCG can be used to localize ischemia onset of arrhythmia [104].

A.2.1 Supra-ventricular Tachycardia

Supra-ventricular tachycardia (SVT) or Paroxysmal Supra-ventricular tachycardia (PSVT) is a rapid heart rate, which is caused by electrical impulses that raise above the heart's ventricles. In general, this includes atrial flutter, fibrillation, sinus tachycardia, and atrioventricular (AV) reentrant tachycardia. Yamada et al. [105] have found that the reentrant circuit of reentrant arrhythmia can be visualized via magnetic source movement, something which cannot be done using body surface maps. One can also differentiate between clockwise and counter-clockwise reentry via observing iso-magnetic field vector orientations over time. During propagation the magnetic field (MF) takes on a pattern sequence made up of three characteristic mechanisms. During a reentrant paroxysmal atrial flutter attack, the automatic mechanism during tachycardia, was seen as a strong MF peak, which then deteriorates into the distorted pattern of atrial fibrillation then

transforms into the circular pattern of atrial flutter before returning to the sinus rhythm single peak.

Early depolarization occurring in the PR region results in a short PR, which is defined as the region between R-peak and P-peak in a cardiac cycle. Because it is shorter than a specific range (from cardiologists perceptive), it is called short PR, a delta wave and prolonged QRS, which is a region of three peaks in a cardiac cycle-depolarization. When this region becomes longer in some cardiac conditions it's called prolonged QRS and when there are some fluctuations between the Q and R peaks it's called a delta-wave.

Pre-excitation sites are localised by looking at the position of the MCG minimum with respect to the maximum in the QRS complex [106, 107]. Differentiation of right-wall pathways is determined by source location above sink (maximum) and leftward current dipoles as activation occurs from right to left ventricle. Positions of source and sink reverse and currents are opposite for the left-sided pathway [18]. The magnetic dipole model was found to be the most accurate source localisation method out of three computationally simple source models in a semi-infinite conducting space: the current dipole, the magnetic dipole and the truncated current multi-pole models [18].

Atrial Fibrillation

Atrial fibrillation is represented in MF maps as a distributed, disorganized pattern with no defined single peak present [105]. Diagnostic of P-wave for this group of patients is significant. P-wave is defined as the first peak of depolarisation in a cardiac cycle. The magnetic P-wave duration has been proven longer in AF patients than in normals and differs in conduction types and the P-wave MF distribution characteristics are very different [18]. They also studied the applicability of MCG mapping in separating Wolff-Parkinson-White syndrome (WPW) patients with AF from those not affected. Patients with AF attacks were found to have more dispersed atrial depolarization distributions compared to patients without AF. By inspection of spatial iso-field maps during atrial depolarization, the risk of atrial fibrillation was classified correctly in 11/20 (55%) patients with documented atrial fibrillation, and in 4/6 (67%) patients without atrial fibrillation. 55% patients with AF problems were found to have more than two extrema in the atrial depolarization maps, compared to (67%) of non-AF patients, who had bipolar MCG maps.

Reproducibility of atrial depolarization signals has been found to be superior to ECG [108]. Time-frequency analysis can differentiate multiple reentrant wavelets from focal triggered activation [109]. The intra-atrial conduction pathways can now be differentiated and help diagnose fibrillation as the dominance of the margin of fossa ovalis as well as multiple pathway conduction is a trend in AF patients [110]. This is done by observing the change in pseudo current orientations during atrial activation.

Atrial Flutter

Atrial flutter is caused by the signal macro-reentry mechanism, which physiologically explains a reentrant circuit that can cover a vast area of the atrium. For instance, a circuit runs between the top and the bottom of the right atrium and produces atrial flutter. Another example could be a reentry circuit that uses a bundle branch for antero-grade conduction and another for retrograde conduction to produce the highly malignant bundle branch reentry ventricular tachycardia. This is characterised by a circular MF pattern [105, 109]. It can be differentiated between clockwise and counterclockwise flutter via observing iso-magnetic field vector orientations over time [105]. The weak atrial flutter "f-waves" can be extracted from the other components of the P-QRS-T complex. These are too weak to be detected by standard ECG. The extraction is 3-dimensionally localized on a mesh model of a human heart by a beam former technique having a surface action potential activity as its filter output. It allows tracing of the atrial excitation, hence localization of abnormal atrial activation which was separated from the ventricular excitation [77].

Hypertension

The direction and location of single equivalent dipoles over time were similar to those of normals but their dipole moments were increased significantly [107].

Ventricular Fibrillation (VF)- Ventricular fibrillation MF maps tend to be multi-polar, whereas healthy hearts are either mono or mostly bipolar. Bipolar content is assessed to discriminate risk of VT/VF by many groups in similar ways. One way is eigenvector analysis from the covariance matrix of that produced by the

MCG recording. Higher order eigenvectors will have increasing polarity content as their contribution to the total signal energy increases. This can be shown by deriving spatial distributions from QRS-T integral maps, which is an integration measurement at a region of QRS complex and T-wave that can help the cardiologist to diagnose abnormalities [111].

Ventricular Tachycardia (VT)- QRS fragmentation (polarity change) discriminates between VT and non-VT patients after myocardial infarction [112].

A method of calculating the principal component content of QRST integral maps via eigenvalue analysis determines a patient at risk of VT. If there are more than two eigenvalues larger than 1, this corresponds to the number of extrema dipoles in the MF pattern. VT subjects tend to have two or three extrema over the repolarization segment [111, 113]. In electrocardiography the T-wave illustrates the repolarisation of the ventricle in a cardiac cycle. When there is a dispersion on the interval distance from T-wave peak to T-wave end means there is an abnormality in repolarisation or recovery in a cardiac cycle. Dispersion can happen at re- and/or de- polarisation. When there is a dispersion on the interval, the distance starts at the repolarisation (T-wave) to the end of it.

Late fields - Time domain parameters differ significantly between post-infarction VT and normals; QRS-d, root mean square amplitude (RMS) and Low amplitude signal duration (LAS) parameters. For instance, for each heart's function, P,Q,R,S,T, their peak amplitude can be measured and signal-averaged. If it is found that some of them are lower than the level it should be (from cardiologists' perspective) then there are some abnormalities on that specific area. Mean QRS-d is much longer for VT than MI patients. None of these showed any correlation with LV ejection fractions [103]. Ejection fraction (EF) is a significant measurement in determining how well the heart is pumping out the blood in diagnosing and tracking heart failure. Left Ventricular ejection fraction (LVEF) describes left ventricular conductivity in terms of blood cycle.

Furthermore, re-polarization abnormalities- post-infarction patients have significantly larger late T-wave (TPE) parameters (maximum peak value, average of six longest and the mean of all channels). QT dispersion did not discriminate VT, differing from the ECG findings [103].

Ectopic Beats/ PVC (premature ventricular contraction)- During the propagation the MF pattern takes on a single peak during sinus rhythm or a triggered activity such as a premature complex initiation [84, 105].

B_x, B_y and B_z MF components have been Fourier transformed to produce waveforms and MF distributions for each position and direction. A covariance matrix and eigenvalue equation can then be used to calculate the principal component analysis (PCA) percentage in each direction. The frequency distributions of those score proportions highlight a discrepancy between PVC and healthy subjects, where PVC cases are dominated by significantly lower frequencies. Furthermore, the B_x component shows a different pattern from the other two directions in PVC [114]

Pre-excitation Syndromes (Wolff-Parkinson-White-WPW)- Localisation of Kent's bundle and detection of the proportion of the hearts entire electrical signal through it, is a major success of MCG recording. With MCG mapping, the general localization of 1-2 cm is sufficient for use in pre-surgical or pre-ablative evaluation of WPW. This way of mapping allows for the estimation of risk for atrial fibrillation in WPW [18].

MCG waveforms consist of a short PR interval, delta wave and prolonged QRS. During ventricular re-polarisation, isomagnetic maps for right-sided pathways show the source located above the sink and the activation is directed from right to left. For left-sided pathways, the positions and currents are opposite [115]. Location of accessory pathways can be diagnosed through 3D magneto-anatomical mappings (superimposed MCGs on MRs) in patients with WPW that have been treated successfully by catheter ablation [116]. Another research has been by Brisinda et al. [117]. They studied on classification of Ventricular pre-excitation using multi-site mapping, which showed accuracy with 94% of accessory pathway AP localisation, versus 64% and 67% with ECG during sinus rhythm and pacing-induced maximal ventricular pre-excitation (VPx). A 3D MCG localisation of the AP corresponds to ablation sites.

Right-Bundle Branch Block- Large S- and R-waves along with long durations are common in complete right bundle branch block (CRBBB). Mean angle of maximum-current arrow during ST segment changes significantly for CRBBB patients compared to little variation for healthy subjects [118], up to 160 degree rotation. For right bundle branch this abnormal current flow direction is positive,

corresponding to a clockwise magnetic current change from left to right above the upper-right ventricle. Moreover, T-peak current arrow map (CAM) orientation is not like in normal subjects. Whole-Heart-Electrical-Activation Diagrams (W-HEADS) for CRBBB patients and normals show that the conduction pathway probabilities differ with CRBBB cases having main conduction from posteromedian septum left ventricle to posteromedian free wall [119].

Furthermore,Whole-Heart-Electrical Bull's Eye Maps (W-HEBEMS) show the main current vectors and their distribution zones for CRBBB for S- and R-waves. These show that the large S-wave vector only occurs in the anterior septum but the R-wave is distributed over the anterior and posterior heart [120].

Left-Bundle Branch Block- According to Kandori et al. [118] it is possible to separate left-and right-BBB by observing the propagation of activation with time through the heart. The left BBB has not been studied as thoroughly but the application of MCG to this condition should be as successful.

Cardiomyopathies

Cardiomyopathy are heart muscle diseases. We can classify cardiomyopathies functionally, as involving dilation, hypertrophy, or restriction. Re-polarization processes in patients with cardiomyopathy were different from those in normal subjects on current vector maps [121]. For general cardiomyopathy subjects it was found that analysis of the tangential component (B_xy) rather than the normal (B_z) results in abnormalities in the form of multi-dipoles (50% cases) and shifts in the maximum current vector direction (50% cases) [121].

In addition, Kandori et al. [122] included a subgroup of eight cardiomyopathies of three types in a study on three ST segment current vector shifts, which are all independent of the distance between the heart and scanner. This resulted in 100% true negatives and 100% true positives for cardiomyopathies. Four years after that, another study [123] used a 36-channel MCG to compare with 12-lead ECG parameters. They found that Jt end, Qt end, T peak-end and Qt dispersion parameters were significantly longer for left ventricular hypertrophy (LVH) patients compared to normals (Jt end is a measurement of repolarisation over a time period of a cardiac cycle and it starts from J point (after QRS complex and before T) to end of T-wave).

Dilated - Weakening and enlargement, leading to abnormal electrical activity, meaning the heart cannot pump blood efficiently at this situation. The decreased heart function can affect the lungs, liver, and other body systems. In 2001, Kandori et al.[84] found that ECG often shows sinus tachycardia or AF, VA left atrial abnormalities, and sometimes intra-ventricular conduction defects and low voltage. Echo-cardiogram shows left ventricular dilatation with normal or thinned walls and reduced ejection fraction of less than 40%. Cardiac catheterization and angiography are often performed to exclude Ischemic Heart Disease-IHD. Chronic/Acute Echo, X-ray, Stress test T-end parameters are always significantly longer for VA patients with cardiomyopathy dilation and other intervals also tend to be longer. The presence of bundle branch block show all related parameters abnormal. The key mechanism in cardiomyopathy is abnormal depolarization rather than delay. Hence, T-end and late fields were not markers for dilated cardiomyopathy via exclusion of late conduction.

Hypertrophic (HCM/LVH)- Hypertrophic cardiomyopathy (HCM) is a condition, in which the heart muscle becomes thick. The thickening makes it harder for blood to leave the heart, forcing the heart to work harder to pump blood. This mainly happens around the left heart muscle (LVH). The main underlying diseases of hypertrophy are essential hypertension, aortic stenosis and/or regurgitation and mitral regurgitation. From as early as 1992 [115] it was shown that detection of the increased electromotive forces related to hypertrophy is more specific than when using ECG. This was done via computation of the single equivalent current dipoles from the MCG recording at various points throughout the cardiac cycle to analyze the activation sequence. This is known as the single moving dipole method. Estimation of the amplitude of the source allows location of the hypertrophy. In 2007, Schirdewan et al. [124], were able to discriminate not only HCM patients from normals but also between the obstructive and non-obstructive subtypes. This was done by a new method of quantifying the topology differences between map sequences in terms of entropy against an average reference map. This was most successful for the ST segment between normals and patients, although the QRS complex did provide fragmented high entropy value intervals. The QRS segment was best in differentiation between the subtypes. To improve the power of discrimination, mean normalized MF distributions during QRS were produced and MF strengths of individual grids compared.

Earlier in 2002, Karvonen et al. [86], compared current ECG parameters with

MCG parameters of the same segment as well as two new parameters based on the QRST interval. The QRS integrals successfully separated patients from controls and the additional QRST integral and angle parameters proved more correlated to LV mass. QRST angle was superior to ECG in a small sample of overweight cases.

Furtherer research done by Comani et al. [125] compared the gold standard echo with ECG and MCG diagnosis. Patients with recent mild to moderate arterial hypertension were examined. All patients showed no hypertrophy evidence via ECG, however, ECHO showed a greater LV mass index and concentric remodeling and MCG found significant differences between QRS integrals.
Ischemic - Ischemic cardiomyopathy describes patients, who have reduced heart pumping (squeezing) due to coronary artery disease. These patients often have congestive heart failure. Ischemic means that an organ (such as the heart) is not getting enough blood and oxygen. This has not yet been investigated using magnetocardiography.

Myocardial Infarction- MI (Heart Attack)

According to Weismuller and co-workers [126] the algorithm of Simson determined late fields for ECG data. Averaged, non-filtered signals were baseline corrected visually. The single current dipole model was used in their research. Eight patients post MI with ventricular late potentials and four control subjects were examined. Healthy subjects showed no delay in ventricular fields, whereas these occurred in all patients. The abnormalities were located within the myocardial infarct zones in six patients. Patients were separated from normals via single MCG channel evaluation. Criteria for patient discrimination was a minimum rms 98 fT in one channel and maximum length of terminal low amplitude signal of 38 ms. The composite MCG signal could not distinguish between groups.

In 2000, intra-QRS fragmentation for ECG and MCG were compared [127] by quantifying the number or peaks M and a score S, which was the product of M and the sum of the peak amplitudes. The first 80 ms and the total QRS were used. Late potential and late fields were also analyzed for the same time intervals. Both ECG and MCG provided better results using the fragmentation parameters with the same sensitivities and higher specificity for MCG. Several studies have

been done [18, 24, 66, 102, 126, 128] on QT and QRS prolongation caused by myocardial abnormality using simple late field and QT dispersion techniques.

MCG at rest showed the largest differences between post MI patients and healthy group during re-polarization, which is more prominent in patients with inferior MI, whereas in BSPM they have been found during depolarization [39]. The duration of the QRS complex in the magnetocardiogram was significantly longer in patients with ventricular tachycardia after an old myocardial infarction compared to patients with infarction but without tachycardia, with the sensitivity of 80%.They also showed ST-slope and T-wave amplitude decrease during bicycle exercise testing were the best markers of post-MI with triple vessel-disease.

Remarkably, it is found that [67] MCG can detect 'healed' MI both in patients with Q-wave and non-Q-wave MI via measurement of waveform parameters (QRS, ST-segment, T-wave and ST-T wave integrals, ST-segment and T-wave amplitude and QRS and ST-T wave MF map orientations). Orientation of the MFMs were only significantly different in the ST-T waveform maps, not in QRS. Re-polarisation abnormalities are more pronounced in Q-wave patients than non-Q-wave and are common in healed MI, thus should not always be interpreted as present ongoing ischemia. The QRS-T discordance, defined as the absolute value of the ST, T and ST-T- wave integrals subtracted from the QRS area, showed significant separation power as they were all larger for the MI group than controls. Another research [129] showed that cluster patterns of wave-front vectors during ST-T provide a parameter for statistical classification of Q-MI and myocardial disease.

In 2009, Lim et al. [33] combined ten parameters based on currents and angles that were derived from the re-polarisation interval and T-wave peak with two types of maps depicting MF at the T-wave peak and spatiotemporal activation. Normals had never more than four MCG abnormal parameters whilst 95% of NSTEMI patients had more than four that were abnormal. The STAG and T-MFM results showed significant deviations evident from observation alone.

Another group in the same year [130] compared ECG and MCG in the identification of MI via spatiotemporal correlation analysis to quantify homogeneity of re-polarization. This was done by calculating the correlation coefficient between the QRS and T-max with the MCG signal. 110 patients were investigated a month after MI and revascularisation surgery. Eleven parameters derived based on the whole heart beat were found to all be significantly different for post-MI patients.

ECG detected MI in 72.5%, whereas MCG sudden cardiac arrest (SCA) identified 80.2%. The study included patients, who had non-diagnostic ECGs that were diagnosed via the spatial correlation analysis of QRS and T-wave maxima. In 2010, Leeuwen et al. [131] used the non-dipolar content method for MF maps to classify patients with a history of STEMI. This is assessed via Karhunen-Loeve transformation of the MCG matrix, with the percentage of the contribution of all eigenvectors beyond the third as the non-dipolar content. It was found that STEMI patients produce MF maps with increased non-dipolar content during repolarization, but not significantly during depolarization. T-wave coherence in the dipolar maps differed even more so between normals and patients.

Risk Assessment:

Leder et al. [132] determined the location of the late potentials that are markers for arrhythmogenic events after MI. Current density on the surface of the left ventricle was computed and compared to the entire current distribution for the QRS complex and high frequency late potential signals. Sites of infarctions were characterized by closely matching low current density areas of the QRS and high density areas of the late potential signals.

A new method was developed [122] to determine the state of fibrosis and ischemia of myocardial cells using three ST segment current vector shifts, which are all independent of the distance between the heart and scanner. The four criteria parameters are: two total vectors at T1 and T2, a variance vector and a flatness factor between the first two. Scoring three out of four abnormal parameters judges a patient to have poor muscle status at risk.

Statistical classification would be another method that can be vital for myocardial viability based on Bayes Theorem [129].

The method uses 2D wave-front vectors and cluster patterns from MF maps to obtain a parameter that when applied to Bayes theorem, gives a probability of a patient belonging to a disease group. The ST-T interval was used for 6 old MI patients and 15 normals with result of: specificity 100%, sensitivity 83%, positive predictive value 100% and negative predictive value 94%. Furthermore, myocardial viability with regard to myocardial scarring was evaluated by [133] in single vessel disease patients, who had suffered previous MI. Patients were divided into three categories: no scar segments, scar in 1-3 segments or more than three

segments. Time and area parameters were extracted automatically from each baseline-corrected data set.

Lim et al. [77] found that 15 different parameters significantly separated NSTEMI patients from controls with the max field map angle and T-wave peak max current angle the most sensitive markers. Prolonged QRS duration (QRSd) in MCG is associated with increased mortality after MI. Patients with filtered QRSd>121 ms had more arrhythmic events and significantly increased risk of cardiac death compared to those <121 ms. Kandori et al. [92] found that in multivariate analysis with clinical parameters like age and previous MI, the MCG was only an independent predictor of arrhythmic events, not cardiac death. Previous MI information was needed to make the prediction with MCG. However, ECG was a strong independent predictor of death.

According to Park et al. [134] the 3-Year predictive value investigated four MCG MF map parameters; direction of vector from plus to minus pole, change in this angle, change in distance between poles and the ratio change of pole strengths. They concluded that for NSTEMI and acute chest pain patients, having one out of four parameters abnormal identifies patients at risk of 3-year mortality, whilst rapid changes in these parameters were characteristic of CAD. In the patients with abnormal MCG, 17% died, whereas in the 75 patients with normal MCGs only one died.

Goernig et al. [130] compared MCG and positron emission tomography (PET) for assessment of myocardial viability, by using Bull's eye plots. MCG plots were produced using MF maps over the left ventricle, and by solving the inverse problem. Six out of nine patients showed significant correlation between current density (CD) and PET. The reconstructed CD magnitudes were low in scar segment but also in segments with preserved metabolic activity.

Myocarditis

Agrawal et al. [135] revealed the ability of MCG to monitor the development of myocarditis, which is today, only reliably done via myocardial biopsy. The MCG mean current dipole tracing over time was used to compute a parameter relating the instantaneous current with its localization between consecutive heart beats-the electrical circulation (EC). It was found that the EC value is less than 1 for normals and typically much larger for patients with myocarditis. The mean initial EC value was 4.2, which decreased to 1.5. The myocardial biopsies determined the

count of the cytoplasm of pro-thymocytes (CD3) cells in the myocardium, which decreased from 3.5 to 1.8. This resulted in a strong correlation between the MCG electrical circulation parameter and the lyphocytic infiltration biopsy parameter. The MCG parameters showed no significant change in follow-up of patients with either no significant immunohistological (chemical history) change or persisting inflammation as determined by biopsy.

Myocardial Ischemia (Ischemic Heart Disease-IHD)

Early on, Cohen, et al. [37] revealed changes relating to ischemia not detected by ECG. The TQ baseline elevation and ST depression were found after exercise testing in CAD patients. Ischemic ST depression appeared in the MCG from CAD patients, indicating a greater ST amplitude shift/R amplitude ratio in MCG than that found in ECG [38, 39].

According to Hanninen et al. [39], despite the smaller spatial mapping area of the MCG compared to BSPM, MCG was capable of detecting reciprocal ischemia-induced changes in the ST-segment and T-wave parameters. It was able to detect exercise-induced myocardial ischemia caused by stenosis in any of the main coronary arteries, regardless of presence or absence of a remote infarction. ST-segment parameters and T-wave amplitude, performed equally well in ischemia detection. In non-MI patients, ST elevation and increase in ST slope performed best. In post-MI patients, decrease in ST slope and in T-wave amplitude were best. The optimal locations for ischemia-induced ST depression, decrease in ST slope, decrease in T-wave amplitude and decrease in ST-T integral area were over the middle inferior thorax and abdomen. Moreover, information on physiological stages of ischemia development and resolution can be found in the ST-segment and T-wave upon exercise testing.

Also, transient acute myocardial ischemia is well-recognized in MCG. In addition, the localization of Myocardial by MCG has been successfully attempted using a current density reconstruction method [40]. Tavarozzi et al. [41] added that transient acute myocardial ischemia causes well recognizable changes in the MCG on the ST segment and the T-wave, to determine these changes, the orientation of the maximum spatial gradient of the MF was used. MCG abnormalities during the re-polarization phase were detected in all patients with severe coronary lesions in vector arrow maps and iso-integral maps.

Remarkably, MCG parameters from ST interval and T-wave in IHD patients at rest were found to be sensitive markers for myocardial ischemia [31, 42–45].

Another study [46] used Machine Learning as their diagnostic tool. Machine learning for diagnosing ischemia teaches a computer to learn patterns of MF maps and to differentiate between healthy and IHD patients, Direct Kernel based Self-Organizing Maps (DK-SOMs) were used for unsupervised learning and Direct Kernel Partial Least Squares (DK-PLS) and (Direct) Kernel Ridge Regression for supervised learning.

Hanninen et al. [47] also found it is possible to differentiate between different stenosed vessel regions, with T-wave and ST segment giving equal capability. Optimal locations for detection of exercise-induced ischemia depend strongly on ischemic regions.

In a study with 13 parameters [48], the most successful in separating ischemic patients from controls was RSI (Re-polarization stabilization interval) measured post-exercise, with post-exercise ST- T integrals in both channels and the T-wave amplitude over the upper left thorax also performing well. The best parameters at rest were; T-wave amplitude, ST slope and ST-T integral in the channel over the upper left thorax.

For the detection of re-polarization abnormalities, 7 parameters around the peak of the T-wave were used (pre-peak T-wave mean frontal angle, trajectory, angle deviation; post-peak T-wave mean frontal angle, trajectory, angle deviation; and difference in mean frontal angle between pre- and post-peak T-wave). It was found that the MCG effective magnetic dipole vector score had the strongest relationship with an ischemic outcomes, when compared to ECG and stepwise logistic regression analysis [42].

Myocardial Fibrosis

Myocardial fibrosis is the abnormal thickening of heart valves. A person has inflammation of the heart caused by a buildup of oenophiles-white blood test in the heart muscle. It can result in enlargement of the heart and congestive heart failure.

In 2000 Kandori et al. [122] developed a new method to determine the state of fibrosis and ischemia of myocardial cells using three ST segment current vector shifts, which are all independent of the distance between the heart and scanner.

The four criteria parameters are: two total vectors at T1 and T2, a variance vector and a flatness factor between the first two. Scoring three out of four abnormal parameters judges a patient to have poor muscle status at risk.

The gold standard is still biopsy of the myocardium, generally done in the setting of angiography. Agrawal et al. [135] showed myocardial inflammation can be suspected on the basis of ECG results and elevation of certain proteins. The ECG findings most commonly seen are diffuse T-wave inversions; saddle-shaped ST-segment elevations may be present (these are also seen in pericarditis). ECG examines low voltage QRS complexes in leads I, II and III and a right axes deviation. This is caused by the risen pressure on the right chamber. This leads to right ventricular hypertrophy.

Appendix B

Systematic Review

B.1 Quality Assessment

For the systematic review we used the Quality Assessment of Diagnostic Accuracy Studies (QUADAS 2) tool [74]. For each study, the risk of bias was evaluated according to the quality assessment tool shown in Table B.1.

Domain	Item	Definition
Patient Selection	Risk of bias?	Could the selection of patients have introduced bias?
Index Test	Risk of bias?	Could the conduct/interpretation of the index test have introduced bias?
Reference Standard	Risk of bias?	Is it likely to correctly classify the target condition? Could the conduct/interpretation of the test have introduced bias? Were the test results interpreted without knowledge of reference standard?
Flow And Timing	Acceptable Delay between tests? Withdrawals explained?	Is the time period between reference standard and index test short enough? so that the target condition did not change between the two tests? Were withdrawals from the study explained?

Table B.1: Quality data assessment

B.2 Study Characteristics

We extracted the study characteristics for all the 40 studies, these are shown in Table B.2.

Author (Year)	Study Design	Test	Control	Room (#channels)
Endt, 2000,	Registry	Patients who suffered MI more than 6 months earlier with documented VT within 2 years after MI (20)	Patients who suffered MI more than 6 months earlier with no malugnant VT (11)	Shielded (1)
Fenici, 2004	Case-control	Patients with iHD and angographically proven > 70% coronary stenosis and positive stree/ SPECT (19)	Healthy volunteers (20)	Unshielded (36)
Gapelyuk, 2010	Case-control	Patients with symptomatic stable CAD and angiographically proven >50% stenosis in main coronary arteries (101)	Healthy subjects with no CAD history (59)	Shielded (7)
Gapelyuk, 2007	Case-control	Patients with stable CAD and angiographically proven > 50% stenosis. (101)	Healthy subjects with normal findings in ECG and bicycle ergometry (59)	Shielded (7)
Godde, 2001	Case-control	Patients with CAD and angiographically proven > 70% stenosis with history of documented sustained VT/VF (43)	Patients with CAD and angiographically proven > 70% stenosis with history of MI who remained free of tachyarrythmic events (42)	Shielded (49)
Goering, 2009	Case-control	Patients who suffered MI more than 28 days earlier with angographically proven stenosis > 70% stenosis (108)	Healthy subjects (70)	Shielded (31)

Hailer, 2005	Case-control	Patients with stable angina and CAD angiographically proven ≥ 50% stenosis of a vessel (177)	Healthy subjects with no history of cardiovascular disease, normal ECG at rest and stress and normal echocardiogram at rest (117)	Unshielded (4)
Kandori, 2010	Case-control	Patients with CHD and angographically proven > 75% stenosis of a vessel (56)	Healthy subjects (101)	Shielded (64)
Kanzaki, 2003	Case-control	Patients with CAD and angographically proven > 75% stenosis of a vessel (17)	Healthy volunteers and Patients with chest symptoms with normal coronary angiograms (13)	Shielded (64)
Korhonen, 2001	Case-control	Patients with remote MI and history of documented sustained monomorphic VT (53)	Patients with MI > 6 months ago and no history of sustained VT (83)	Shielded (Not specified)
Korhonen, 2000	Case-control	Patients with remote MI and history of documented sustained monomorphic VT (38)	Patients with MI > 6 months ago and no history of sustained VT (62)	Shielded (Not specified)
Kwon, 2010	Case-control	Patients admitted to hospital with suspected ACS diagnosed CAD with angiographically proven > 50% stenosis of a vessel (237)	Patients with angiographically proven nonobstructive CAD (127)	Shielded (64)
Leithauser, 2013	Registry	Parients with CAD and BBB chosen from patients with ACS and NSTEMI angiographically proven > 50% stenosis (46)	Patients with ACS and BBB angiographically proven nonobstructive CAD (16)	Unshielded (Not specified)
Lim, 2009	Case-control	Patients with unstable angina pectoris and NSTEMI patients (193)	Young subjects with normal ECG and no history of heart diseas, Age-matched controls admitted to hospital for chest pain, normal clinical results (203)	Shielded (64)

Ogata, 2009	Case-control	Patients with CHD and angographically proven > 75% stenosis of a vessel (56)	Subjects with normal ECG and no history of cardiovascular disease (101)	Not specified (64)
Park, 2005	Registry study	Patients presenting with chest pain diagnosed as CAD with ECG, troponin elevation, echocardiography or coronary angiography (143)	Subjects with normal ECG, troponins or coronary evaluation presenting with chest pain (42)	Unshielded (Not specified)
Park, 2004	Case-control	Patients with symptoms of unstable angina, who were diagnosed with CHD angogographically (53)	Patients with normal troponin levels in whom CHD could be ruled out (33)	Unshielded (13)
Park, 2008	Registry study	Patients with angiographically proven ≥ 70% stenosis of a vessel (42)	Patients with angiographically proven nonobstructive CAD (58)	Shielded (55)
Steinberg, 2005	Registry study	Patients with suspected CAD and angiographically proven > 50% stenosis (19)	Patients with angiographically proven nonobstructive CAD (10)	Unshielded (9)
Tantimongcolwat, 2008	Case-control	Patients with MI (29)	Healthy subjects with no evidence of cardiac abnormal symptoms (22)	Not specified (Not specified))
Tolstrup, 2006	Registry study	Patients presenting with acute chest pain, diagnosed as acute coronary syndrome (55)	Subjects with ECG, troponin or angiographic results not consistent with CAD (70)	Unshielded (9)
Van Leeuwen, 2011	Case-control	Patients with STEMI who received successful invasive diagnosis (97)	Healthy subjects with no history of cardiovascular diseas and normal resting ECG and echocardiograms (39)	Shielded (61)
Van Leeuwen, 2003	Case-control	Patients with CAD and angiographically proven > 75% stenosis and no prior MI (65)	Healthy subjects proven angiographically or volunteers with no history of cardiac disease (20)	Shielded (37)

Wu, 2013	Registry study	Patients with CAD and angiographically proven stenosis (51)	Patients with angiographically proven nonobstructive CAD (24)	Shielded (64)
Brisinda, 2003	Case-control	Patients with documented coronary artery disease by angiography (4 by SPECT and exercisetest) (21)	Healthy subjects (13)	Unshielded (36)
Chen,2014	Case-control	Patients with CAD and angiographically proven > 70% stenosis in at least one coronary artery (15)	Healthy subjects (38)	Shielded (61)
Fenici, 2005	Case-control	Patients classified as ischemic on the basis of clinical criteria (41)	Healthy subjects with no evidence of cardiac diseas at clinical history, normal physcial examination and echocardiography (33)	Unshielded (Not specified)
Hren, 1999	Case-control	Patients with CAD and spontanous episodes of VT or VF documented by ECG (29)	Healthy subjects with no history of cardiac disease and normal ECG, echocardigram and physcial exam (22)	Shielded (Not specified)
Karvonen, 2002	Case-control	Patients with pressure overload induced LVH by gender-specific echocardiographic criteria (42)	Healthy subjects (12)	Not specified (Not specified))
Kwon,2006	Case-control	Patients presenting with chest pain diagnosed as CAD with angiographically proven stenosis > 50% and positive treadmill test if available (69)	Symptomatic patients (70)	Shielded (2)
Lim, 2007	Case-control	NSTEMI patients (83)	Subjects presenting with chest pain but there was no clinical evidence to indicate MI (57)	Shielded (64)

Wu, 2008	Case-control	Patients with CAD and angiographically proven stenosis > 50% of a vessel (51)	Healthy volunteers and subjects with angiographically proven nonobstructive CAD (40)	Shielded (Not specified)
Wu, 2013	Case-control	Patients with CAD documented by angiography (28)	Healthy subjects (50)	Unshielded (4)
Wu, 2014	Registry study	Patients with suspected CAD and angiographically proven ≥ 70% stenosis of a vessel (36)	Patients with angiographically proven nonobstructive CAD (19)	Shielded (64)
Van Leeuwen, 2006	Case-control	Patients with CAD and angiographically proven stenosis ≥ 75% of a vessel (94)	Patients with angiographically proven nonobstructive CAD and healthy volunteers (50)	Shielded (37)
Park, 2015	Registry study	Patients with CAD and angiographically proven ≥ 50% stenosis of a vessel (42)	Patients with angiographically proven nonobstructive CAD (5)	Shielded (66)
MakiJarvi, 1993	Case-control	Patients with documents sustained ventricular tachycardia and old MI (10)	Patients with old MI without history of sustained VT or cardiac arrest (10)	Shielded (1)
Muller, 1999	Case-control	Patients with CHD and history of sustained VT and angiographically proven stenosis > 75% in at least one vessel (43)	Post MI patients without arrhythmic event (42)	Shielded (49)
Lin, 2011	Registry study	Patients with suspected ACS with STEMI (144)	Patienst with NSTEMI (143)	Shielded (Not specified)

TABLE B.2: Study Characteristics.

Appendix C

Ethics and Study Protocol

C.1 Ethical Arrangements

All participants were asked to provide written, informed consent. The participants were recruited in a cardiology clinic and there was plenty of time available for considering trial information. Ethical approval was granted by Leeds East Research Ethics Committee and review provided by the local research ethics committee (LREC), with ethics certificate number 12/YH/0562. The trial was conducted in accordance with Medical Research Council (MRC).The University of Leeds was the sponsor for the trial. The Trial Steering Committee (TSC) and the Trial Management Group (TMG) included of the Chief Investigator (prof Mark Kearney), Academic Supervisor (Prof Ben Varcoe), myself, Principal Investigator (prof Mark Kearney) at single site-Leeds General Infirmary, project manager (Leanne Burgin), statistician (Sarah Brown) and research nurses (Rowan Byroom and Lorraine Folk). The Data Monitoring and Ethics Committee (DMEC) involved of an independent statistician (Sarah Brown), and the Chief Investigator-cardiologist (prof Mark Kearney), who were asked to review trial data at regular intervals and implement stopping rules in accordance with MRC guidance.

C.2 Data Management

Trial data were collected on the case report form and follow-up form and then entered by the research nurses into an on-line database provided on a secure central server by the Leeds General Infirmary, LGI. Quality control procedures were applied to validate the trial data. Data will be collated at the Experimental Quantum Information group (QIX) laboratory, University of Leeds and reviewed to characterize the image markers, based on a number of analytical and observational parameters in order to produce a manual of summary features for ischemic heart disease and normal heart images that will allow training of assessors. Two research fellows and myself conducted the data analysis and reporting. The first step was to recruit 5 patients and 5 healthy normal volunteers that have been taken by research nurses. Data from the first five patients and first five healthy volunteers were be reviewed to determine if there are large differences between normal and abnormal images. Monthly outcomes were generated for the group, summarizing baseline characteristics of patients recruited, follow-up rates, data completion and adverse events by study group.

C.3 Trial Progress

The project started on 16 September 2013. We planned to recruit staff and gain ethical and governance approvals in a year before. First group of recruitment completed in months 9–11 plus data analysis and generating report. Actual trial progress was slower than anticipated: patient recruitment was slower than expected, and the trial was terminated to the target of 120 recruitments in one year study. In addition to trial training to the nurses, I had to have received formal training in Good Clinical Practice (GCP), which teaches us how to get best information to carry out the duties in the site as we are involved in conducting a trial.

C.4 Design and Methodology

The design is a technical performance study and is an academic proposal using an in-house manufactured Magneto-Cardiogram imaging prototype. The apparatus is non-invasive, non-contact, field and emission free. The design of the study was chosen to assess the differences in data parameters between cardiac images obtained from healthy volunteers and patients with existing ischaemic heart conditions. For this we need to evaluate the device in an NHS clinical setting on patients, who have already been diagnosed with ischemic heart conditions, including a subset of patients who have suffered a recent myocardial infarction. This is a single-centre study of 120 participants (60 patients and 60 age gender-matched healthy volunteers) to be conducted at the Cardiology clinic at Leeds General Infirmary.

C.4.1 Scanning Procedure

On day 1, the participant will be scanned twice by one operator. A follow-up session will be held one week later on day 8 (-2, +7) at which two MCG scans will be taken; one by the same operator as on day 1, and one by a second operator. The follow-up time point is standardised across participants, and chosen such that the condition of the patient is sufficiently stable so that any changes in the image represent a difference in technical performance rather than deterioration (or improvement) in heart conditions.

C.4.2 Development of the Manual of Image Markers

Data from 30 patients with an ischaemic heart disease and 30 healthy volunteers were used to identify and characterize the markers of the images (training cohort). Data were collated at the Experimental Quantum Information group (QIX) laboratory and reviewed to characterize the image markers, based on a number of analytical and observational parameters in order to produce a manual of summary features for ischemic heart disease that allowed training of the "raters". The remaining data from 30 patients and 30 healthy volunteers were enrolled to evaluate the technical performance of the device (validation cohort) using the information generated from the set of data used to characterise the markers.

C.5 Assessments

Initial assessment (Day 1)
All participants:
Demographic data: date of birth, gender, height, weight, smoking history, medical history (COPD/ hypertension)
Personal data:initials
Clinical data: Blood pressure, heart rate, 12-lead ECG, ECHO cardiogram
Concomitant medications
Adverse events
Procedural outcome measures (by operators): ease of use, time taken to do scan

Patients only
Clinical History: diagnosis of heart condition, duration of ischaemic heart disease, diabetes history, blood test results (obtained from patients notes)

Follow-up assessment (Day 8 (-2,+7))
All participants:
Adverse events
Procedural outcome measures (by operators): ease of use, time taken to do scan
Participant's assessment of the procedure

Appendix D

Publication

A Portable Diagnostic Device for Cardiac Magnetic Field Mapping

J. W. Mooney, S. Ghasemi-Roudsari, E. Reade Banham, C. Symonds, N. Pawlowski, and B. T. H. Varcoe

School of Physics and Astronomy, University of Leeds, Leeds LS2 9JT, UK

June 2016

Abstract. In this paper we present a portable magnetocardiography device. The focus of this development was delivering a rapid assessment of chest pain in an emergency department. The aim was therefore to produce an inexpensive device that could be rapidly deployed in a noisy unshielded ward environment. We found that induction coil magnetometers with a coil design optimized for magnetic field mapping possess sufficient sensitivity ($104fT/\sqrt{Hz}$ noise floor at 10Hz) and response ($813fT/\mu V$ at 10Hz) for cycle averaged magnetocardiography and are able to measure depolarisation signals in an unshielded environment. We were unable to observe repolarisation signals to a reasonable fidelity. We present the design of the induction coil sensor array and signal processing routine along with data demonstrating performance in a hospital environment.

PACS numbers: 06.30.Ka, 41.20, 87.19, 87.57.-s

1. Introduction

Chest pain is responsible for one of the highest rates of emergency hospital visits in industrialized countries [1] and accounts for a large proportion of hospital admissions. Statistics show that around 75% of patients who present at the Emergency Department with chest pain do not have a cardiac related condition [2–5], yet they still need to go through a full diagnostic pathway which can take more than 10 hours [2]. This leads to several thousand people occupying bed spaces placing an additional burden on health care systems. A diagnostic that is capable of rapidly stratifying the cases and removing those patients who don't need an overnight stay is therefore valuable in both triage and cost saving [2].

Magnetocardiography (MCG) involves capturing Magnetic Field Maps (MFM's) of current distributions resulting from cardiac action potentials [6–14]. It has been shown that MCG gives significant improvements in diagnostic capability over an ECG [15–26]. Significantly, in this respect, it has been demonstrated that MCG is capable of reliable detection of Non-ST-Elevated Myocardial Infarction (NSTEMI) [15, 22], which are by definition difficult to detect using ECG. For this reason all ECG negative chest

Bibliography

[1] G. Bison. Development of an optical cardio-magnetometer. *Ph.D thesis*, 2004.

[2] R. Fenici, D. Brisinda, and A. Meloni. Clinical application of magnetocardiography. *Expert review of molecular diagnostics*, 5:291–313, 2005.

[3] G. Baule and R. McFee. Detection of the magnetic field of the heart. *American Heart Journal*, 66(1):95–96, 1963.

[4] J. Mahon, S. Chaplin, and R. Hodgson. UK chest pain A&E attendance statistics. *Health Economics Consortium, The Universty Of York, York*, 2015.

[5] R. Rude, W. Poole, J. Muller, Z. Turi, J. Rutherford, C. Parker, R. Roberts, D. Raabe, H. Gold, P. Stone, J. Willerson, and E. Braunwald. Electrocardiographic and clinical criteria for recognition of acute myocardial infarction based on analysis of 3,697 patients. *The American journal of cardiology*, 52(8):936–42, November 1983.

[6] K. Wrennl. Protocols in the emergency room evaluation of chest pain: do they fail to diagnose lateral wall myocardial infarction? *General Internal Medicine*, pages 86–67, 1987.

[7] T. Lee, G. Rouan, M. Weisberg, D. Brand, D. Acampora, C. Stasiulewicz, J. Walshon, G. Terranova, L. Gottlieb, B. Goldstein-Wayne, D. Copen, K. Daley, A. Brandt, J. Mellors, R. Jakubowski, E. Cook, and l. Goldman. Clinical characteristics and natural history of patients with acute myocardial infarction sent home from the emergency room. *American Journal of Cardiology*, (60):219–224, 1987.

[8] H. Lim, Y. Lee, and N. Chunge. The evolution and future of magnetocardiography in identification of heart disease-induced electro physiological changes. *Proceedings of the World Medical Conference*, pages 74–77, 2010.

[9] D. Geselowitz. Clinical application of magnetocardiography. *IEEE Transactions on Biomedical Engineering*, BME-26(9):497–504, 1979.

[10] G. Bison, N. Castagna, A. Hofer, P. Knowles, J. Schenker, M. Kasprzak, H. Saudan, and A. Weis. A room temperature 19-channel magnetic field mapping device for cardiac signals. *Applied Physics Letters*, 95(17):173701–3, 2009.

[11] K. Tashiro. Proposal of coil structure for air-core induction magnetometer. In *Sensors, 2006. 5th IEEE Conference on*, pages 939–942, 2006.

[12] D. Cohen. Review of measurements of magnetic fields produced by natural ion currents in humans. *Magnetics, IEEE Transactions on*, 6(2):344–345, 1970.

[13] F. Mancoff, J. Dunn, B. Clemens, and R. White. A giant magnetoresistance sensor for high magnetic field measurements. *American Institute of Physics Letters*, 77(12):1879–1881, 2000.

[14] J. Nenonen. Magnetocardiography. *Braginski A and Clarke J and eds. SQUID handbook. Wiley-VCH Verlag, Berlin*, 2002a.

[15] J. Nenonen, J. Montonen, and M. Mäkijärvi. Principles of magnetocardiographic mapping. *Shenasa M, Borgreffe M, Breithardt G, eds. Futura Publishing Co, Mount Kisco, NY*, 2002b.

[16] I. Tavarozzi, S. Comani, C. Del Gratta, S. Di Luzio, G. Luca Romani, S. Gallina, M. Zimarino, D. Brisinda, R. Fenici, and R. De Caterina. Magnetocardiography: current status and perspectives. part ii: clinical applications. *Italian l Heart Journal*, 3:151–165, 2002b.

[17] S. Erne and J. Lehmann. Magnetocardiograph, an induction. in squid sensors:fundamental fabrications and applications. *Weinstock H (Ed),Kluwer Academic publishers, Boston, USA*, pages 395–412, 1996.

[18] M. Makijarvi, J. Nenonen, L. Toivonen, J. Montonen, T. Katila, and P. Siltanen. Magnetocardiography:supraventricular arrhythmias and pre-excitation syndrome. *European Heart Journal*, 14(4):46–152, 1993.

[19] M. Saarineen, P. Karp, T. Katila, and P. Siltanen. The magnetocardiogram in cardiac disorders. *Cardiovascular*, 44(6):820–830, 1974.

[20] M. Saarineen, P. Siltanen, P. Karp, and T. Katila. The normal magnetocardiogram: I morphology. *Morphology Annual Clinic*, suppl. 21:1–43, 1978.

[21] R. Fenici, G. Romani, S. Barbanera, P. Zeppilli, P. Carelli, and I. Modena. High resolution magnetocardiography: non-invasive investigatiion of the hispurkinjesystem activity in man. *Italian Journal Cardiology*, pages 1366–1370, 1980.

[22] R. Fenici, G. Melillo, and M. Masselli. Clinical magnetocardiography:10 years experiences at catholic university. *International Journal of Cardiovascular Imaging*, pages 151–167, 1991.

[23] P. Van Leeuwen, G. Stroink, B. Hailer, A. Adams, S. Lange, and D. Grönemeye. Rest and stress magnetocardiography in coronary artery disease. *Med. Biol. Eng. Comput*, 37:1482–1483, 1999.

[24] B. Hailer, P. Van Leeuwen, S. Lange, and M. Wehr. Spatial distribution of QT dispersion measured by magnetocardiography under stress in coronary artery disease. *Journal of Electrocardiology*, 32(3):207–16, 1999.

[25] P. Van Leeuwen, B. Hailer, S. Lange, M. Pilath, and D. Gronemeyer. Spatial distribution of repolarization times in patients with coronary artery disease. *Pacing Clin Electrophysiol*, 26:1706–1714, 2003.

[26] M. Tsukada, I. Yamaguchi, H. Kanzaki, S. Kamakura, and K. Miyatake. Magnetocardiographic mapping characteristic for diagnosis of ischemic heart disease - Computers in Cardiology 2000. *IEEE-Computers in cardiology*, pages 505–508, 2000.

[27] R. Hoekema, C. Gürlek, M. Brouwer, I. Chaikovsky, F. Verheugt, and M. Gmbh. The use of magnetocardiography and body surface potential mapping in the detection of coronary artery disease in chest pain patients with a normal electrocardiogram. pages 389–392, 2004.

[28] I. Chaikovsky, J. Kohler, Th. Hecker, B. Hailer, S. Eisernitz, and V. Sosnytsky. Detection of coronary artery disease in patients with normal or unspecifically changed ECG on the basis of magnetocardiography. *In: Biomag*

2000 Proceedings of the 12th International Conference on Biomagnetism. Helsinki: University of Technology, Espoo, pages 1–4, 2000.

[29] D. Brisinda, A. Meloni, and R. Fenic. First 36-channel magnetocardiographic study of CAD patients in an unshielded laboratory for interventional and intensive cardiac care. *Conference: Functional Imaging and Modeling of the Heart, Second International Workshop, Lyon, France*, pages 122–131, 2003.

[30] B. Hailer, I. Chaikovsky, S. Auth-Eisernitz, H. Schäfer, and P. Van Leeuwen. The value of magnetocardiography in patients with and without relevant stenoses of the coronary arteries using an unshielded system. *Pacing and clinical electrophysiology*, 28(1):8–16, January 2005.

[31] J. Park, P. Hill, N. Chung, P. Hugenholtz, and F. Jung. Magnetocardiography Predicts Coronary Artery Disease in Patients with Acute Chest Pain. *Annals of noninvasive electrocardiology*, 10(0049):312–323, 2006.

[32] K. Hyukchan, K. Kiwoong, K. Jin Mok, L. Yong Ho, L. Hyun Kun, and K. Tae Eun. Classification of magnetocardiographic parameters based on the probability density function. *Journal- Korean Physical Society*, 48(5):2004–2006, 2006.

[33] L. Kyoon, K. Kim, Y. Lee, and N. Chung. Detection of non-ST-elevation myocardial infarction using magnetocardiogram: new information from spatiotemporal electrical activation map. *Annals of medicine*, 41(7):533–46, January 2009.

[34] K. Ogata, A. Kandori, Y. Watanabe, A. Suzuki, K. Tanaka, Y. Oka, H. Takaki, H. Kanzaki, S. Nakatani, K. Miyatake, S. Watanabe, I. Yamaguchi, T. Miyashita, and S. Kamakura. Repolarization spatial-time current abnormalities in patients with coronary heart disease. *Pacing and clinical electrophysiology : PACE*, 32(4):516–24, April 2009.

[35] H. Kwon, K. Kim, Y. Lee, J. Kim, K. Yu, N. Chung, and Y. Ko. Non-Invasive magnetocardiography for the early diagnosis of coronary artery disease in patients presenting with acute chest pain. *Circulation Journal*, 74(7):1424–1430, 2010.

[36] A. Kandori, K. Ogata, M. Tsuyoshi, Y. Watanabe, H. Takaki, and H. Kanzaki. Subtraction magnetocardiogram for detecting coronary heart disease. *Annals of noninvasive electrocardiology*, 15(4):360–8, October 2010.

[37] D. Cohen and D. McCaughan. Magnetocardiograms and their variation over the chest in normal subjects. *American Journal Cardiology*, 29:678–685, 1972.

[38] M. Saarinen, P. Karp, and P. Siltanen T. Katila. The magnetocardiogram in cardiac disorders. *Cardiovascular Research*, 8(6):820–34, 1974.

[39] H. Hanninen. Multichannel magnetocardiography and body surface potential mapping in exercise-induced myocardial ischemia. *Ph.D. Thesis*, 2002.

[40] R. Killmann, G. Jaros, P. Wach, R. Graumann, W. Moshage, M. Renhardt, and P. Fleischmann. Localisation of myocardial ischaemia from the magnetocardiogram using current density reconstruction method: computer simulation study. *Medical & biological engineering & computing*, 33(5):643–51, 1995.

[41] I. Tavarozzi, S. Comani, C. Del Gratta, S. Di Luzio, G. Romani, S. Gallina, M. Zimarino, D. Brisinda, R. Fenici, and R. De Caterina. Magnetocardiography: current status and perspectives. Part II: Clinical applications. *Italian Heart Journal*, 3(3):151–65, 2002.

[42] K. Tolstrup. Non-invasive resting magnetocardiographic imaging for the rapid detection of ischaemia. *European Cardiovascular Disease*, pages 1–5, 2006.

[43] M. Lowe, L. Peterson, K. Monahan, and D. Packer S. Asirvatham. Electroanatomical mapping to assess phrenic nerve proximity to superior Vena Cava and Pulmonary Vein Ostia. *Academic journal*, 90:24, May 2004.

[44] J. Park and F. Jung. Qualitative and quantitative description of myocardial ischemia by means of magnetocardiography. *Biomedical Technique Berlin*, 49:267–273, 2004.

[45] B. Hailer, I. Chaikovsky, and S. Auth-Eisernitz. Magnetocardiography in coronary artery disease with a new system in an unshielded setting. *Clinical Cardiology*, 26:465–471, 2003.

[46] M. Embrechts, B. Szymanski, K. Sternickel, T. Naenna, and R. Bragaspathi. Use of machine learning for classification of magnetocardiograms. *Systems, Man and Cybernetics, IEEE International Conference*, pages 1400–5, 2003.

[47] H. Hanninen, P. Takala, M. Makijarvi, P. Korhonen, L. Oikarinen, K. Simelius, J. Nenonen, T. Katila, and L. Toivonen. ST-Segment Level and Slope in Exercise-Induced Myocardial Ischemia Evaluated with Body Surface Potential Mapping. *American Journal of Cardiology*, 88, November 2001.

[48] J. Chen, P. Thomson, V. Nolan, and J. Clarke. Age and sex dependent variations in the normal magnetocardiogram compared with changes associated with ischemia. *Annals of Biomedical Engineering*, 32:307–312, 2004.

[49] K. Kim, Y. Lee, H. Kwon, J. Kim, I. Kim, and Y. Park. Optimal sensor distribution for measuring the tangential field components in MCG. *Neurology and Clinical Neurophysiology*, 60:1–4, November 2004.

[50] K. On, S. Watanabe, S. Yamada, N. Takeyasu, Y. Nakagawa, and H. Nishina. Integral value of JT interval in magnetocardiography is sensitive to coronary stenosis and improves. *Circulation journal*, 10:1586–92, October 2007.

[51] A. Gapelyuk, A. Schirdewan, R. Fischer, and N. Wessel. Cardiac magnetic field mapping quantified by Kullback-Leibler entropy detects patients with coronary artery disease. *Physiological measurement*, 31(10):1345–54, 2010.

[52] R. Prance, T. Clark, and H. Prance. Compact room-temperature induction magnetometer with superconducting quantum interference device level field sensitivity. *Review Sci. Instrument*, 74:3735, 2003.

[53] D. Cohen. Magnetic fields around the torso: Production by electrical activity of the human heart. *Science*, 156(3775):652–654, 1967.

[54] K. Estola and J. Malmivuo. Air-core induction-coil magnetometer design. *Journal of Physics E: Scientific Instruments*, 15(10):1110, 1982.

[55] R. Schmid and G. Thews. Physiologie des mensche. *Springer (Berlin, Heidelberg)*, 1997.

[56] J. Wikswo. Biomagnetic sources and their models. *Proceedings of the Seventh International Conference on Biomagnetism, New York*, 1989.

[57] E. Carmeliet and J. Vereecke. Cardiac cellular electrophysiology. *Springer*, 2002.

[58] W. Andra and H. Nowak. Magnetism in Medicine. *A Handbook. Wiley-VCH*, 2, 2007.

[59] K. Peuhkurinen. Ischemic heart disease at the cellular level. *International Journal of Bioelectromagnetism*, 2(1), 2000.

[60] J. Taniguchi, A. Noma, and H. Irisawa. Modification of the cardiac action potential by intracellular injection of adenosine triphosphate and related substances in guinea pig single ventricular cells. *Circulation Research*, 53(2):131–139, August 1983.

[61] J. Weiss and K. Shine. Effects of heart rate on extracellular [K+] accumulation during myocardial ischemia. *The American journal of physiology*, 250:982–91, June 1986.

[62] J. Tranum-Jensen, M. Janse, W. Fiolet, W. Krieger, C. D'Alnoncourt, and D. Durrer. Tissue osmolality, cell swelling, and reperfusion in acute regional myocardial ischemia in the isolated porcine heart. *Circulation Research*, 49(2):364–381, August 1981.

[63] E. Aiello, R. Jabr, and W. Cole. Arrhythmia and delayed recovery of cardiac action potential during reperfusion after ischemia. *Circulation Research*, 77(1):153–162, 1995.

[64] D. Mirvis. Spatial variation of QT intervals in normal persons and patients with acute myocardial infarction. *The American College of Cardiology*, (3):625–31, 1985.

[65] M. Malik and VN. Batchvarov. Measurement, interpretation and clinical potential of QT dispersion. *Journal of American College of Cardiology*, 36(6):1749–66, November 2000.

[66] P. Van Leeuwen, B. Hailer, and M. Wehr. Spatial distribution of QT intervals: An alternative approach to QT dispersion. *Pacing Clinic Electrophysiology*, 19:1894–1899, 1996.

[67] H. Hanninen, M. Holmstrm, P. Vesterinen, M. Karvonen, H. Väänänen, L. Oikarinen, M. Mäkijärvi, J. Nenonen, K. Lauerma, T. Katila, and L. Toivonen. Magnetocardiographic assessment of healed myocardial infarction. *Annals of noninvasive electrocardiology*, 11(3):211–21, 2006.

[68] G. Yan, R. Lankipalli, J. Burke, S. Musco, and P. Kowey. Ventricular repolarization components on the electrocardiogram: cellular basis and clinical significance. *Journal of American College Cardiology*, 42:401–409, 2003.

[69] H. Lim, H. Kwon, N. Chung, Y. Ko, I. Kim J. Kim, and Y. Park. Usefulness of magnetocardiogram to detect unstable angina pectoris and Non-ST elevation myocardial infarction. *The American Journal of Cardiology*, 103:448–454, 2009.

[70] J. Stinstra, S. Shome, B. Hopenfeld, and R. MacLeod. Modeling passive cardiac conductivity during ischaemia. *Medical Biology Engineering Computing*, 43:776–782, 2005.

[71] P. Takala, H. Hanninen, J. Montonen, P. Korhonen, M. Makijarvi, J. Nenonen, L. Oikarinen, L. Toivonen, and T. Katila. Heart rate adjustment of magnetic field map rotation in detection of myocardial ischemia in exercise magnetocardiography. *Basic Research Cardiology*, 97:88–96, 2002.

[72] Quarterly activity and emergency admissions statistics, NHS and independent sector organisations in England. *Quarterly time series 2004-05 onwards with Annual*.

[73] B. Lindahl. Acute coronary syndrome – the present and future role of biomarkers. *Clinical Chemistry and Laboratory Medicine*, 51(9):1699–706.

[74] P. Whiting, A. Rutjes, M. Westwood, S. Mallett, J. Deeks, J. Reitsma, M. Leeflang, J. Sterne, and P. Bossuyt; QUADAS-2 Group. QUADAS-2: A revised tool for the quality assessment of diagnostic accuracy studies. *Annals of Internal Medicine*, pages 529–36, 2011.

[75] Y. Takwoingi and J. Deeks. METADAS: A SAS macro for meta-analysis of diagnostic accuracy. *Available from: http://srdta.cochrane.org.*, 2010.

[76] H. Muller, P. Godde, K. Czerski, M. Oeff, R. Agrawal, P. Endt, W. Kruse, U. Steinhoff, and L. Traluns. Magnetocardiographic analysis of the two-dimensional distribution of intra-QRS fractionated activation. *Physics in Medicine and Biology*, 44:105–20, 1999.

[77] H. Lim, N. Chung, K. Kim, Y. Ko, H. Kwon, Y. Lee, J. Kim, B. Joung, J. Kim, K. Yu, J. Cho, I. Kim, and J. Park. Can magnetocardiography detect

patients with non-ST-segment elevation myocardial infarction? *Annals of medicine*, 39(8):617–27, January 2007.

[78] M. Goernig, M. Liehr, C. Tute, M. Schlosser, J. Haueisen, H. R. Figulla, and U. Leder. Magnetocardiography based spatiotemporal correlation analysis is superior to conventional ECG analysis for identifying myocardial injury. *Annals of Biomedical Engineering*, 37:107–11, 2009.

[79] L. Lin, F. ang, N. Hua, and H. Lu. Contrast between magnetocardiography and electrocardiography for the early diagnosis of coronary artery disease in patients with acute chest pain. *Computing Cardiology*, 38:641, 2011.

[80] B. Leithauser, J. Park, P. Hill, Y. Lam, and F. Jung. Magnetocardiography in patients with acute chest pain and bundle branch block. *International Journal of Cardiology*, 168:582–3, 2013.

[81] B. Steinberg, A. Roguin, S. Watkins, P. Hil, D. Fernando, and J. R. Resar. Magnetocardiogram recordings in a nonshielded environment–reproducibility and ischemia detection. *Annals of Noninvasive Electrocardiology*, 10:152–60, 2005.

[82] P. Leeuwen, B. Hailer, S. Lange, and D. H. Grönemeyer. 'Changes in dipolar structure of cardiac magnetic field maps after ST elevation myocardial infarction. *Annals of Noninvasive Electrocardiology*, 16:379–87, 2011.

[83] J. Park, E. Shin, S. Ann, M. Godde, J. Park, and J. Brachmann. Validation of magnetocardiography versus fractional flow reserve for detection of coronary artery disease. *Clinical Hemorheology and Microcirculation*, 59:267–81, 2008.

[84] P. Korhonen, J. Montonen, M. Mäkijärvi, T. Katila, MS. Nieminen, and L.Toivonen. Magntocardiographic intra-QRS fragmentation analysis in the identification of patients with sustained ventricular tachycardia after myocardial infarction. *Pacing Clinic Electrophysiology.*, 24:1179–1186, 2001.

[85] T. Tantimongcolwat, T. Naenna, C. Isarankura-Na-Ayudhya, M. Embrechts, and V. Prachayasittikul. Identification of ischemic heart disease via machine learning analysis on magnetocardiograms. *Computers in Biology& Medicine*, 38:817–25, 2008.

[86] M. Karvonen, L. Oikarinen, P. Takala, M. Kaartinen, M. Rossinen, H. Hanninen, and J. Motonen. Magnetocardiographic indices of left ventricular. *Journal of Hypertension*, 20(11), 2002.

[87] P. Ripka. Induction sensors Magnetic Sensors and Magnetometers. *measurement Science and Technology*, pages 47–74, 2001.

[88] R. Prance, T. Clark, and H. Prance. Room temperature induction magnetometers Encyclopedia of Sensors. *Valencia, CA:American Scientific Publishers*, 10:1–12, 2006.

[89] C. Cavoit. Closed loop applied to magnetic measurements in the range of 0.1–50 MHz. *Review of Scientific Instrument*, pages 1–12, 2006.

[90] M. Burrows. Extremely low frequency communications antennas. 1978.

[91] F. Grover. Inductance calculations, working formulas and tables. 1946.

[92] P. Korhonen, T. Husand, V. Ilkka, M. Heikki, K. Markku, T. Katila, and L. Toivonen. Increased intra-QRS fragmentation in magnetocardiography as a predictor of arrhythmic events and mortality in patients with cardiac dysfunction after myocardial infarction. *Journal of cardiovascular electrophysiology*, 17(4):396–401, 2006.

[93] G. Bison, R.Wynands, and A. Weis. Optimization and performance of an optical cardiomagnetometer. *The American Journal of Cardiology*, 22:77–87, 2005.

[94] G. Bison, R.Wynands, and A. Weis. Dynamical mapping of the human cardiomagnetic field with a room-temperature, laser-optical sensor. *Optics Express*, 11:904–909, 2003.

[95] P. Leeuwen, B. Hiler, W. Bader, J. Geissler, E. Trowizsch, and D. Gronemeyer. Magnetocardiography in the diagnosis of fetal arrhythmia. *British Journal of Obstetrics and Gynaecology*, 106:1200–1208, 1999.

[96] G. Lancaster, S. Dodd, and P. Williamson. Design and analysis of pilot studies: recommendations for good practice"Journal of Evaluation in Clinical Practice. *Journal of Evaluation in Clinical Practice*, 10:1088–1099, 2004.

[97] A. Kandori, K. Ogata, T. Miyashita, Y. Watanabe, K. Tanaka, M. Murakami, Y. Oka, S. Hashimoto H. Takaki, Y. Yamada, K. Komamura,

W. Shimizu, S. Kamakura, S. Watanabe, and I. Yamaguchi. Standard template of adult magnetocardiogram. *Annals of Noninvasive Electrocardiology*, pages 391–400, 2008.

[98] A. Kandori, K. Oqata, Y. Watanabe, N. Takuma, K. Tanaka, M. Murakami, T. Miyashita, N. Sasaki, and Y.Oka. Space-Time database for standardization of adult magnetocardiogram-making standard MCG parameters. *Pacing and Clinical Electrophysiology*, 31:422–431, 2008b.

[99] Y. Li, Z.Che, W. Quan, R. Yuan, Y. Shen, Z. Liu, W. Wang, H. Jin, and G. Lu. Diagnostic outcomes of magnetocardiography in patients with coronary artery disease. *International Journal of Clinical and Experimental Medicine*, 8:2441–2446, 2015.

[100] H. Hanninen, M. Makijarv P. Takala, J. Montonen, P. Korhonen, L. Oikarinen, J. Nenonen, T. Katila, and L. Toivonen. Detection of exercise-induced myocardial ischemia by multichannel magnetocardiography in single vessel coronary artery disease. *Annals of noninvasive electrocardiology*, 5:147–157.

[101] K. Sternickel and A. Braginski. Biomagnetism using SQUIDs: status and perspectives. *Superconductor Science and Technology*, 19:S160–S171, 2006.

[102] P. Korhonen, J. Montonen, M. Mäkijärvi, T. Katila, MS. Nieminen, and L. Toivonen. Late fields of the magnetocardiographic QRS complex as indicators of propensity to sustained ventricular tachycardia after myocardial infarction. *J Cardiovascular Electrophysiology*, 11:413–420, 2000.

[103] P. Korhonen. Magnetocardiography in assessment of ventricular arrhythmia risk. *PhD thesis*, 2002.

[104] K. Pesola, J. Nenonen, R. Fenici, J. Lötjönen, M. Mäkijärvi, P. Fenici, P. Korhonen, K. Lauerma, M. Valkonen, L. Toivonen, and T. Katila. Bioelectromagnetic localization of a pacing catheter in the heart. *Physics in Medicine and Biology*, 44:2565–2578, 1999.

[105] S. Yamada, K. Tsukada, T. Miyashita, Y. Noguchi, T. Ebashi, Y. Terada, K. Kuga, and I. Yamaguchi. Analysis of more complex arrhythmias using the tangential components of the cardiac magnetic field. *In: Proceedings of the 12th International Congress on Biomagnetism*, pages 2–5, 2003.

[106] M. Mäkijärvi, J. Nenonen, M. Leiniö, J. Montonen, L. Toivonen, MS. Nieminen, and T. Katila P. Siltanen. Localization of accessory pathways in Wolff-Parkinson-White syndrome by high-resolution magnetocardiographic mapping. *Journal of Electrocardiology*, 25:143–155, April 1992.

[107] M. Nomura, K. Nakayasu, Y. Nakaya, Y. Miyoshi, T. Wakatsuki, K. Saito, S. Bando, and S. Ito. Single moving dipole obtained from magnetic field of the heart in patients with left ventricular hypertrophy. *Clinical cardiology*, 15(10):752–8, October 1992.

[108] R. Koskinen, M. Lehto, H. Vaananen, J. Rantonen, L. Voipio-Pulkki, M. Makijarvi, L. Lehtonen, J. Montonen, and L.Toivonen. Measurement and reproducibility of magnetocardiographic filtered atrial signal in patients with paroxysmal lone atrial fibrillation and in healthy subjects. *Journal of Electrocardiology*, 38:300–6, April 2005.

[109] S. Yamada and I. Yamaguchi. Magnetocardiograms in clinical medicine: unique information on cardiac ischaemia, arrhythmias, and fetal diagnosis. *Journal of Internal Medicine*, 44:1–19, 2005.

[110] R. Jurkko, V. Mäntynen, M. Lehto, M. Jari, J. Tapanainen, J. Montonen, H. Parikka, and L. Toivonen. Interatrial conduction in patients with paroxysmal atrial fibrillation and in healthy subjects. *International Journal of Cardiology*, pages 455–460, December 2010.

[111] R. Hren, U. Steinhoff, C. Gessner, P. Endt, P. Goedde, R. Agrawal, M. Oeff, and L. Trahms. Value of magnetocardiographic QRST integral maps in the identification of patients at risk of ventricular arrhythmias. *Pacing Clinic Electrophysiology*, 22(9):1292–304, September 1999.

[112] P. Endt, H. Hahlbohm, D. Kreiseler, O. Steinhoff, and L. Trahms. Fragmentation of the band-pass filtered QRS complex of patients prone to malignant arrhythmia. *Medical Biology, Engineering and Computing*, 36:723–728, 1998.

[113] B. Schless, H. Müller, M. DeMelis, A. Pasquarelli, S. Erné, and V. Hombach. Analysis of the ST-segment in terms of principal components: application on multichannel magnetocardiographic recordings. *Journal of Medical Engineer Technology*, 28(2):56–60, March 2004.

[114] K. Kobayashi. Development of a three-dimensional biomagnetic measurement system with 39-channel. *Biomagnetism*, pages 35–38, 1999.

[115] N. Masahiro, N. Yutaka, S. Ken, K. Fumiko, W. Tetsuzo, M. Hirokazu, N. Akiyoshi Nishikado, B. Shigenobu, I. Susumu, N. Hiromu, W. Masao, F. Satoshi, and I. Tamura. Noninvasive localization of accessory pathways by magnetocardiographic imaging. *Clinical Cardiology*, 17(10):239–244, May 1994.

[116] S. Yamada, K. Tsukada, T. Miyashita, Y. Noguchi, T. Ebashi, Y. Terada, K. Kuga, and I. Yamaguchi. Analysis of more complex arrhythmias using the tangential components of the cardiac magnetic field. *Proceedings of the 12th International Congress on Biomagnetism*, pages 2–5, 2001.

[117] D. Brisinda and R. Fenici. Noninvasive classification of ventricular preexcitation with unshielded magnetocardiography and transesophageal atrial pacing and follow-up. *PACE: Pacing and Clinical Electrophysiology*, 30 Suppl 1:S151–5, January 2007.

[118] A. Kandori, W. Shimizu, M. Yokokawa, T. Noda, S. Kamakura, K. Miyatake, M. Murakami, T. Miyashita, K. Ogata, and K. Tsukada. Identifying patterns of spatial current dispersion that characterise and separate the Brugada syndrome and complete right-bundle branch block. *Medical Biology Engineering Computing*, 42(2), March 2004.

[119] A. Kandori, T. Miyashita, K. Ogata, W. Shimizu, and Y. Wataru. Electrical space-time abnormalities of ventricular depolarization in patients with Brugada syndrome and patients with complete right-bundle branch blocks studied by magnetocardiography. *Pacing and clinical electrophysiology*, 29(1):15–20, January 2006.

[120] A. Kandori, T. Miyashita, K. Ogata, W. Shimizu, M. Yokokawa, S. Kamakura, K. Miyatake, K. Tsukada, S. Yamada, S. Watanabe, and I. Yamaguchi. Magnetocardiography study on ventricular depolarization-current pattern in patients with brugada syndrome and complete right-bundle branch. *Pacing Clinic Electrophysiology*, 29(12), December 2006.

[121] J. Shiono, H. Horigome, A. Matsui, Y. Terada, T. Miyashita, and K.Tsukada. Detection of repolarization abnormalities in patients with cardiomyopathy using current vector mapping technique on magnetocardiogram. *The International Journal of Cardiovascular Imaging*, 19, April 2003.

[122] A. Kandori, H. Kanzaki, K. Miyatake, S. Hashimoto, S. Itoh, N. Tanaka, T. Miyashita, and K. Tsukada. A method for detecting myocardial abnormality by using a total current-vector calculated from ST-segment deviation of a magnetocardiogram signal points. 39:21–28, 2000.

[123] D. Brisinda, A. Meloni, A. Largo, and R. Fenici. Magnetocardiographic study of ventricular repolarization in hypertensive patients with and without left ventricular hypertrophy. *Neurol Clin Neurophysiol.*, 13:2002–2005, 2004.

[124] A. Schirdewan, A. Gapelyuk, R. Fischer, L. Koch, H. Schütt H, U. Zacharzowsky, R. Dietz, L. Thierfelder, and N. Wessel. Cardiac magnetic field map topology quantified by Kullback–Leibler entropy identifies patients with hypertrophic cardiomyopathy. *Chaos An Interdisciplinary Journal of Nonlinear Science (CHAOS)*, 17:015118–10, 2007.

[125] S. Comani, S. Gallina, A. Lagatta, M. Orlandi, G. Morana, S. De Luzio, D. Brisinda, R. De Caterina, R. Fenici, and GL. Romani. Concentric remodeling detection by magnetocardiography in patients with recent onset arterial hypertension. *PACE: Pacing and clinical electrophysiology*, 27(6pt1), 2004.

[126] P. Weismüller, K. Abraham-Fuchs, R. Killman, P. Richterand W. Härer, M. Höher, M. Kochs, T. Eggeling T, and V. Hombach. Magnetocardiography: three-dimensional localization of the origin of ventricular late fields in the signal averaged magnetocariogram in patients with ventricular late potentials. *Eurropean Heart Journal*, 14:61–68, June 1993.

[127] P. Endt, J. Montonen, M. Mäkijärvi, J. Nenonen, U. Steinhoff, L.Trahms, and T. Katila. Identification of post-myocardial infarction patients with ventricular tachycardia by time-domain intra-QRS analysis of signal-averaged electrocardiogram and magnetocardiogram. *Medical Biological Engineering Computing*, 38(6):659–65, 2000.

[128] L. Oikarinen, M. Paavola, J. Montonen, M. Viitasalo, M. Mäkijärvi, L. Toivonen, and T. Katila. Magnetocardiographic QT interval dispersion in postmyocardial infarction patients with sustained ventricular tachycardia: validation of automated QT measurements. *Pacing Clinical Electrophysiology*, 21(10):1934–42, 1998.

[129] Y. Ono, A. Ishiyama, N. Kasai, S. Yamada, K. On, S. Watanabe, I. Yamaguchi, T. Miyashita, and K.Tsukada. Bayesian classification of myocardial

excitation abnormality using magnetocardiogram maps for mass screening. *Neurology & clinical neurophysiology : NCN*, 2004:43, 2004.

[130] M. Goernig, J. Haueisen, J. Schreiber, and U. Leder. Comparison of current density viability imaging at rest with FDG-PET in patients after myocardial infarction. *Computerized medical imaging and graphics*, 33(1):1–6, 2009a.

[131] P. Van Leeuwen, B. Hailer, A. Beck, W. Sherifa, G. Eiling, and D. Grönemeyer. Magnetic field map orientation in patients after ST elevation myocardial infarction. *17th International Conference on Biomagnetism Advances in Biomagnetism – Biomag2010*, 28:436–439, 2010.

[132] U. Leder, F. Schrey, J. Haueisen, L. Dörrer, J. Schreiber, M. Liehr, G. Schwarz, O. Solbrig, H. Figulla, and P. Seidel. Reproducibility of HTS-SQUID magnetocardiography in an unshielded clinical environment. *International journal of cardiology*, 79(2-3):237–43, 2001.

[133] A. Morguet, S. Behrens, O. Kosch, Ch. Lange, M. Zabel, and D. Selbig. Myocardial viability evaluation using magnetocardiography in patients with coronary artery disease. *Coronary artery diseases*, pages 155–162, 2004.

[134] J. Park, B. Leithauser, P. Hill, and F. Jung. *Annals of noninvasive electrocardiology : the official journal of the International Society for Holter and Noninvasive Electrocardiology, Inc.*

[135] R. Agrawal, K. Czerski, P. Goedde, and U. Kuehl. Non-invasive follow up of evolution of myocarditis with magnetocardiography. *Nenonen J, Ilmoniemi RJ, Katila T, editors. Proceedings of 12th Intern. Conf. on Biomagnetism*, pages 13–17, 2001.